DISSERTATION

Submitted to the
Combined Faculties for the Natural Sciences and for Mathematics
of the
Ruperto-Carola University of Heidelberg, Germany
for the degree of
Doctor of Natural Sciences

Presented by:
Supriya Saraswati
Born in: Dehradun, India

Oral examination: 23rd May, 2017

The Role of *Asap1* in Physiology and Tumor Metastasis

Referees: Prof. Dr. Jonathan P. Sleeman
Prof. Dr. Nicholas S. Foulkes

Zusammenfassung

Tumorwachstum ist ein mehrschrittiger und komplexer Vorgang, der ultimativ im Auswachsen von Metastasen endet. Da Metastasen für die Mehrheit der krebsbedingten Todesursachen verantwortlich sind, sind neue Ansätze um das Metastasieren von Krebszellen therapeutisch zu unterbinden unerlässlich. Voraussetzung für neue therapeutische Ansätze ist es, die zugrundeliegenden Mechanismen der Dissemination von Krebszellen vom Primärtumor an entfernt liegende Orte im Organismus zu verstehen.

Asap1 (Arf-GAP with SH3-domains, Ankyrin-repeats and PH-domains) wurde in unserem Labor durch einen unvoreingenommenen Screen als prometastatisches Gen identifiziert. Es wurde dabei auch gezeigt, dass Asap1 funktionell zum Tumorwachstum in experimentellen Mausmodellen beiträgt und die Expression von Asap1 mit schlechter Prognose und verkürztem metastasenfreiem Überleben von Kolorektalkrebspatienten korreliert.

Um die Rolle von Asap1 in normaler Physiologie und Krebs zu verstehen, habe ich in meiner Doktorarbeit Asap1 Knockout-Mäuse (Asap1$^{GT/GT}$) untersucht, die durch gezielte Depletion des Asap1 Gens in unserem Labor generiert wurden. Meine Untersuchungen ergaben, das Asap1$^{GT/GT}$ Mäuse bis ins Erwachsenenalter leben, obwohl es eine Reduktion der erwarteten Anzahl an homozygoten Knockout-Jungen gibt. Die Abwesenheit von Asap1 resultiert in Wachstumsverzögerung, in Atemnot und verminderter Angiogenese in überlebenden Jungen. Diese physiologischen Unterschiede sind transient und adulte Asap1 Knockout-Mäuse unterscheiden sich morphologisch nicht von Wildtyp-Mäusen.

Zusätzlich habe ich die Rolle von Asap1 im Tumorwachstum und der Metastasierung in autochtonen Brustkrebsmodellen unter Verwendung von Asap1$^{GT/GT}$ Mäusen untersucht. Meine Ergebnisse zeigen, dass der Verlust von Asap1 in MMTV-PyMT Mäusen zu einem früheren Beginn des Tumorwachstums, schnellerem

Tumorwachstums und mehr Lungenmetastasen führt. Weiter habe ich die Effekte von Asap1 Defizienz auf das Verhalten von Brustkrebszellen und Fibroblasten, die von Asap1$^{+/+}$ und Asap1$^{GT/GT}$ Mäusen isoliert wurden, untersucht. Zusammengefasst zeigen meine Ergebnisse, dass *Asap1* ein wichtiger Regulator von Zellmotilität ist und der Verlust von *Asap1* zu Entwicklungsdefekten in neugeborenen Mäusen führt. Weiter hat die Abwesenheit von ASAP1 Effekte, die sich nicht nur auf Tumorzellen beschränken, und führt zu einer erhöhten Anzahl an Metastasen im murinen MMTV-PyMT autochtonen Brustkrebsmodell.

Summary

Tumor progression represents an array of complex events that ultimately lead to metastasis, the end-stage of cancer that is responsible for the majority of cancer-related mortalities. Improved ways to target the spread of cancer are thus imperative to treat cancer effectively. Understanding the mechanisms that regulate the dissemination of cancer cells from the primary site to distant places is a pre-requisite for such strategies.

Asap1 (Arf-GAP with SH3-domains, Ankyrin-repeats and PH-domains) was identified by our lab in an unbiased screen to identify genes whose expression is associated with the metastatic phenotype. It was shown to be functionally involved in tumor progression in experimental animal models and this expression was correlated with poor metastasis-free survival and prognosis in colorectal cancer patients.

To understand the role of *Asap1* in normal physiology and in cancer, in my thesis work I studied *Asap1* knockout (Asap1$^{GT/GT}$) mice, generated in our lab by targeted deletion of the gene. I observed that Asap1$^{GT/GT}$ mice can live to maturity, although there is a reduction in the expected number of homozygous knockout offspring at birth. Deletion of *Asap1* results in growth retardation, respiratory distress and reduced angiogenesis in the surviving pups. This physiological phenotype in the absence of *Asap1* is transient, and adult Asap1$^{GT/GT}$ mice are morphologically undistinguishable from the wild-type mice.

I further studied breast tumor development and metastasis in Asap1$^{GT/GT}$ mice using autochthonous models of breast cancer. My results demonstrate that loss of *Asap1* in MMTV-PyMT mice leads to an earlier tumor onset, faster tumor growth and increased metastasis to the lungs. I also examined the effect of ASAP1 deficiency on the behaviour of breast cancer cells and fibroblasts taken from Asap1$^{+/+}$ and Asap1$^{GT/GT}$ mice. Taken together, my results show that *Asap1* is a critical regulator of cellular motility and its absence gives rise to developmental defects in newborn mice. Deficiency of ASAP1 also has tumor cell non-autonomous effects, and leads to

increased numbers of metastases in the MMTV-PyMT autochthonous mouse model of breast cancer.

Contents

1. Introduction

Cancer has been recognized to be a major health problem worldwide. Understanding the molecular basis of the complex mechanisms driving the process of cancer metastasis is crucial to build more potent therapeutic regimes to treat this disease. This study focuses on establishing and understanding the role of *Asap1,* a gene that has previously been correlated with metastasis of a wide variety of cancer types. The study describes the first reported attempt to understand the role of *Asap1* in normal physiology and in a specific pathophysiological context, namely breast tumor metastasis in a murine model.

1.1 *Asap1*: Discovery as a metastatic gene

A transcriptomic screen using suppression subtractive hybridization (SSH) was performed by our lab that led to generation of metastasis-associated gene expression profiles for two rat adenocarcinoma models, namely rat mammary and pancreatic adenocarcinomas (Nestl et al., 2001). Pairs of clonal rodent tumor cell lines – one metastasizing and the other non-metastasizing, were used from both the rat tumor models. Subtractive libraries were generated when the transcripts from the non-metastasizing tumor cell line were subtracted from those of the metastasizing cell line. Upon screening the two subtractive tumor libraries, 268 differentially expressed genes were identified. This approach led to several important outcomes, for example, it confirmed that the expression of previously known genes correlated with the metastatic phenotype, it associated already characterized genes that had not yet been linked with metastasis to the metastatic phenotype, and most importantly, it identified novel metastasis-exclusive genes.

Subsequent to this screening, our lab performed a secondary screening on the panel of 268 genes that were previously identified (Müller et al., 2010). In order to identify genes that may have a general function in tumor progression, the gene profile generated from metastatic mammary and pancreatic carcinoma was probed with cDNA derived from a

prostatic tumor progression model. By doing this, 68 genes were thus found to be upregulated in three different metastatic tumor models. They represented potential candidate genes that may be involved with tumor progression of many cancer types and *Asap1* was one of these genes. Importantly, expression of ASAP1 is able to increase metastasis formation in experimental animal models (Müller et al., 2010), demonstrating a functional role for the protein in metastatic dissemination. Furthermore, its expression in colorectal cancer samples correlated with poor patient prognosis (Müller et al., 2010).

1.1.1 Structure and function of ASAP1

ASAP1 stands for ***A***rf-GAP protein with ***S***H3 domains, ***a***nkyrin repeats and ***p***leckstrin homology domain. This reflects that fact that ASAP1 is a multi-domain protein that belongs to the Arf-GAP family. ADP-ribosylation factor (Arf) proteins are small GTPases that are involved in vesicle trafficking and modulating actin structures. The activity of Arf proteins is regulated by a class of proteins called Arf-GAPs, of which ASAP1 is a member. In addition, ASAP1 interacts with many different proteins through its various domains to bring about pleiotropic changes within the cell. The structure of ASAP1 and its splice variants is discussed here before the function of ASAP1 in various cellular processes and its association with many cancer types is described.

1.1.1.1 Structure of ASAP1

ASAP1 belongs to AZAP-family of Arf-GAPs that contains multiple domains, which dictate its subcellular localization and function. From the N-terminus, the sequence of its domains is a BAR (Bin–Amphiphysin–Rvs) domain, a PH (pleckstrin homology) domain, a zinc finger motif, a proline-rich region containing SH3 ligand motifs, eight repeats of the sequence (E/DLPPKP), and an SH3 domain at the C-terminus (Figure 1).

The zinc finger motif is embedded within an evolutionary conserved Arf-GAP sequence, and is required for GAP activity. Sequence similarities are observed between the zinc finger motif found in ASAP1 and other proteins similar to ASAP1 that have a PH domain

at the N-terminus of the zinc finger and ankyrin repeats C-terminal to it. Together, the PH-Zinc finger-Ankyrin domains constitute the PZA module that is the minimal subunit of ASAP1 required for its GAP activity. This sequence is evolutionarily conserved, being also found in plants, worms and flies. The PH domain of ASAP1 contributes to phosphoinositide-dependent activation of ArfGAP domain and hence to regulation of Arfs. However, PIP_2 binding to Arf is also important for the GAP activity of ASAP1, and hence phosphoinositide binds to both the enzyme, PZA, and the substrate, Arf, thus exhibiting dual roles in the regulation of Arf (Brown et al., 1998).

BAR domains were first studied in the context of the mammalian proteins Bin and amphiphysin, and yeast proteins Rvs167 and Rvs161 (Lombardi and Riezman, 2001; Wigge and McMahon, 1998; Zhang and Zelhof, 2002). The BAR domain dimerizes to form a crescent-shaped structure that induces or detects membrane curvature and binds to acid phospholipids and other proteins (Farsad et al., 2001; Peter et al., 2004). The BAR domain of ASAP1 has been shown to be involved in the formation of transport intermediates, by mediating physical changes of the membranes of endocytic organelles and is also responsible for ASAP1-dependent regulation of cell spreading and EGFR recycling (Nie et al., 2006).

ASAP1 also contains an SH3 binding domain through which it interacts with Src. This interaction likely affects the activity and localization of ASAP1 (Brown et al., 1998). ASAP1 contains a unique sequence repeat (E/DLPPKP) with proline rich regions that may facilitate homodimerization of ASAP1, as detected both *in vitro* and *in vivo* (Kam et al., 2000).

Three known alternatively spliced variants of ASAP1 exist, namely, ASAP1a, ASAP1b (human) and rASAP1c (rat) (Brown et al., 1998; Müller et al., 2010). The two variants described in humans differ in their proline rich regions, in that ASAP1b lacks one of the three proline rich regions present in ASAP1a. The third splice variant, described in rat, lacks one of the three proline rich regions, like ASAP1b, and also a short sequence contained between the BAR domain and PH domain, that encodes 15 amino acid

residues. All three spliced variants retain the ArfGAP activity (Brown et al., 1998; Müller et al., 2010).

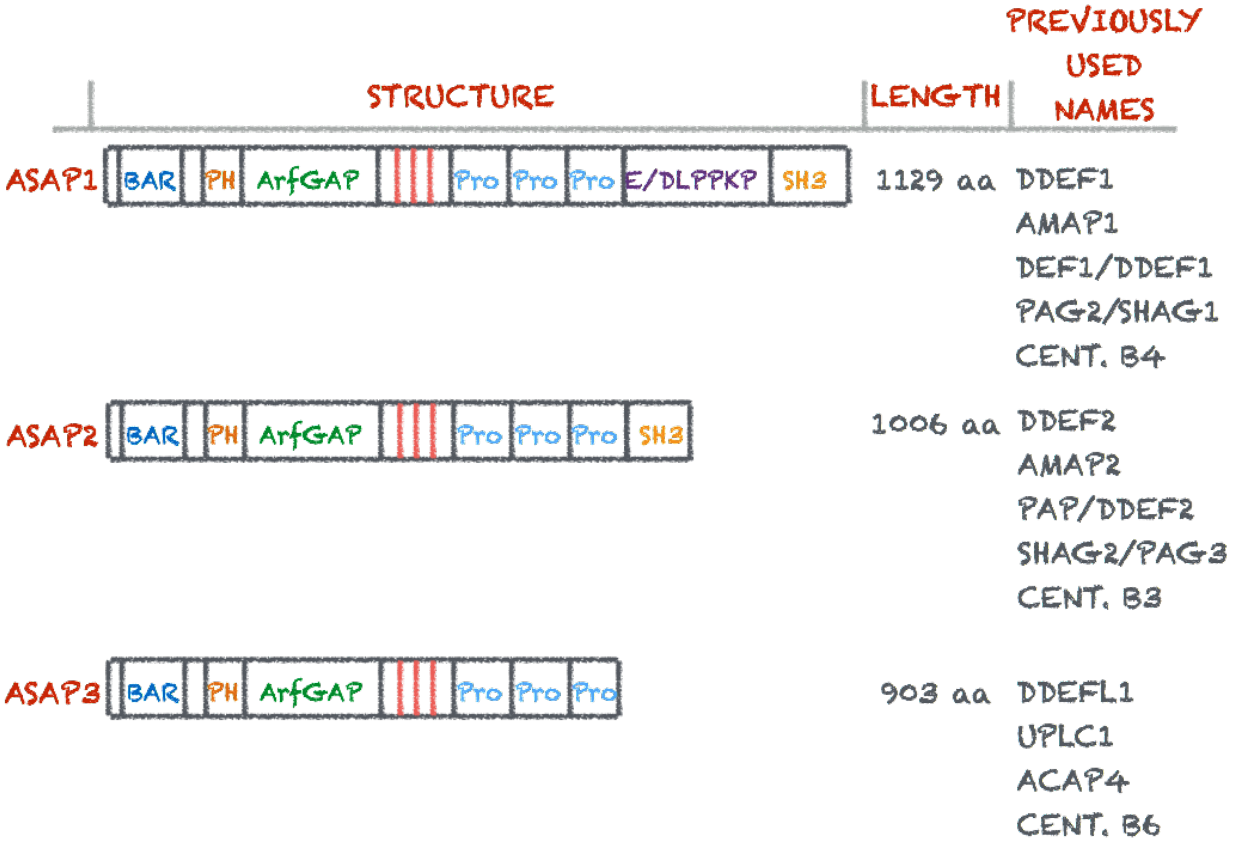

Figure 1. Members of ASAP family of proteins.
Schematic representation of structure, length and aliases of ASAP family members. Various domains like the BAR, PH, ArfGAP and proline-rich SH3 domains are shown for all the three members of ASAP family. Previously used nomenclature for each of the member is given.

ASAP1 is closely related to other members of the ASAP family (Figure 1). ASAP2 also has PIP_2-dependent GAP activity (Andreev et al., 1999) and acts as an adapter protein that recruits many endocytic proteins to site of Arf6 activation (Hashimoto et al., 2005). ASAP3 lacks the SH3 domain at the C-terminus, unlike ASAP1 and ASAP2. Like ASAP1, ASAP3 is associated with focal adhesions (FAs) and central dorsal ruffles (CDRs), but is not required for invadopodia formation (Ha et al., 2008). This shows independent functions for different ASAP family members despite a common localization.

1.1.1.2 Cellular functions of ASAP1

The most intensively studied function of ASAP1 is its role as an Arf-GAP. I will therefore describe the function of Arf-GAP proteins in general as well as the specific Arf-GAP functions of ASAP1, before considering other functions of ASAP1.

1.1.2 The Ras superfamily of small GTPases

Small GTPases are regulatory proteins that participate in cellular signaling by acting as 'molecular switches' that begin their function when guanine nucleotide exchange factors (GEFs) facilitate GTP binding on them and terminate their function when GTPase activating proteins (GAPs) dissociate the bound GTP by hydrolyzing it. Small GTPases are enzymes that bring about a wide range of cellular processes (Wennerberg et al., 2005). The Ras superfamily of small guanosine triphosphatases (GTPases) encompasses more than 150 proteins distributed across five major groups. These protein families are classified on the basis of their sequences and function. Due to lack of functional data, a definitive classification of these proteins has not been possible yet. The biochemical mechanism of action is common across these sub-families, and that is, all of these small GTPases act as binary molecular switches (Vetter and Wittinghofer, 2001). All of these proteins also share a highly conserved ~ 20 kDa of GTP/GDP-binding sequence, the G box located at their N-terminus. Small GTPases have high affinity for GDP/GTP binding, but they do not have the ability to hydrolyze GTP or exchange GDP for GTP. For this, they depend on other regulatory proteins called guanine nucleotide exchange factors (GEFs) and GTPase activating proteins (GAPs). Each of the classified group within the Ras superfamily uses distinct set of GEFs and GAPs. As outlined (Figure 2), the five groups of proteins that make up the Ras superfamily of GTPases are the Ras, Rho, Rab, Ran and Arf families.

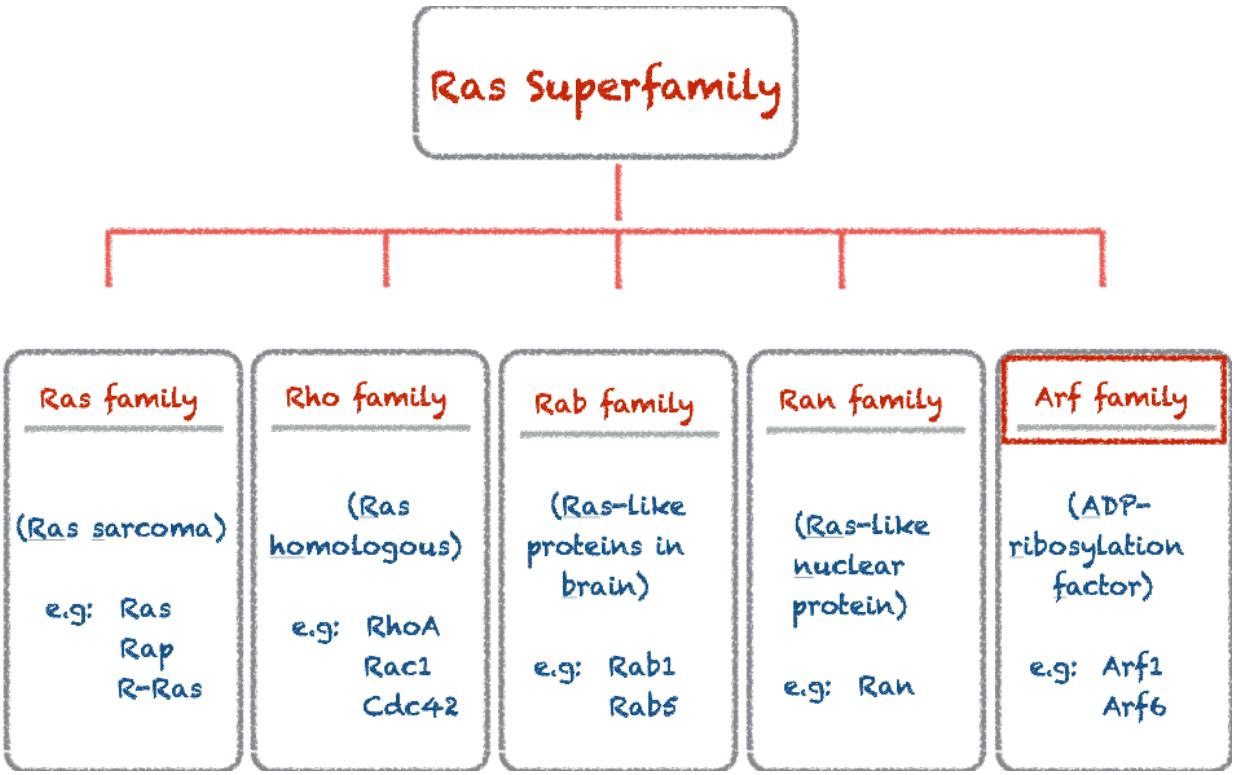

Figure 2. The Ras superfamily of GTPases.
The five major groups – Ras, Rho, Rab, Ran and Arf – that comprise the Ras superfamily of GTPases are shown schematically. Examples of members of each family is given. Arf family is highlighted, and is discussed in the following sections.

1.1.3 The Arf family of GTPases

The ADP-ribosylation factor family represents a class of myristoylated, low molecular weight, guanine nucleotide binding (G) proteins (D'Souza-Schorey and Chavrier, 2006). These proteins are important regulators of organelle structure and modulate actin structures. They also participate in vesicle trafficking by recruiting coat proteins that facilitate sorting of cargo into vesicles. There exist three classes into which the six mammalian Arf GTPases have been categorized. ARF1, ARF2 and ARF3 belong to Class I; ARF3 and ARF4 to Class II and ARF6 represents Class III. Apart from these, more than 20 ARF-like (ARFL) proteins exist that perform more pleiotropic roles than ARFs (Gillingham and Munro, 2007). As mentioned earlier, there are two classes of regulatory proteins that enable ARFs to function. These are ARF GEFs and ARF GAPs.

ARF GAPs regulate ARFs in a spatio-temporal manner, in that they undergo conformational changes upon GTP-binding. Arf-GAP proteins remain in close proximity to membranes owing to an amphipathic helix at their N-terminus that allow them to dock into the membrane, as well as through the lipid modification in which myristoyl groups are added either co- or post-translationally that help recruit Arf-GAPs to the membranes. Although ARF1 and ARF3 are released from the membrane upon GTP hydrolysis, ARF4 and ARF5 have been found to remain attached to ER-Golgi intermediate compartment (ERGIC) membrane in their GDP-bound conformation (Chun et al., 2008). ARF6 appears to be bound to membranes as well (Duijsings et al., 2009). The literature suggests that the nucleotide state of these membrane bound ARFs may dictate various cellular signaling pathways.

1.1.4 Arf-GTPase activating proteins: Arf-GAP domains

The Arf-GAP domain was first identified in rat as the domain responsible for induction of GTP hydrolysis on Arf1 (Cukierman et al., 1995). The Arf-GAP domains are highly conserved and exist in the earliest eukaryotes. In the yeast *Saccharomyces cerevisiae* at least five Arf-GAPs have been identified while the mammalian Arf-GAPs have been shown to range from small proteins to large multi-domain proteins functioning as scaffolds for cellular signaling. Over a period of about a decade, scientists have agreed upon the following nomenclature for human Arf-GAP domain containing proteins. The 31 human genes that encode proteins containing the Arf-GAP domain have been divided into 10 subfamilies (Figure 3). This classification is based on sequence similarities and the conservation of domain architecture within each subfamily (Kahn et al., 2008).

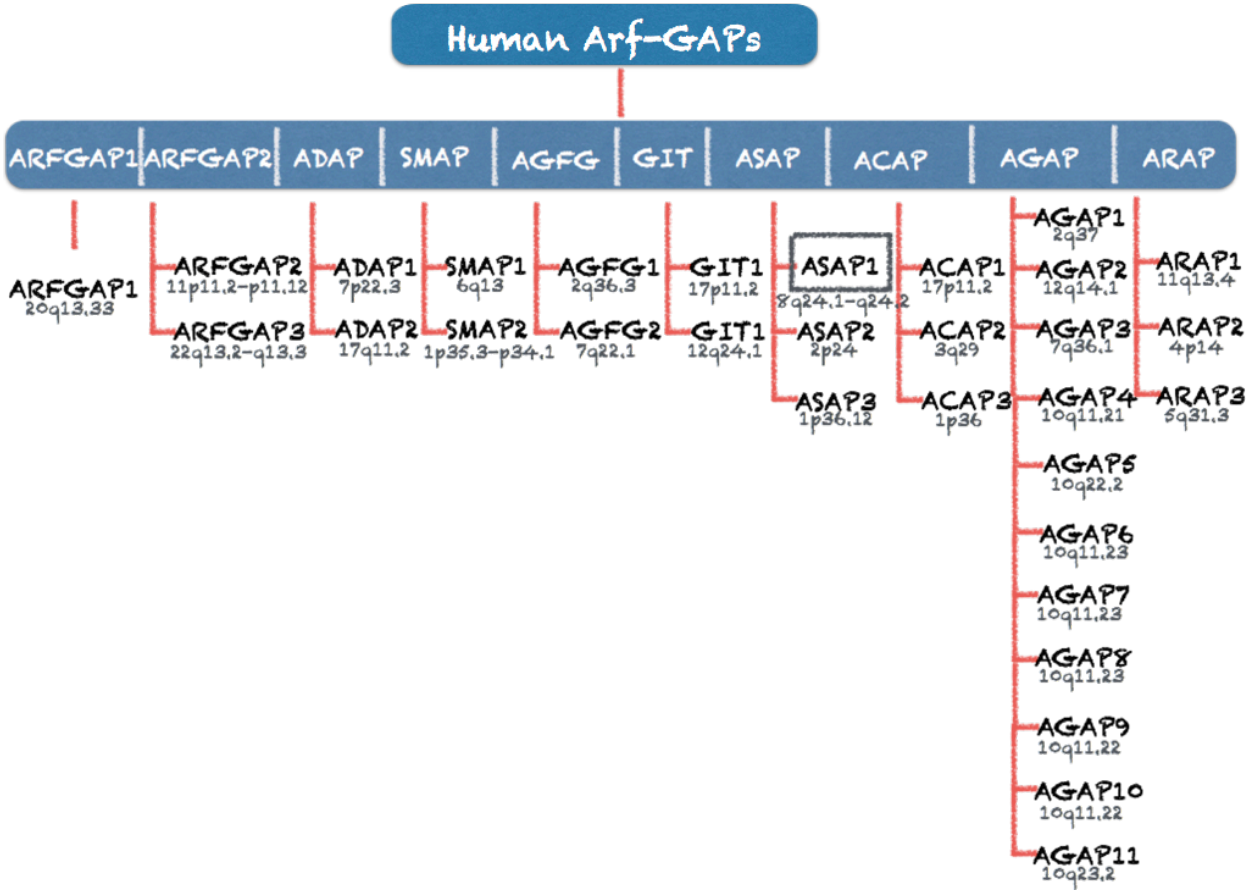

Figure 3. Human Arf-GAPs.
Schematic outline of the 31 genes in humans that encode Arf-GAPs, as classified into ten families. The chromosomal location of each gene is shown. ASAP1, belonging to the ASAP family, is highlighted.

1.1.5 Role of ASAP1 Arf-GAP domain in the regulation of cell motility

GAP activity of ASAP1 is stimulated specifically by the signaling lipid phosphatidylinositol 4,5- bisphospate (PIP_2) (Brown et al., 1998). PIP_2 binds to PH domain of ASAP1, which can serve to both recruit ASAP1 to a membrane surface and to induce an activating conformational change in the protein (Che et al., 2005). Ectopic ASAP1 enhances cell migration toward platelet-derived growth factor (PDGF) and Insulin-like growth factor-1 (IGF-1). This chemotactic effect appears to result from a

general increase in cell motility, as ASAP1-expressing cells also exhibit enhanced basal and chemokinetic motility. The increase in cell motility is dependent on GAP activity. Inhibition of cell spreading by ASAP1 is not GAP-dependent, indicating that spreading and motility are altered by ASAP1 through different pathways. A possible model for general enhancement of cell motility by ASAP1 could depend on the ability of ASAP1 to destabilize focal adhesions. Such a destabilization could lead to an increase in basal, chemokinetic and chemotactic migration rates. Focal adhesion disruption has been documented in transiently transfected ASAP1 NIH3T3 cells. The ability of ASAP1 to increase cell motility in a GAP-dependent manner suggests this effect is mediated by deactivation of the ASAP1 substrate Arf1. Interestingly, Arf1 and Arf6 appear to function antagonistically, with Arf1 activation being anti-migratory and Arf6 activation being pro-migratory (Furman et al., 2002). In contrast, overexpression of ASAP1 inhibits the formation of PDGF-induced membrane ruffles in a GAP dependent manner (Randazzo et al., 2000).

1.1.5.1 Other functions of ASAP1 domains

ASAP1 serves as an important regulator of a wide variety of physiological events occurring within a cell (Figure 4). ASAP1 binds to proteins that function as part of the endocytic machinery, such as CIN85, POB1 and amphiphysin IIm (Hashimoto et al., 2004; Kowanetz et al., 2004). CD2AP, a protein highly related to CIN85, binds to ASAP1 and recruits it to the plasma membrane (Liu et al., 2005). The SH3 domain of ASAP1 mediates binding to POB1, and POB1 simultaneously binds to the Ral binding protein, RalBP. Together, the ASAP1-POB1-RalBP complex regulates actin remodeling by controlling RhoGTP levels, thereby coordinating changes in the actin cytoskeleton with membrane trafficking. This is also important for maintenance of invadopodia (Ikeda et al., 2001; Oshiro et al., 2002).

ASAP1 binds to several protein kinases, including c-Src, focal adhesion kinase (FAK), and the FAK homologue Pyk2 (Brown et al., 1998; Liu et al., 2002). Src phosphorylates ASAP1 and this is required for the formation of invadopodia and podosomes. These are

actin rich adhesion structures on the ventral surface of cells that mediate adhesion, extra-cellular matrix (ECM) degradation and tumor invasion. Src and Pyk2 directly phosphorylate ASAP1 and this inhibits GAP activity for Arf1 (Kruljac-Letunic et al., 2003).

Crk and CrkL are adapter proteins that bind to ASAP1 (Oda et al., 2003). CrkL binds to paxillin and ASAP1 binding to Crk and CrkL is necessary for the association of ASAP1 with focal adhesions.

Cortactin is a multi-domain protein that is found in peripheral membrane ruffles and invadopodia. ASAP1 and cortactin associate with invadopodia in invasive breast cancer cell lines (Onodera et al., 2005). ASAP1 and cortactin have been proposed to be a part of the invasive machinery in cancer cells. This complex links the highly tubulated membranes found in invadopodia and podosomes to polymerized and branched actin (Randazzo et al., 2007). ASAP1 may function as a regulated signaling platform to control the dynamics of invadopodia and podosomes. These structures are labyrinths of tubulated membranes associated with polymerized actin (Buccione et al., 2004). The BAR, PH and Arf-GAP domains of ASAP1 bind to Arf-GTP to induce membrane tubulation, hence ASAP1 could be considered as an Arf effector (Nie et al., 2006). ASAP1 must be phosphorylated by Src to function at podosomes. Therefore, ASAP1 integrates three signals – those from Arf-GTP, PIP2 and Src.

ASAP1 associates with CDRs (Randazzo et al., 2000). CDRs are induced by growth factors like platelet-derived growth factor (PDGF). These structures are rings of dynamic remodeling, polymerized actin at the dorsal surface of cells associated with plasma membranes undergoing extensive endocytosis. The BAR domain of ASAP1 contributes to the formation of tubules from synthetic large unilamellar vesicles *in vitro* and Arf contributes to this ASAP1-mediated tubulation. Therefore, the membrane curvature-inducing function of ASAP1 is coupled with Arf signaling (Nie et al., 2006).

The Rab11-family interacting protein 3 (FIP3) was found to stimulate the GAP activity of ASAP1. It was found to directly interact with the BAR domain of ASAP1. ASAP1 participates in transferrin trafficking through a Rab11-dependent pathway (Inoue et al., 2008). Ablation of ASAP1 abolishes ciliary targeting and causes formation of actin rich, periciliary membrane projections that accumulate mislocalized rhodopsin. ASAP1 serves as a scaffold that brings together the proteins necessary for transport of the cilia including GTP binding protein Arf4 and the G protein of Rab family Rab11 and Rab8, linked by the Rab 8 exchange factor, Rabin 8 (Wang et al., 2012).

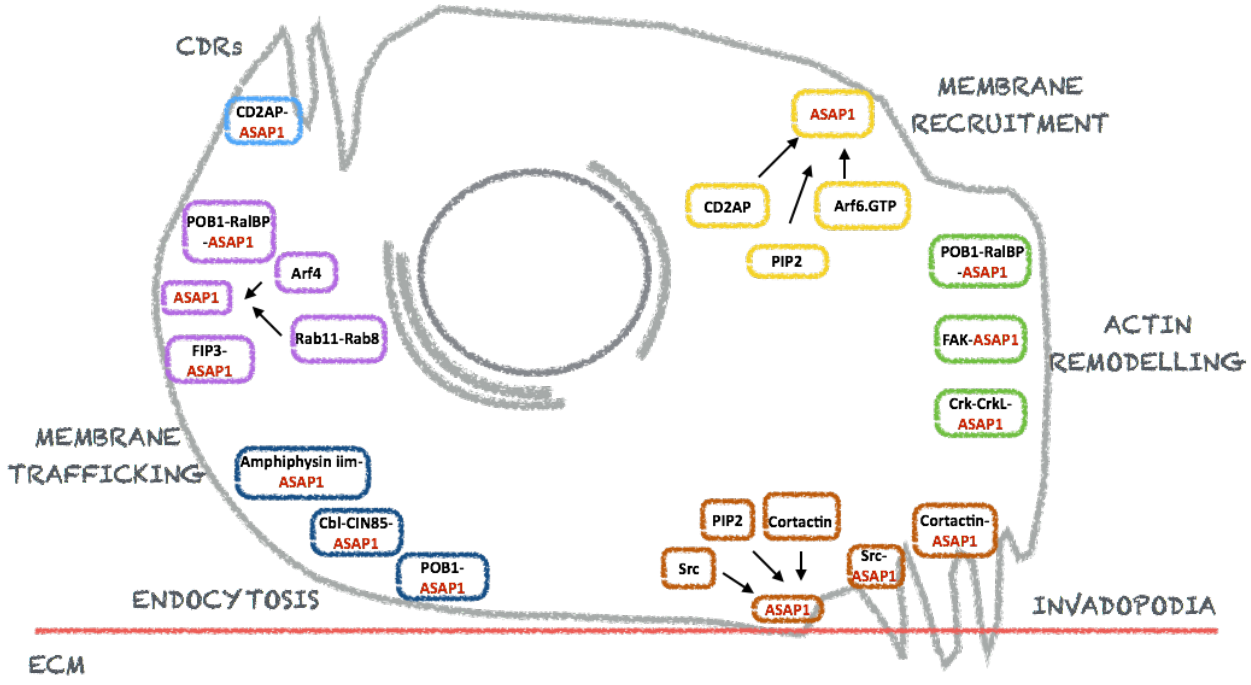

Figure 4. Pleiotropic functions of ASAP1 in the cell.
ASAP1 is involved in regulating a wide variety of cellular processes. ASAP1 is able to bind to many different proteins to form complexes and thus bring about cellular functions. Shown here are its interaction partners that are implicated in membrane recruitment (in yellow boxes); ASAP1 may influence cytoskeletal remodeling (green boxes); it is a known functional component of invadopodia (orange boxes); ASAP1 binds proteins that are part of endocytic machinery (blue boxes); ASAP1 regulates membrane trafficking (purple boxes) and ASAP1 associates with CDRs (light blue box).

ASAP1 overexpression inhibits cell spreading and alters paxillin localization to focal adhesions (Liu et al., 2002). Mislocalization or reduced expression of ASAP1 inhibits cell spreading and migration by influencing Arf1-GTPase cycling. CD2AP stably associates with ASAP1. Mislocalization of ASAP1 to mitochondria with a CD2AP mito fusion protein inhibits fibronectin-mediated cell spreading and migration. siRNA mediated ASAP1 reduction retards cell spreading and inhibits cell migration. Mislocalization or siRNA mediated reduction of ASAP1 causes an increase in intracellular Arf1-GTP and loss of paxillin from cell adhesions. Given previous findings, it was concluded that ASAP1 contributes the process of adhesion assembly by regulating dynamic GTP/GDP cycling of Arf1-GTPase (Liu et al., 2005). CD2AP localizes to membrane ruffles and therefore the interaction of CD2AP with ASAP1 provides a possible mechanism by which ASAP1 localization on the plasma membrane is further refined upon growth factor receptor engagement. Abrogation of ASAP1 function with different approaches caused similar phenotypes to those observed with ASAP1 overexpression, suggesting an important role for the dynamic cycling of Arf1-GTPase in adhesion assembly rather than its active GTP-bound form. Depletion of ASAP1 leads to inhibition of common pathways that partially compensate for the motility defects induced by the loss of ASAP1 function. It is possible that other compensatory Arf-GAPs are exploited by growth factors under ASAP1 depleted conditions (Liu et al., 2005).

The importance of the SH3 domain of ASAP1 in promoting metastasis has been highlighted by mutational analysis in our lab that suggests that binding to SH3 domain-containing proteins, such as SLK (Ste-20-like kinase), is essential for ASAP1 to promote metastasis. SLK was shown to co-immunoprecipitate with ASAP1b and ASAP1c and thus interactions through SH3 domain of ASAP1 may be functionally involved in regulating metastasis (Müller et al., 2010).

Previous work from our group has implicated ASAP1 in the process of metastasis (Nestl et al., 2001; Müller et al., 2010), and ASAP1 expression has been associated with a wide variety of cancer types. My thesis work the involvement of ASAP1 in cancer, and

specifically breast cancer metastasis. In the next section I therefore present the basics of breast cancer and current models and evolving paradigms in the field of metastasis.

1.2 Breast cancer: our knowledge from the bed and the bench

Breast cancer comprises a group of heterogeneous diseases that develops as a local lesion but has the potential to metastasize to various sites in the body (Weigelt et al., 2005). It is the most common malignant disease affecting women worldwide, and it is estimated that over 508,000 women died of this disease in 2011 (Global health estimates, WHO, 2013). In 2012, the estimated annual incidence of breast cancer in 40 European countries was found to be 94.2/100,000 and the mortality to be 23.1/100,000 (Ferlay et al., 2013). In most of the Western countries the mortality rate has decreased, owing to better treatment outcomes and earlier detection. In European women, however, breast cancer remains the leading cause of cancer-related deaths (Allemani et al., 2015; Autier et al., 2010).

1.2.1 Clinical features of breast cancer

The diagnosis of breast cancer is made on the basis of imaging and clinical assessment that includes bilateral mammography and ultrasound of the breast and regional lymph nodes and palpation of the breast and locoregional lymph nodes. Apart from rendering prognostic value, pathological assessment of the primary tumor also leads to pre-treatment disease evaluation. Physical attributes like tumor size, histological examination of the tumor and lymph node involvement contribute to the tumor-node-metastasis (TNM) staging system of breast cancer. This system addresses the histological type, grade and immunohistochemical (IHC) evaluation of hormone receptor status (estrogen receptor (ER), progesterone receptor (PR) and human epidermal growth factor 2 receptor (HER2)). Based on tumor histology (*Table 1.1)*, breast tumors are stratified into several subtypes (Senkus et al., 2015).

Breast cancer represents a heterogeneous group of malignancies originating from the ductal epithelium. The mammary epithelium is bilayered, with a central luminal epithelial cell layer surrounded by an outer myoepithelial cell layer and basement membrane (Nelson and Bissell, 2006). Using traditional histological approaches, three subtypes of breast tumors with different biological behavior have been identified - luminal and basal breast tumors that resemble the luminal and basal breast epithelium, and the HER2-positive breast tumors that overexpress HER2 but lack ER and PR (Kittaneh and Glück, 2011). However, patients with breast cancer of the same stage can differ significantly in their disease outcomes and therapy responses because the strictly clinical predictors may fail to accurately classify the breast tumors. To address this, considerable research has been performed in recent years to better stratify breast cancer patients into more meaningful breast cancer subtypes (Kittaneh et al., 2013; van ’t Veer et al., 2002).

1.2.2 Gene profiling of breast tumors

As a novel approach to predicting prognosis in breast cancer patients, the expression pattern of a panel of specific tumor-related genes has been studied. The specific gene expression patterns have the ability to identify tumors with more aggressive biology and thus can help with precise and more accurate quantification of prediction of recurrence as compared to traditional clinical methods (Kittaneh et al., 2013). The genetic paradigm has led to two important outcomes – it has been possible to identify new intrinsic subtypes of breast cancer, and predictive genomic signatures have been established for breast cancer.

1.2.2.1 Identification of new intrinsic breast cancer subtypes

An integrated approach to profile breast cancers into different subtypes utilizing information from both the clinical features and gene expression signatures has enabled identification of at least 7 different biologic subtypes of breast cancer (Kittaneh and Glück, 2011; Sørlie et al., 2001, Table 1).

Luminal-like breast cancer

This subtype has a gene expression profile similar to the normal luminal breast epithelium. Luminal A breast tumors comprise about 40% of all breast cancers and correlate with a favorable prognosis. This subtype has been shown to overexpress ER-regulated genes and under expression of the HER2 gene cluster (Hu et al., 2006; Kennecke et al., 2010). Luminal B breast tumors represent about 20% of breast cancers and are associated with a higher risk of relapse and poor prognosis. These tumors have lower ER-related genes and varying expression of the HER2 gene cluster (Voduc et al., 2010). A third subtype, namely Luminal C has been found with high expression of a set of genes with presently no known functions (Sørlie et al., 2001).

HER2 enriched breast cancer

Comprising about 20-30% of all breast cancers, this subtype is characterized by high expression of the HER2 cluster of genes and low expression of the luminal cluster genes that include cytokeratins (CKs) CK7, CK8, CK18 and CK19. This breast cancer subtype has poorer prognosis as compared to Luminal A breast cancer (Sørlie et al., 2003).

Basal-like breast cancer

This breast cancer subtype derives its name from the shared gene expression pattern with normal basal epithelial cells and represents about 15% of the invasive ductal breast cancers. Owing to a low expression of luminal and HER2 gene clusters, this breast cancer subtype is often considered 'triple negative'. However the term is not synonymous with basal-like breast cancer (Kennecke et al., 2010).

Claudin-low breast cancer

This subtype is characterized by low expression of luminal differentiation markers and high expression of genes involved in cell migration, differentiation, angiogenesis and immune-related genes. Histologically, this breast cancer subtype is negative for hormone receptor and HER2 expression and often part of the basal intrinsic subtype (Prat et al., 2010).

Normal breast-like breast cancer

Genes expressed in this subtype of breast cancer are similar to those expressed by adipose tissue and other nonepithelial cell types. These tumors exhibit low expression of luminal epithelial genes and a high expression of basal epithelial genes (Sørlie et al., 2001).

Breast Cancer Subtype		Clinicopathologic Surrogate		
		ER	PR	HER2
Luminal A	'Luminal A-like'	+	high	-
Luminal B				
	'Luminal B-like HER2-negative'	+	low	-
	'Luminal B-like HER2-positive'	+	high/low	+
Luminal C*				
HER2 overexpression	'HER2-positive (non-luminal)'	-	-	+
Basal-like	'Triple-negative (ductal)'	-	-	-
Claudin-low*		-	-	-
Normal breast-like*				

Table 1. Breast cancer subtypes and their clinicopathologic surrogate markers.
*Recently identified breast cancer subtypes.

1.2.3 The role of the microenvironment in breast cancer progression

Tumor growth does not just rely on the growth of malignant cells, but also on the various stromal cells found in the surrounding environment of the primary tumor. It has been well established that a tumor cell begins its growth as a neoplastic lesion, most often in epithelial cells, and is contained within a defined boundary of basement membrane (BM). The cells adjacent to this growing lesion, namely the immune cells, blood vessels and fibroblasts, together with the extracellular matrix (ECM) and BM that surround the

lesion, constitute the stroma (Hanahan and Weinberg, 2000; Rønnov-Jessen et al., 1996). In the case of the breast, the epithelium is embedded within the mammary stroma that accounts for 80% of the breast volume and is formed by adipose tissue, interstitial connective tissue and blood vessels (Nelson and Bissell, 2006).

Tumor cells from the primary tumor detach and enter the vasculature as circulating tumor cells (CTCs) that can be transported to distant secondary sites as disseminated tumor cells (DTCs) that may then form metastatic tumors (Sleeman et al., 2011). Distinct microenvironments function at each step of this process and thus regulate disease progression.

1.2.3.1 Stromal regulation of the primary tumor

A neoplastic lesion embedded within the epithelium, and contained by a defined BM, is termed carcinoma *in situ* (CIS). The surrounding stroma of CIS is called 'reactive stroma'. Studies indicate a bidirectional influence of CIS and the reactive stroma on each other, mediated through the BM barrier (Rønnov-Jessen et al., 1996). Whereas a normal stroma contains a certain number of fibroblasts, the reactive stroma maintains a higher number of fibroblasts, increased capillary density and type-I collagen. Experiments on cancer-prone chickens show that the reactive stroma promotes tumorigenesis through oncogenic signals (Sieweke et al., 1990).

The stromal components that have been implicated in promoting primary tumor growth include endothelial cells that are a part of the lymphatic and blood circulatory system, pericytes, fibroblasts and many bone marrow-derived cells (BMDCs) such as macrophages, neutrophils, mast cells, myeloid cell-derived suppressor cells (MDSCs) and mesenchymal stem cells (MSCs) (Sleeman and Cremers, 2007).

Fibroblasts form a very prominent part of the tumor-stromal compartment. Normal mammalian fibroblasts are a heterogeneous cell population that are widely distributed and identified by their characteristic elongated, spindle-shaped morphology (Tarin and

Croft, 1969). The physiological roles of fibroblasts include regulation of ECM by contributing to ECM deposition and also secretion of matrix-degrading enzymes like matrix metalloproteinases (MMPs) (Simian et al., 2001; Tomasek et al., 2002). During wound repair, fibroblasts invade the lesion and generate ECM that acts as a scaffold for various cell types, thereby mediating scar formation and tissue fibrosis. Fibroblasts possess cytoskeletal elements that promote contractions of the healing wound. It has been observed that fibroblasts isolated from a fibrotic tissue or a tissue undergoing wound healing, are 'activated' and proliferate and secrete higher levels of ECM constituents than those fibroblasts isolated from healthy organs. Once the process of wound healing is completed, the number of such 'activated' fibroblasts decreases, thus restoring the resting cell phenotype (Tomasek et al., 2002). Tumors have previously been described as wounds that do not heal, and hence cells that have roles in injury-response, such as fibroblasts are important and are involved with cancer initiation and progression (Dvorak, 1986; Kalluri and Zeisberg, 2006). 'Activated' fibroblasts within the tumor stroma are called cancer associated fibroblasts (CAFs). In breast cancer, 80% of stromal fibroblasts acquire the activated phenotype (Sappino et al., 1988, Figure 5).

Tumor stroma forms most of the tumor mass, and the growth of the stroma is supported by the tumor cells in that tumor cells secrete pro-fibrotic growth factors that promote growth and activation of stromal fibroblasts (Elenbaas et al., 2001). Overexpression of transforming growth factor ß (TGFß) in pancreatic cancer corresponds to a fibrotic response, although it is unclear whether the fibrotic response is a wound-healing mechanism by CAFs to repair the lesion or TGFß stimulates the accumulation of CAFs (Lohr can res 2001). PDGF is secreted by tumor cells, and although tumor cells do not express PDGF receptors, it has been shown that this growth factor exerts its effects via paracrine signaling that involves fibroblasts and endothelial cells (Forsberg et al., 1993). Another growth factor, basic fibroblast growth factor 2 (bFGF2) has been demonstrated to induce proliferation in 3T3 fibroblasts, involvement in tissue fibrosis and induction of angiogenesis (Folkman et al., 1988; Strutz et al., 2000).

To support growth and development of the tumor at early stages, an important step is the induction of angiogenesis (Folkman, 1971). While tumor cells are able to secrete VEGF, it is the stromal components – specifically, fibroblasts and inflammatory cells, that provide the bulk of VEGF required for tumor angiogenesis (Fukumura et al., 1998).

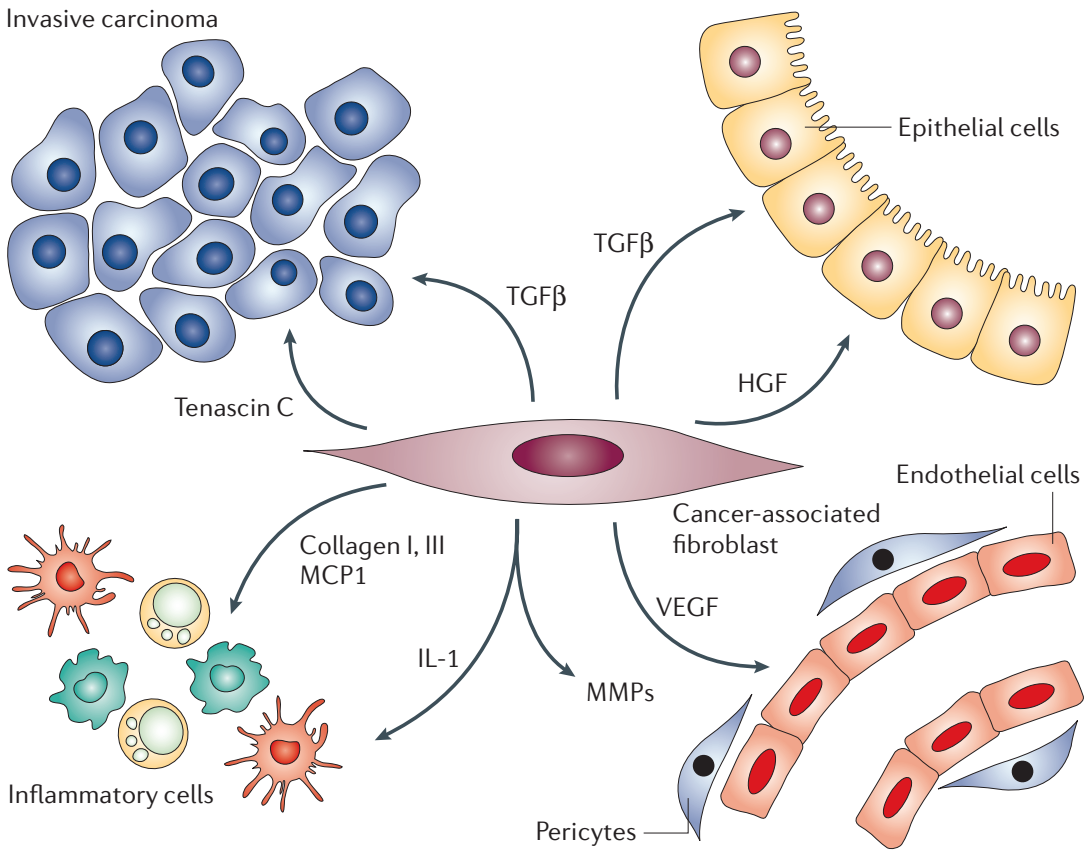

Figure 5. Interactions of activated fibroblasts in tumor stroma.
Various communications of activated fibroblasts with cancer cells, stromal epithelial cells, endothelial cells and pericytes, facilitated by growth factors and chemokines (Zeisberg and Kalluri, 2006).

Progression of cancer to metastasis is a systemic disease process. Cells from the primary tumor invade the local tissue. In the process of intravasation, they enter capillaries, from where they are taken to distant sites. The circulating tumor cells (CTCs) exit the circulatory system in a process known as extravasation and enter the secondary sites. At each of these steps of the invasion-metastasis cascade, key events like

changes in cell adhesive properties and acquisition of motile phenotypes by the tumor cells, occur (Sleeman, 2000). Cellular motility is central to the spread of cancer cells as it helps in local invasion of connective tissues, lymphatic system and the vasculature (Wang et al., 2005).

1.2.3.2 Local invasion and intravasation: cellular structures enabling motility

Cellular motility is of paramount importance in physiological events such as development and immune responses, as well as in many pathological events, like cancer metastasis and cardiovascular diseases (Parsons et al., 2010). The movement for most cells begins when the cell membrane protrudes to form adhesion structures that connect the actin filaments at the leading edge of the cell to the substratum, and the cell moves forward along the actin while the rear end of the cell disengages adhesions (Parsons et al., 2010; Sheetz, 1999). Cells of a tumor detach by remodeling their actin cytoskeleton, they are able to invade ECM and migrate into the bloodstream to be transported to secondary sites following extravasation (Talmadge and Fidler, 2010). Cellular motility is a key process that facilitates these steps of the invasion-metastasis cascade. Distinct, organized adhesive structures mediate interactions between cellular cytoskeleton and ECM.

The cell membrane of a migratory cell is capable of undergoing extensive reshaping to fulfill specific physiological requirements (Buccione et al., 2004). Morphologically and functionally distinct structures are formed by invagination or protrusion of cell membranes. These structures are called lamellipodia, filopodia and the phagocytic cup. The formation of these cellular processes is dependent upon the assembly of filamentous- (F)-actin and its associated proteins. In order to form these surface-specialized structures, a certain network of proteins is needed, and often includes F-actin, Arp2/3 complex, N-WASP (neural-Wiskott Aldrich syndrome protein), along with Rho family of GTPases (Linder and Aepfelbacher, 2003). Based on this protein network that constitutes the actin-based machinery, a cell may distort membranes transiently

and form different membrane structures like podosomes, invadopodia and circular dorsal ruffles (Buccione et al., 2004).

Podosomes are found on the ventral side of cells like osteoclasts, macrophages and endothelial cells and are utilized to degrade ECM. Podosomes in osteoclasts arrange themselves in such a way to form a rosette, that is a compartment in which bone cells can be efficiently degraded (Gimona et al., 2003). The podosomes of lymphocytes bear pores through endothelial cells (Carman et al., 2007). Highly motile cancer cells have been shown to possess sites of rapid actin polymerization and matrix degradation. These sites are podosome-like actin-rich structures, and are called invadopodia (Weaver, 2006).

When the leading edge of a migratory cell connects with the substratum, many integrin containing adhesion structures are formed inside the cell. These adhesion structures unite to form focal adhesions (FAs) which are the sites of actin cytoskeleton attachment within the cell (Geiger et al., 2009). FAs are one of the most well characterized adhesive structures that are made up of transmembrane integrin receptors and they are responsible for cell traction and reorganization of ECM (Albiges-Rizo et al., 2009). Invadopodia and podosomes both have a central actin-based machinery that is surrounded by multimeric protein complex of integrins and its associated proteins like talin, vinculin and paxillin (Desai et al., 2008; Mueller et al., 1992). In the case of FAs, the relationship between the actin-based machinery and associated proteins in not well understood. It is known that vinculin transiently associates with the Arp2/3 complex when cells attach to fibronectin (DeMali et al., 2002). Focal adhesion kinase (FAK) may influence actin stress fiber formation. FAK has been shown to interact with Arp2/3 complex and WASP, and it is postulated that FAK and Arp2/3 may interact during early cell spreading (Serrels et al., 2007).

Through the processes of cell migration and invasion, tumor cells enter the lymphatic or blood vasculature, and are taken to distant organs where they may form metastasis (Chambers et al., 2002). Cancer cells produce proteases that are required to physically

invade into the vasculature by the process of proteolytic degradation. The tumor stroma provides the principal source of proteases such as matrix metalloproteinases (MMPs), cysteine cathepsins and serine proteases (Joyce and Pollard, 2009). Activated fibroblasts secrete MMPs that enable tumor cells to invade local tissues and also detach from the primary tumor (Kalluri and Zeisberg, 2006). MMP3, produced by fibroblasts, has been shown to directly affect cancer cell motility and invasiveness (Lochter et al., 1997). The mechanisms by which proteases lead to invasion and intravasation include cleaving cell-adhesion molecules like E-cadherin, that leads to disruption of cell-cell junctions (Masterson and O'Dea, 2007). Once the cellular junctions are disabled, cancer cells are able to migrate into the surrounding tissues and vasculature. Tumor associated macrophages (TAMs) play a critical role in tumor progression by driving cell invasive phenotypes at the leading edge of the tumor (Condeelis and Pollard, 2006). Aside from their roles in facilitating invasive phenotypes, TAMs secrete proteases such as cysteine cathepsins that work towards promoting tumor progression (Shree et al., 2011).

In order to invade local tissues, tumor cells utilize the same basic strategies that are used by non-neoplastic cells during physiological processes like embryonic morphogenesis and wound healing. Additionally, tumor cells are able to use different modes of motility to infiltrate neighboring tissue matrices. They either move as single cells to bring about 'individual cell migration', or they disseminate in solid cell sheets or clusters, known as 'collective migration' (Friedl and Wolf, 2003).

1.2.3.3 Survival of CTCs in circulation and extravasation

From the millions of cancer cells shed into circulation, only about 0.01% survive to produce metastases (Fidler, 1970). Shear forces in the circulation that lead to mechanical destruction of these CTCs or immune surveillance by natural killer (NK) cells contribute to making the blood a difficult environment for the cancer cells to survive (Joyce and Pollard, 2009). Cancer cells can express the receptors for coagulation, namely VIIa and X, leading to platelet aggregation that acts as a shield for the cancer cells and protects them from shear forces and also NK cell-mediated lysis (Palumbo et

al., 2007). Intravital video microscopy has allowed the extravasation of CTCs into different organs like lung, liver and brain to be studied (Condeelis and Segall, 2003). It has been shown by real-time imaging that extravasation through endothelial capillaries involves active transmigration through holes in the vascular wall (Kienast et al., 2010). Studies on metastatic and non-metastatic cells show that CTCs that will not produce metastases may still retain the ability to extravasate (Schlüter et al., 2006; Kienast et al., 2010).

1.2.3.4 The metastatic tumor microenvironment

It has been widely accepted that the interactions between the tumor cells and its microenvironment largely regulate formation of metastases. Way back in 1889, Stephen Paget, an English surgeon put forth a landmark concept of 'seed and soil' to explain the process of metastasis, when he wrote "*When a plant goes to seed, its seeds are carried in all directions. But they can only live and grow if they fall on congenial soil.*" He argued that cancer cells (seeds) could grow to form secondary tumors only in certain organs (soil) that were somehow predisposed (Paget, 1889). More recent studies point out the ability of the primary tumor to secrete certain factors that home the tumor cells to particular organs. MDA-MB-231 xenograft tumors on one side of the mouse, were shown to secrete osteopontin and hence mobilize bone marrow precursors to home to secondary sites where a less malignant cell line could grow (McAllister et al., 2008). In organ-specific dissemination, chemokines and their receptors have been implicated. Tumor cells express cognate receptors on their surface and through these, detect chemokines expressed in specific organs and respond with increase in chemotaxis and invasiveness (Müller et al., 2001). Breast cancer cells express CXCR4 and CCR7, and lung, liver and bone marrow exhibit peak levels of expression of their cognate ligands, SDF-1/CXCL12 and CCL12. These organs – lung, liver and bone marrow - represent important sites of breast cancer metastasis. Signaling through the chemokine receptors CXCR4 and CCR7 results in actin polymerization and pseudopodia formation and induces chemotactic and invasive responses in breast cancer cells (Müller et al., 2001).

In line with Paget's hypothesis of metastasis, and in fact, furthering the idea is the concept of metastatic niche and the stromal progression model of metastasis (Psaila and Lyden, 2009; Sleeman et al., 2012). These concepts highlight the role of microenvironmental conditions local to the cancer cells, that potentially affect the growth and survival of these DTCs. Formation of a metastatic niche can be dictated remotely by factors produced by the primary tumor, before the DTCs arrive at secondary sites (called the pre-metastatic niche), and also by modification of the microenvironment endogenous to the organ where metastasis would develop (Sleeman, 2012). VEGFR1+ bone marrow-derived hematopoietic progenitor cells home to tumor-specific pre-metastatic sites where they form cellular clusters before the arrival of DTCs (Kaplan et al., 2005). Tumors produce VEGF-A, TGF-ß and TNF-α, which leads to secretion of chemoattractants like S100A8 and S100A9 at the sites of future metastasis. These chemoattractants stimulate expression of SAA3 that induces recruitment of CD11b+ myeloid cells to these sites (Hiratsuka et al., 2006). Remodeling of ECM and vasculature, recruitment of BMDCs, hypoxia, the presence of non-neoplastic cells such as endothelial cells and fibroblasts, all constitute the functional elements of the metastatic niche (Sleeman, 2012; Sleeman and Cremers, 2007).

Upon extravasation, not all the DTCs are capable of forming metastases. Some either die or remain dormant. In some cases, cancer cells have been reported to be dormant for years, and the seeding of these cells may have occurred several years before the diagnosis of the primary tumor (Aguirre-Ghiso, 2007). In other cases, dormant cells maintain a balance of proliferation and apoptosis, and in the absence of an appropriate blood supply, form micrometastasis that do not further develop into overt metastasis. This phenomenon has been termed 'angiogenic dormancy' (Holmgren et al., 1995).

The metastatic niche plays a deciding role in whether the DTCs survive, become dormant or develop into metastases. The functional components of the niche, along with the cues from the primary tumor, have a crucial role in determining the fate of DTCs (Sleeman, 2012). An integrative model, the stromal progression model, has been proposed to explain the process of metastasis (Sleeman et al., 2012). According to this

model, tumor intrinsic properties, for example, genetic aberrations in the primary tumor, driven by an increased genomic instability and epigenetic changes, are not the only factors that decide whether the tumor will progress into fulminant metastases. Stromal progression, marked by modification of ECM, recruitment of BMDCs and non-transformed cells like fibroblasts, induction of angiogenesis, occurs in parallel. As the tumor cells are exposed to new microenvironments at each step of the metastasis cascade, the tumor-stroma undergoes further changes, and this mutual and interdependent cross-regulation between the tumor and the stromal components drives tumor progression as a whole (Sleeman et al., 2012).

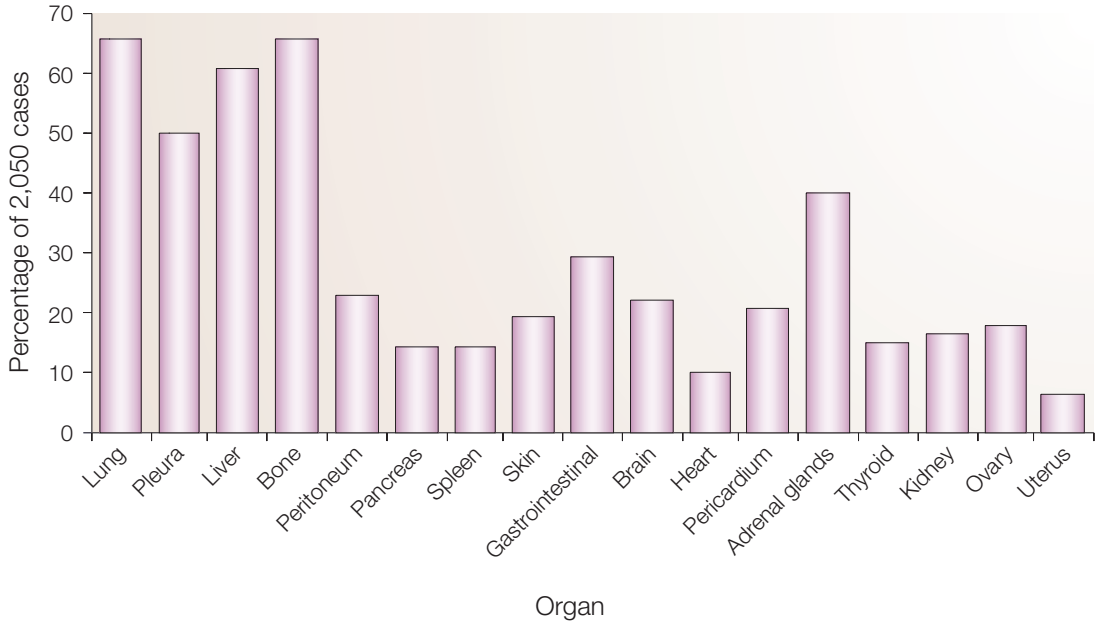

Figure 6. Most common sites of breast cancer metastasis.
Graphical representation of the most common sites of breast cancer metastasis. These include lung, liver and bone. (Weigelt et al., 2005).

Upon dissemination, breast carcinoma cells form metastases in various organs (Figure 6*)*, with lung, bone and liver being the common sites for metastasis. About 10-15% of the breast cancer patients develop an aggressive disease and show metastases within 3 years of initial diagnosis of the primary tumor. There are also cases where patients manifest metastases 10 years or more after the initial detection (Weigelt et al., 2005).

Breast cancer patients are therefore at a lifetime risk of developing metastasis. In-depth studies on genes that promote breast tumor progression is therefore required to fully understand the heterogeneous nature of the disease.

1.3 *Asap1* and cancer: rationale of the study

Subsequent to its identification in a metastasis-associated gene expression profile, our lab showed that as compared to the surrounding non-neoplastic tissue, ASAP1 expression was upregulated in a wide variety of human tumor types including carcinomas of the stomach, gall bladder, colon, breast, ovary, and esophageal and head and neck squamous cell carcinoma (HNSCC) (Müller et al., 2010). Its expression correlated with poor metastasis-free survival and poor overall survival in human colorectal cancer patients, and it was found to promote cell adhesion, motility and invasion and *in vivo* metastasis formation in a syngeneic rat pancreatic cancer model (Müller et al., 2010). Other groups have also reported association of high levels of ASAP1 with tumor progression and metastasis. For example, increased levels of ASAP1 corresponds to poor prognosis and survival after surgery of HNSCC patients (Sato et al., 2014), poor prognosis in epithelial ovarian cancer (Hou et al., 2014) and metastasis of prostate cancer (Lin et al., 2008). An oncogenic role for ASAP1 in the metastasis of laryngeal tumors has also been described (Li et al., 2014).

1.3.1 *Asap1* and breast cancer: what is known so far

Overexpression of ASAP1 has been correlated with malignancy of primary ductal carcinoma of the human breast (Onodera et al., 2005). Most of the current knowledge about how ASAP1 may be involved in the metastasis of breast carcinoma comes from cell line-based models or retrospective studies on patient data. There is evidence to suggest that the EGFR-GEP100-Arf6-ASAP1 signaling pathway is upregulated in malignant breast cancer and used for invasion and metastasis (Onodera et al., 2005). Specifically, co-expression of EGFR and GEP100 (a GEF for Arf6) correlates with malignant breast cancer (Morishige et al., 2008). Ligand activated EGFR directly binds

to GEP100 to activate Arf6 (Someya et al., 2001). Activation of GEP100 by Arf6 perturbs E-cadherin-based cell-cell adhesion of breast cancer cells, and may induce their motile phenotypes (Morishige et al., 2008). Importantly, activated Arf6 recruits ASAP1 to this complex by direct binding (Hashimoto et al., 2005).

Cortactin is a multi-domain protein that is found in the peripheral membrane ruffles and invadopodia. ASAP1 and cortactin associate with invadopodia in invasive breast cancer cell lines (Onodera et al., 2005). It has been shown that ASAP1 and cortactin together form an invasive machinery that links the highly tubulated membranes found in invadopodia and podosomes to polymerized and branched actin (Randazzo et al., 2007). Taken together, these observations suggest that ASAP1 is likely implicated in molecular regulation of the invasive phenotype.

1.3.2 Tools for studying the role of *Asap1* in breast cancer

Given the correlation of ASAP1 with metastasis of cancer types including breast cancer, it is pertinent that the molecular biology underlying this association and the function of ASAP1 should be studied in detail. For this purpose, *Asap1* knockout mice have been generated in our lab (data unpublished). My thesis set out to breed these mice with autochthonous mouse models of breast cancer as a pre-clinical model to understand the role of ASAP1 in breast cancer metastasis. The next sections therefore describe these animal models in more detail.

1.3.2.1 Engineering of *Asap1* knockout mice

One way to knock out genes in the mouse germline in a high throughput manner is to create a gene trap vector that carries a promoterless *lacZ* gene, a splice acceptor upstream to it and an antibiotic resistance marker. Mouse embryonic stem (ES) cells are then transfected with the gene trap vector. Random intronic integration of the gene trap vector into genes in the cells results in disruption of endogenous expression (von Melchner and Ruley, 1989). As depicted (Figure 7), upon transcriptional activation of the

gene, a spliced transcript arising from the upstream exon of gene of interest and *lacZ* gene, is generated. Thus not only is expression of the gene disrupted, expression of the *lacZ* gene serves as an indicator of when the disrupted gene would normally be expressed. Successfully transfected ES cells are screened to determine which gene has been targeted, and can then be used to create knockout mice through standard blastocyst injection methods.

This gene trap vector approach was used to create *Asap1* knockout mice. Insertion of the gene trap vector into the second intron of the mouse gene locus of *Asap1* was confirmed by whole genome sequencing. As the promoter of *Asap1* drives the expression of the *lacZ* gene, the normal expression pattern of ASAP1 can easily be detected by way of β-gal staining. The *Asap1* mice carrying the gene trap are designated as $Asap1^{GT/GT}$ since in these mice, both the alleles for *Asap1* have been replaced by the gene trap. They represent an *Asap1* knockout mice population. The *Asap1* heterozygous mice and the wild-type mice are denoted as $Asap1^{+/GT}$ and $Asap1^{+/+}$ respectively, as in them either one or none of the *Asap1* alleles has been replaced by the gene trap.

Complete abrogation of the endogenous expression of *Asap1*, as confirmed by RT-PCR analysis on a mouse embryo of stage E11.5 carrying the gene trap, demonstrated successful integration of the gene trap into mouse *Asap1* locus (Figure 8*)*. Sometimes utilizing the gene trap strategy could lead to a scenario where hypomorphic alleles are generated due to alternative splicing, mainly because the insertion event has taken place in an intron. This could result in low expressions of the endogenous gene transcripts (McClive et al., 1998). To rule out any possibility of expression of *Asap1* arising from alternative splicing, the exons downstream of the gene trap insertion site (exons 11-13, exons 21-24, exons 29-30) were analyzed for *Asap1* expression. The expression was also checked at the protein level and it was found that $Asap1^{GT/GT}$ embryos were incapable of expressing endogenous ASAP1.

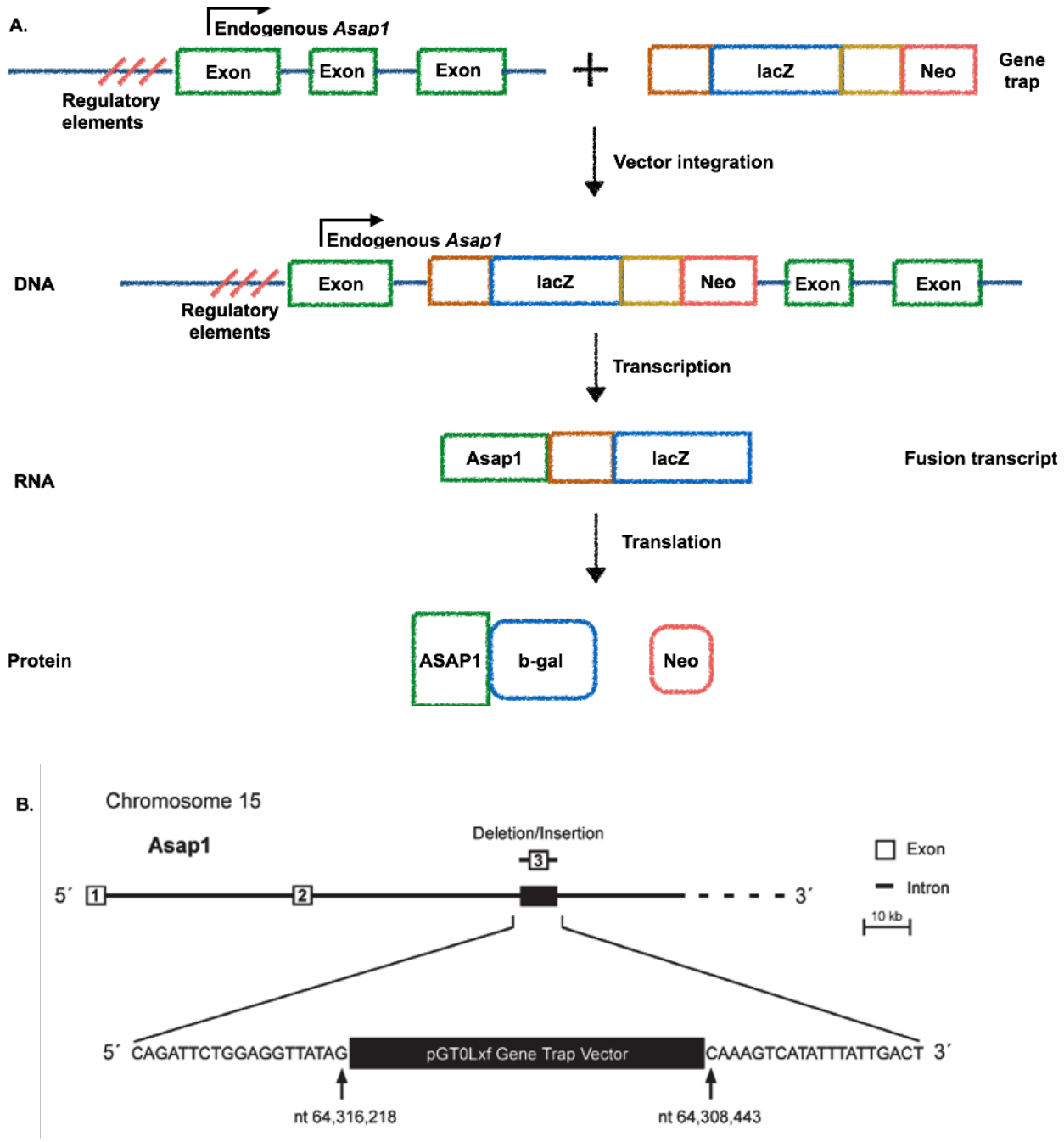

Figure 7. Strategy for trapping *Asap1.*
(A) Schematic representation of gene trap vector insertion into *Asap1* gene locus. Upon a successful insertional event where the gene trap integrated into the intron of *Asap1,* a fusion transcript was generated during the process of transcription. *Asap1* promoter drives the expression of promoterless *lacZ* gene. The *Asap1* is thus trapped and reported. (B) Gene trap vector was introduced into intron 2 of mouse *Asap1* gene locus at chromosome 15 thereby replacing exon 3 and a part of intron 2, leading to disruption of endogenous expression of *Asap1*. The site of gene trap insertion was determined by genomic sequencing.

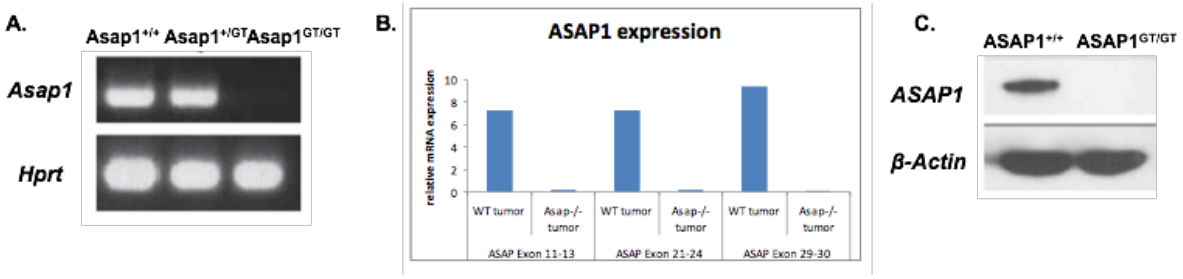

Figure 8. Validation of generation of *Asap1* knockout mice.
(A) RT-PCR analysis of E11.5 embryos confirm deletion of *Asap1*. (B) *Asap1* mRNA expression from exons downstream of site of gene trap introduction was checked to validate gene trap insertion event. None of the exons expressed *Asap1*, therefore any possibility of a partial expression of *Asap1* arising likely from any alternative splicing is ruled out. *Asap1* expression is completely abrogated. (C) Western blot showing no expression of *Asap1* at protein level corroborates *Asap1* deletion in our mouse model. Experiment and analysis performed by Dr. Caroline Schreiber and Dr. Natascha Cremers, CBTM, Mannheim.

At the start of my PhD thesis work, Asap1$^{GT/GT}$ mice had been generated, but their phenotype had been little investigated. Therefore, one of my tasks was to investigate the effect of loss of ASAP1 on normal physiology.

1.3.2.2 Murine models of breast cancer progression

One aim of my PhD thesis was to understand how *Asap1* regulates breast tumor progression. To this end, specific mouse models of breast cancer were bred with knockout mice and tumor growth in these mice was studied. The genetically engineered mouse models (GEMM) used recapitulate events observed in human breast cancer by forming spontaneous tumors when an oncogene is expressed in the mammary epithelium via a tissue-specific promoter. The most frequently utilized promoter is the mouse mammary tumor virus (MMTV) promoter that has been used to drive the expression of many oncogenes like Ras, Her2 (Neu), Cox2, polyoma middle T antigen (PyMT) and Wnt1 in the mammary epithelium, resulting in the formation of breast cancers (Fantozzi and Christofori, 2006).

MMTV-Neu

Primary human breast cancers can carry amplification and overexpression of the proto-oncogene *HER2,* which inversely correlates with the survival of the patients (King et al., 1985). The rodent homologue of *HER2* is *neu. HER2/neu* is a 185-kDa transmembrane protein belonging to the EGF receptor family. To study the tumorigenic potential of this oncogene in the mammary epithelium of transgenic mice, mice lines carrying either the activated or the unactivated rat *neu* under the transcriptional control of the MMTV promoter have been generated (Bargmann and Weinberg, 1988; Guy et al., 1992a). In my thesis work I have utilized the unactivated *neu* oncogene, driven by the MMTV promoter. In MMTV-Neu (unactivated) transgenic mice, focal mammary tumors appear at about 4 months of age, independent of pregnancy status. Histologically, these tumors are identical to those formed by activated *neu*. The oncogene *neu* has been shown to have intrinsic tyrosine kinase activity, and this has been associated with its tumorigenic potential. Consistently, *neu*-induced tumors have been shown to exhibit increased tyrosine kinase activity compared to the adjacent mammary epithelia. Mammary gland-specific expression of *neu* has been documented to induce metastases to the lung, in mice that have borne tumors for several months (Guy et al., 1992a).

MMTV-Wnt1

The *Wnt1* gene encodes a member of a family of poorly soluble, glycosylated, cysteine-rich, secretory proteins. The Wnt family of proteins associate with the ECM and determine cell fate and patterning via their interactions through cell surface receptors. Overexpression of several of the Wnt family members has been associated with the transformation of cultured cells. *Wnt1* overexpression has been shown to morphologically transform mammary epithelial cells (Li et al., 2000). A *Wnt1* transgene driven by the MMTV promoter in mice induces increased alveolar and ductal hyperplasia, independent of the pregnancy status (Tsukamoto et al., 1988). Metastasis was not reported at the time of detection of tumors, but the majority of the Wnt1 transgenic mice showed lung and/or lymph node metastasis after the primary tumor was removed (Li et al., 2000).

MMTV-PyMT

Polyoma virus middle T antigen (PyMT) is associated with a strong tyrosine kinase activity, like the *neu* oncogene, and has been implicated in murine mammary carcinogenesis (Guy et al., 1992b). The tumorigenic capacity of PyMT is mainly attributable to its association and subsequent activation of many *c-src* family members and its interaction with a subunit of phosphatidylinositol 3'-kinase (PI3K). MMTV-PyMT transgenic mice develop multifocal mammary tumors and multiple foci of metastatic mammary adenocarcinomas in the lung parenchyma. The transgenic mice display a short latency period between the expression of the transgene and transformation of the mammary epithelium, and this suggests that the expression of middle T oncogene is sufficient for the induction of mammary carcinogenesis in these mice, without the requirement of any additional genetic events (Guy et al., 1992b). The frequent occurrence of pulmonary metastasis in MMTV-PyMT transgenic mice allows for a systematic monitoring of mammary tumor progression in this model.

1.4 Objectives of the study

In my thesis work my major objective was to understand the function of *Asap1* in normal physiology as well as its role in breast tumor metastasis. I had the following specific aims:

1. Characterize *Asap1* knockout mice and determine the knockout phenotype.

2. Establish whether loss of *Asap1* affects tumor formation and metastasis in transgenic mouse models of breast cancer.

3. Understand the role of *Asap1* in tumor metastasis at the cellular level by studying murine mammary tumor cells and murine fibroblasts.

2. Materials and Methods

2.1 Materials

Material	Company
Acetic acid	Roth, Karlsruhe
Acetone	Merck, Darmstadt
Acrylamide/N, N'-Methylene - bisacrylamide (37,5:1)	Roth, Karlsruhe
Agarose	Sigma, Taufkirchen
Ammonium peroxodisulfate (APS)	Roth, Karlsruhe
BCA protein assay kit	Thermo Fisher Scientific, Schwerte
Bovine serum albumin	Roth, Karlsruhe
Bromophenol blue	Roth, Karlsruhe
Butanol	Roth, Karlsruhe
Cell culture plastic ware	BD Biosciences, Heidelberg
Chloroform	Sigma, Taufkirchen
Dako pen	Dako, Hamburg
Deoxynucleoside triphosphates – dNTPs	Peqlab, Erlangen
Diamidinophenylindole (DAPI)	Sigma, Taufkirchen
Diethylpyrocarbonate (DEPC)	Sigma, Taufkirchen
Dimethylsulfonyloxide (DMSO)	Sigma, Taufkirchen
Disodium hydrogen phosphate	Roth, Karlsruhe
Dithiothritol (DTT)	Fluka, Neu-Ulm
Dream Taq DNA polymerase and buffer	Thermo Fisher Scientific, Schwerte
Dulbecco modified eagle medium (DMEM)	Life Technologies, Darmstadt
ECL, western blotting substrate	Thermo Fisher Scientific, Schwerte
Eosin	Merck, Darmstadt
Epidermal growth factor (EGF)	Sigma, Taufkirchen
Ethanol	Roth, Karlsruhe
Ethidium bromide	Roth, Karlsruhe
Ethylenediaminetatraacetic acid	Thermo Fisher Scientific, Schwerte
Eukitt	Kindler GmBH, Freiburg
Fetal calf serum	Life Technologies, Darmstadt
Fibronectin	Millipore
Fluoromont-G	Southern Biotech

Material	Company
Gelatin	Roth, Karlsruhe
GeneRuler DNA Ladder	Thermo Fisher Scientific, Schwerte
Glutamine	Invitrogen, Karlsruhe
Glycerin	Roth, Karlsruhe
Glycerol	Roth, Karlsruhe
Glycine	Roth, Karlsruhe
H_2O_2	Roth, Karlsruhe
Isopropanol	Roth, Karlsruhe
Mayer's Haematoxylin solution	Merck, Darmstadt
Medical X-ray film	Typon Roentgen-Film, Frankenthal
Methanol	Roth, Karlsruhe
Nonidet P 40	Sigma, Taufkirchen
Oligonucleotides	Metabion
Opti-MEM	Life Technologies, Darmstadt
PageRuler Plus Protein ladder	Thermo Fisher Scientific, Schwerte
Paraformaldehyde	Roth, Karlsruhe
Penicillin/Streptomycin	Life Technologies, Darmstadt
Phalloidin	Promokine
Phenol	Roth, Karlsruhe
Phosphate buffered saline	Life Technologies, Darmstadt
Potassium chloride	Roth, Karlsruhe
Potassium dihydrogen phosphate	Roth, Karlsruhe
Powdered milk	Roth, Karlsruhe
Power SYBR Green Master Mix	Applied Biosystems, Darmstadt
Protease inhibitor complex	Roche Diagnostics, Mannheim
Proteinase K	Dako, Hamburg
Roti-Histol	Roth, Karlsruhe
Sodium chloride	Roth, Karlsruhe
Sodium deoxycholate	Sigma, Taufkirchen
Sodium dodecyl sulfate	Roth, Karlsruhe
Sodium hydroxide	Roth, Karlsruhe
Tetramethylethylendiamine (TEMED)	Roth, Karlsruhe
Tissue Tek O.C.T	Sakura
Tris HCL, Tris base	Roth, Karlsruhe
Triton X 100	Sigma, Taufkirchen
Trizol	Invitrogen, Karlsruhe
Trypsin	Invitrogen, Karlsruhe
Tween 20	Roth, Karlsruhe
β mercaptoethanol	Sigma, Taufkirchen

2.2 Equipment

Equipment	Company
Axio Imager.D1	Carl Zeiss, Jena
Cawomat 2000R	CAWO, Schrobenhausen
Centrifuges	Thermo Fisher Scientific, Schwerte
Diaphragm pump	Vacuubrand, Wertheim
DMI6000b microscope	Leica Microsystems, Wetzlar
Electrophoresis apparatus	Peqlab, Erlangen; Biorad, Muenchen
ELISA reader Multiscan Ascent	Thermo Fisher Scientific, Schwerte
Incubators	Binder, Tuttlingen; Thermo Fisher Scientific, Schwerte
NanoDrop ND-8000 spectrophotometer	NanoDrop Tech, Wilmington, USA
Paraffin embedding station EG1160	Leica, Wetzlar
PCR cycler	Analytic Jena, Jena
SLEE CUT 4060	SLEE medical, Mainz
Sterile hood Hera Safe	Thermo Fisher Scientific, Schwerte
Thermomixer 5436	Eppendorf, Hamburg
Tissue lyzer II	Qiagen, Duesseldorf
UV transilluminator	INTAS, Goettingen
Vortex	VWR International, UK
Water bath	Memmert, Buechenbach

2.3 Antibodies

Antigen	Host	Species Reactivity	Application Comment	Concentration Used	Company
ASAP1	Mouse	Mouse	IF	5 µg/ml	Lab produced
SLK	Rabbit	Mouse	WB	2 µg/ml	Abcam
			IF/IHC	20 µg/ml	
β-actin	Mouse	Mouse	WB	1:10,000*	Sigma
Vinculin	Mouse	Mouse	IF	5 µg/ml	Sigma
Tubulin	Rabbit	Mouse	IF	5 µg/ml	Abcam
Secondary AlexaFluor (546/488)	Goat	Rat	IF	4 µg/ml	Invitrogen
	Goat	Rabbit	IF	4 µg/ml	Invitrogen
	Goat	Mouse	IF	4 µg/ml	Invitrogen
CK14	Rabbit	Mouse	IHC	10 µg/ml	Covance
CK18	Mouse	Mouse	IHC	2 µg/ml	Progen Biotechnik
α-SMA	Mouse	Mouse	IHC	1:100*	Sigma

*Antibody concentration not provided.

2.4 Oligonucleotides

All oligonucleotides are specific for genes in mus musculus, purchased from Oligos Metabion and ordered with standard purification procedure (desalted).

Name	Sequence (5' → 3')
ASAPgeneTrap3´for	TCGATGTAACCCACTCGTGC
ASAPgeneTrap3´rev	CTACTTACTCCTACATCTGAGATCC
ASAPgenomic5 for	GCATCGCCTGTCATCCTACA
RibPO for	GGACCCGAGAAGACCTCCTT
RibPO rev	GCACATCACTCAGAATTTCAATGG

2.5 Cell lines

All cells were cultured in DMEM containing 10% FCS, 1% L-glutamine and 1% penicillin/streptomycin and were maintained at 37°C in a humidified incubator in 5% CO_2 supply.

Cell Type	Cell Line	Source
Murine Embryonic Fibroblasts (MEFs)	Asap1$^{+/+}$ fibroblasts	E13.5 Asap1$^{+/+}$ embryo
	Asap1$^{GT/GT}$ fibroblasts	E13.5 Asap1$^{GT/GT}$ embryo
Primary tumor derived cell lines	PyMT Asap1$^{+/+}$ tumor cells	MMTV PyMT Asap1$^{+/+}$ tumor
	PyMT Asap1$^{GT/GT}$ tumor cells	MMTV PyMT Asap1$^{GT/GT}$ tumor

2.6 Tissue culture methods

2.6.1 Cell culture maintenance

Cells were maintained at 37°C in a humidified incubator with 5% CO_2 supply. They were grown until they were 80-90% confluent, after which they were detached by trypsinization and re-seeded at lower density. Trypsin and the culture medium were pre-warmed at 37°C before they were applied onto the cells. Briefly, culture medium was aspirated and cells were washed with PBS. Cells were detached using 0.25% trypsin, and were incubated for a short time at 37°C to speed up the detachment process. Fresh medium was added to the detached cells and cells were spun down into a pellet, to be re-suspended and plated at desired densities. All cell lines were routinely screened for mycoplasma infection using the VectorGem Myco Detection kit from Vector. For long-term storage of cells, they were stored in freezing medium (90% FCS, 10% DMSO) at -80°C or in liquid nitrogen. The freezing process began when the cells reached about 80% confluence. For this purpose they were harvested and centrifuged at 1000 rpm for 3 minutes. Medium was aspirated and the cell pellet was re-suspended in freezing vials in 1 ml of freezing medium. They were transferred to -80°C for a few days and then later to liquid nitrogen. When required, cells were thawed through fast warming at 37°C in a water bath, following dilution in 5 ml of fresh medium. Cells were spun down to a pellet and re-suspended in fresh medium, to remove residual DMSO.

2.6.2 Isolation of Mouse Embryonic Fibroblasts (MEFs)

Pregnant FVB, Asap1$^{+/GT}$ mice were utilized to isolate embryonic fibroblasts. The experimental animals were maintained under specific pathogen free (SPF) conditions at the animal facility of Institute for Toxicology and Genetics, at Karlsruhe Institute of Technology. The pregnant mice, usually at F7 generation, were sacrificed by cervical dislocation on embryonic day 13.5. In a sterile hood, the abdomen was swabbed with 70% ethanol then cut open to expose the uterine horns, which were immediately transferred to a clean Petri dish containing PBS and placed on ice during the entire procedure. Embryos were carefully dissected in fresh Petri dishes to avoid any contamination with maternal tissue. Yolk sac was removed and later used for

genotyping. Head, heart, liver and spleen were removed from the embryo and the rest of the tissues from the embryo was cut into small pieces. These were washed in cold PBS once and then allowed to settle on ice. After aspirating PBS, the cut tissues from each embryo were transferred to Falcon tubes containing cold 0.25% trypsin. Tissue-digestion was allowed to occur at 37°C for 20 minutes, after which, 5 ml of warm media was added to the tubes and lysed tissue was gently homogenized by pipetting up and down to obtain single-cell suspension. Before plating onto a 10 cm dish, 5 ml fresh medium was added to this suspension. On the next day, the medium was aspirated to remove cell debris and fresh medium was added. Following genotyping results, MEFs from Asap1$^{+/+}$ and Asap1$^{GT/GT}$ were identified and stored in freezing medium at -80°C or liquid nitrogen for long-term storage.

2.6.3 Isolation of MMTV-PyMT Asap1$^{+/+}$ and – Asap1$^{GT/GT}$ tumor derived cells

Tumors from MMTV-PyMT Asap1$^{+/+}$ and – Asap1$^{GT/GT}$ were isolated under sterile conditions. Briefly, tumor-bearing mice were sacrificed by cervical dislocation and their abdominal skin was cut open to expose the breast tumor. Mammary tumors were then carefully excised from the animals and placed on clean, sterile Petri dish. Using a sterile scalpel, the tumor was cut into fine pieces. Pre-warmed fresh medium was added to the finely cut tumor pieces and they were incubated in culture dishes overnight at 37°C. Tumor pieces that resisted being cut into smaller pieces were removed from the cell culture dish the following day using sterile forceps, and the medium was replenished. Cells were then allowed to grow until they achieved about 80% confluency. This usually took about 8-10 days. Medium was changed twice a week. Once cells were confluent, they were stored in freezing medium.

2.6.4 Cell motility assay

For each experiment, 5 x 10^5 cells/well from three Asap1$^{+/+}$ and Asap1$^{GT/GT}$ (MEFs or tumor-derived) cell lines were seeded in 12 well plates. On the following day, a ‘wound’ was created in the monolayer of confluent cells by using a sterile 20 µl pipette tip. The scraped-out cells from creating the wound were washed away by changing the medium

and images were taken at desired time points. The distance between the cells fronts was analyzed with ImageJ software. Percentage wound healing was calculated.

2.6.5 Cell spreading assay

Cells at a density of 1 x 10^5 cells/well were seeded in slide chambers coated with 10 μg/ml fibronectin for 30 minutes at room temperature. After incubation at 37°C for the desired time points, cells were fixed with 4% PFA for 10 minutes at room temperature. The chamber compartment was taken off the slides and slides were sealed with coverslips. Spread and non-spread cells were counted in five representative high power fields. Spread cells were defined as large, elongated cells, adhering to the substrate (fibronectin-coated slide) and non-spread cells were defined as small cells with no (or very little) membrane protrusions.

2.6.6 EGF stimulation of MEF cells

Coverslips were coated with 0.25% gelatin in PBS. Excess gelatin was aspirated and the coverslips were air-dried and placed in 6 cm cell culture dishes. Cells were serum-starved for 6 hours, then harvested and seeded at 2 x 10^5 cells per 6 cm dish onto the coverslips. Cells were treated with 10 ng/ml EGF for the specified time points after which they were fixed in 4% PFA for 10 minutes at room temperature. They were then washed twice with PBS and either stored at 4°C or used immediately for immunofluorescence staining.

2.6.7 Immunofluorescence staining

Cells grown on coverslips were PFA fixed, then washed twice with PBS and treated with 0.1% Triton X 100 in PBS for 2 minutes at room temperature to allow permeabilization. After three PBS washes, cells were blocked with goat serum for 1 hour at room temperature. Cells were then incubated with the desired primary antibodies diluted in 0.1% goat serum/10% FCS/PBS for 1 hour at room temperature. Cells were washed again three times with PBS to get rid of excess antibodies and then incubated with appropriate secondary Alexa Fluor secondary antibodies diluted in 0.1% goat serum/10% FCS/PBS for 30 minutes in the dark, at room temperature. Wherever

phalloidin staining was required, it was added together with the secondary antibodies at specified concentrations. After secondary antibody incubation, cells were washed with PBS, three times, to remove excess antibody and then incubated with 0.5 μg/ml DAPI for 2 minutes in the dark at room temperature. After a final PBS wash, the coverslips were carefully turned onto microscopic slides with the cell-coated side facing down, and mounted with Fluoromont-G. The samples were kept at -20°C in the dark for at least an overnight before taking images.

2.7 Biochemical methods

2.7.1 Cell lysis

To analyze protein expression, lysates from cells were prepared. After the medium was aspirated, cells were washed with ice-cold PBS and harvested using an appropriate volume of lysis buffer. After about 15 minutes of incubation of cells on ice, they were sonicated for 10 to 20 seconds at 50 or 60 Hz for mechanical disruption and to break the DNA. Cells were centrifuged at 13000 rpm for 5 minutes and protein concentration was determined using a commercially available bicinchoninic acid (BCA) assay kit, using a calibrated curve generated from known concentrations of bovine serum albumin. A 1:5 dilution of the lysate was used for the colorimetric assay. The color development in each sample was proportional to the amount of protein, and was measured at 595 nm with an ELISA reader. Protein concentration was calculated using Ascent software. Lysates containing 50-100 µg proteins were diluted with 4x sample buffer and incubated for 5 minutes at 95°C.

Reagent		Concentration
Lysis buffer	Tris pH 7.5	50 mM
	Sodium Chloride	150 mM
	EDTA	5 mM
	Triton X 100	1%
	PMSF	1 mM
	Protease inhibitor cocktail	1x dilution
Sample buffer	SDS	8%
	Tris-HCl pH 6.8	100 mM
	Glycerin	40%
	Bromophenol blue	0.02%
	DTT	400 mM

2.7.2 SDS-PAGE

Protein samples were loaded onto SDS gels containing a stacking and a resolving part for separation of proteins based on size. The sample containing gel was run in running buffer, at 60-100 V until the dye front from the sample buffer reached the lower end of the gel.

Reagent		Concentration
Stacking gel	Acrylamide/bisacrylamide	3%
	Tris-HCl pH 6.8	125 mM
	SDS	0.10%
	APS	0.10%
	TEMED	0.10%
Resolving gel	Acrylamide/bisacrylamide	8-12%
	Tris-HCl pH 8.8	375 mM
	SDS	0.10%
	APS	0.10%
	TEMED	0.10%
Running buffer	Tris	25 mM
	Glycine	192 mM
	SDS	0.10%

2.7.3 Western blot

Upon completion of SDS-PAGE, gels were incubated in transfer buffer for 10 minutes. The PVDF membrane was activated by soaking it in 100% methanol for 15 seconds and rehydrated in water for 2 minutes, after which it was equilibrated in transfer buffer for 5 minutes. The blotting assembly was prepared using Whatman filter paper and sponges in the order, from cathode to anode: sponge pads, filter paper, gel, membrane, filter paper and sponge pads. Avoiding any air bubbles within this assembly, gels were electro-blotted on the membrane in transfer chambers filled with cold transfer buffer, overnight at 30 V at 4°C, and constant stirring. After transfer, the PVDF membrane was given a gentle wash with washing buffer and incubated with blocking buffer for an hour, at room temperature, followed by another hour of incubation (at room temperature) with the desired primary antibody diluted in blocking buffer. Excess antibody was washed away and the membrane was incubated with secondary horseradish peroxidase (HRP)-conjugated antibodies at appropriate dilutions (made in blocking buffer). Incubations in blocking buffer and antibodies were carried out with gentle shaking. Protein bands on the membrane were visualized with the help of ECL (enhanced chemiluminiscence) pipetted onto the membrane. After a minute, the membrane was exposed to X-ray films for a few minutes, depending on signal strength.

Reagent		Concentration
Transfer buffer	Tris	20 mM
	Glycine	192 mM
	SDS	0.01%
	MeOH	20%
Blocking buffer	Tris-HCl pH 7.4	50 mM
	Sodium chloride	150 mM
	Tween-20	0.03%
	Powdered milk	4%
Wash buffer	Tris-HCl pH 7.4	50 mM
	Sodium chloride	150 mM
	Tween-20	0.03%

2.7.4 Preparation of Formalin-Fixed Paraffin Embedded (FFPE) tissues

Fresh tissue (tumor and/or lung) isolated from the experimental animals was fixed in formalin overnight at room temperature and subjected to an automated dehydration procedure using a Hypercenter XP (Thermo Fisher Scientific) tissue processor with the following program:

1. Formalin, 1.5 h, repeated twice
2. 70% ethanol, 1.5 h
3. 80% ethanol, 1.5 h
4. 96% ethanol, 1.5 h
5. 100% ethanol, 1.5 h
6. Xylol, 1.5 h, repeated twice
7. Paraffin, 1.5 h

Samples were embedded in paraffin and stored at 4°C overnight before they were cut into 5 µM sections. These sections were allowed to dry overnight at 37°C and then immersed in Roti-histol (twice, 5 minutes each), followed by immersion in descending ethanol concentrations (100%, 96%, 80%, 70%; 2 minutes in each). The samples were then ready to be used either for immunohistochemistry or haematoxylin and eosin (H&E) staining.

2.7.5 Immunohistochemical staining of FFPE-tissue

Sections were incubated in citrate buffer (pH 6.0) at 60°C for 30 minutes to facilitate antigen retrieval. They were then cooled down and immersed in PBS for 5 minutes. Endogenous peroxidase activity was quenched by immersing samples in 3% H_2O_2 for 5 minutes. Slides were then washed in PBS (twice, 5 minutes each) and blocked by incubation with 10% goat serum for 30 minutes. The desired primary antibody was diluted as required in blocking solution, and samples were incubated at 4°C overnight. The next day, slides were washed in PBS (3 times, 5 minutes each) and incubated with secondary antibody diluted in blocking buffer at 1:200 ratio at specified concentrations. Samples were incubated for 30 minutes at room temperature, after which they were

washed with PBS (3 times, 5 minutes each) and incubated with ABC reagent for 30 minutes (prepared and incubated in the dark for 30 minutes at room temperature). This was followed by another PBS wash (3 times, 5 minutes each). Subsequently, the NovaRed peroxidase substrate was applied to the samples for 2 to 4 minutes or until visible coloration appeared on the sample. The samples were then washed in water for 5 minutes. Slides were subsequently immersed in ascending concentrations of ethanol (70%, 80%, 96%, 100%; 2 minutes in each) and Roti-histol (3 times, 5 minutes each). The slides were covered in Eukitt mounting medium and mounted with coverslips.

2.7.6 Haematoxylin and Eosin (H&E) staining of FFPE-tissue

FFPE sections, after being treated with Roti-histol and decreasing concentrations of ethanol were immersed in haematoxylin for 10 minutes and the then placed under running tap water to wash off excess stain. Slides were then immersed in eosin for 5 minutes and quickly passed through increasing concentrations of ethanol (70%, 80%, 96%, 100%; 2 minutes each) and then in Roti-histol (3 times, 5 minutes each). Slides were then covered in Eukitt mounting medium and mounted with coverslips.

2.8 Animal experiments

All procedures involving mice were carried out in accordance with the local regulatory board (Regierungspraesidium, Karlsruhe). The FVB strain of mice was used in this study and mice were housed under specific pathogen free (SPE) conditions at the animal facility of Institute for Toxicology and Genetics, at Karlsruhe Institute of Technology. Light conditions (12 hours light, 12 hours dark) and temperature (21°C) were controlled, and mice were fed commercial mouse chow (Purina) and tap water *ad libitum.* The mice were kindly genotyped by Annette Gruber and Gitta Theide, at CBTM, Mannheim.

2.8.1 β-galactosidase staining of embryos

Embryos at appropriate stages were dissected and transferred immediately to a clean petri dish containing PBS, placed on ice. For early embryonic stages like E9.5 and E10.5, a light microscope was used to carry out the dissection process. Yolk sac and/or

embryonic tails were used for genotyping. Each dissected embryo was then placed in individual wells of a 24-well plate containing PBS, also kept on ice. The embryos were fixed in 4% PFA at room temperature, with gentle shaking for 1 hour (early stage embryos) or 2 hours (late stage embryos), after which they were washed with detergent containing wash buffer three times, 20 minutes each, also at room temperature and with constant gentle shaking. X-gal was added freshly to the staining solution, taking care not to expose it to light. After the final wash, staining solution was added to the embryos and it was ensured that they were covered in the staining solution. They were incubated at 37°C overnight. The following day, *Asap1*$^{+/+,}$ *Asap*$^{+/GT}$ and *Asap1*$^{GT/GT}$ embryos could be identified respectively on the basis of no stain, weak blue stain and intense blue stain. Where possible, phenotypes were confirmed by PCR.

Reagent		Concentration
Wash buffer	Disodium hydrogen phosphate pH 7.3	100 mM
	Sodium dihydrogen phosphate pH 7.3	100 mM
	Magnesium chloride	2 mM
	Sodium deoxycholate	0.10%
	Nonidet P-40	0.02%
	BSA	0.05%
Staining solution	Potassium ferricyanide ($K_3Fe(CN)_6$)	5 mM
	Potassium ferrocyanide ($K_4Fe(CN)_6$)	5 mM
	Sodium chloride	7.2 mM
	X-gal (reconstituted in DMF at 50 mg/ml; added freshly)	0.3 mg/ml

2.8.2 Genotyping of Asap1 mice

Genotyping of Asap1 mice was performed by PCR amplification of genomic DNA extracted from either mouse tails or yolk sac (in case of embryos). Tails (or yolk sac) were lysed overnight in 400 μl of SNET buffer for genomic dna isolation and 10 μl of proteinase K at 55 °C, with light shaking at 750 rpm. The next day, the tubes were centrifuged at 13000 rpm for 10 minutes at RT. Supernatant (350 μl) was transferred into a fresh Eppendorf tube and 250 μl isopropanol was added and incubated at RT for

10 minutes. Tubes were centrifuged at 13000 rpm for 15 minutes, after which the supernatant was discarded. The pellet was air dried, and then 100 μl dd-water was added to it. PCR to assess the genotype was set up as given below.

	Reagent	Concentration
PCR setup	DreamTaq Buffer (10x)	2.5 μl
	dNTPs 10 mM	0.5 μl
	Primer ASAPgeneTrap3' for (10 μM)	1 μl
	Primer ASAPgeneTrap3' rev (10 μM)	1 μl
	PrimerASAPgenomic5 for (10 μM)	1 μl
	Template (DNA)	2 μl
	Taq polymerase	0.1 μl
	dd-water	16.9 μl

After preparing all the PCR samples on ice, these were put directly into the cycler with the following program.

95 °C	2 min	
95 °C	1 min	33x
59 °C	1 min	
72 °C	1 min	
72 °C	5 min	

The amplified DNA was stored at 4 °C and was electrophoresed using TAE agarose gel electrophoresis. Agarose (1% (w/v)) was dissolved in TAE buffer by heating. Ethidium bromide (0.2 μg/ml) was added before pouring the solution into a casting tray. Samples were mixed with 6x DNA loading dye, and the gel was run with 3-6 V/cm. A 1 Kb DNA-ladder was used for size reference, and Asap1 heterozygous, Asap1 knockout and wild-type along with water control was also run. DNA was visualized under UV-light.

	Wild-type ($Asap1^{+/+}$)	Heterozygous ($Asap1^{+/GT}$)	Knockout ($Asap1^{GT/GT}$)
Expected band sizes	330 bp	330 bp + 680 bp	680 bp

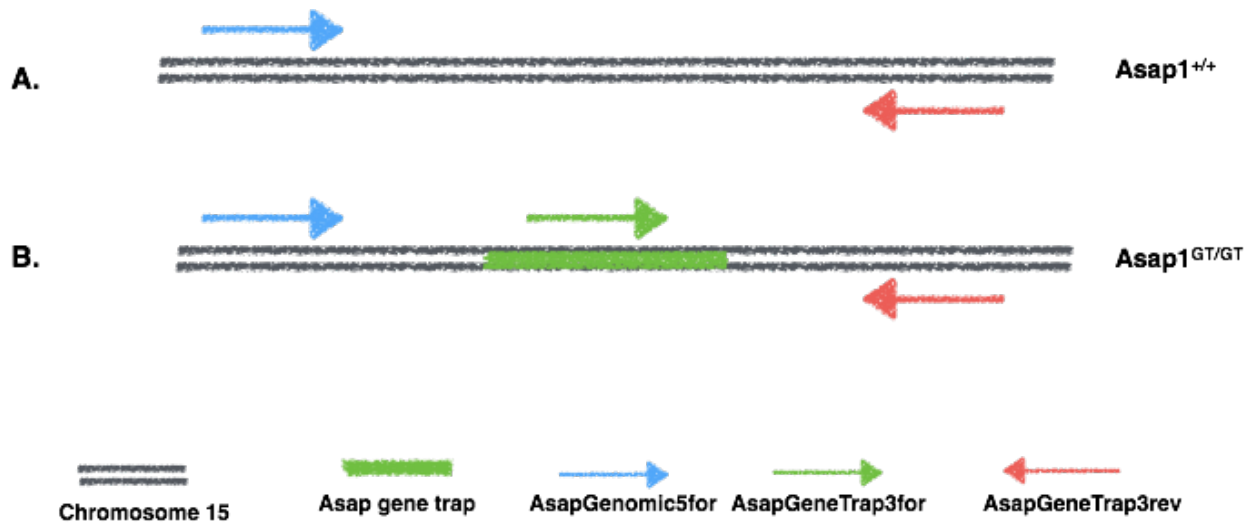

Figure 9. Genotyping Asap1 mice.
Chromosome 15 of a wild-type mouse where AsapGenomic5for and AsapGeneTrap3rev primers bind and upon polymerase chain reaction, produce an amplicon of 330 bp. (B) $Asap1^{GT/GT}$ allele with gene trap inserted into intron 2, as determined by genomic sequencing, and which contains complimentary sequence for AsapGeneTrap3for primer to bind and amplify, along with AsapGeneTrap3rev primer. The primer pair AsapGeneTrap3for and AsapGeneTrap3rev produce an amplicon of 680 bp. Heterozygous Asap1 mouse DNA produces two bands of 330 bp and 680 bp each.

2.8.3 Alcian blue/Alizarin red staining of Asap1 embryos

Asap1 embryos at specific stages (E15.5, E18.5) were obtained following cesarean section. The embryos were scalded in hot tap water (about 70 °C) for 20-30 sec, and their skin was removed carefully with the help of forceps. Internal organs were removed from the embryos so as to obtain their skeletons. These were then fixed in 95% ethanol overnight at RT. The next day, these mice were put in acetone and incubated overnight at RT. After briefly rinsing the mice with deionized water, they were stained for cartilage with alcian blue for 24 h. Next, the mice were washed in 70% ethanol for 6-8 h and then

transferred to 1% KOH overnight. Once the tissues were visibly cleared, they counterstained with alizarin red to stain their bone. The samples were cleared in 1% KOH/20% glycerol and stored in 1:1 glycerol: ethanol solution.

2.8.4 Respiratory and growth parameters measurements

Respiratory rate measurement

Pups from a litter, when taken out of the cage for analysis, were kept together on a wad of tissues and placed on a metallic plate maintained at room temperature. This was done to keep the pups warm and comfortable thereby reducing any stress induced by the analysis. Pups were monitored one by one and the respiratory rate per minute per pup was recorded. Three measurements were made per pup and the average respiratory rate was calculated and used for analysis. Care was taken that the pups were returned to their mother as soon as possible to minimize stress.

Size and weight measurement

Embryos at appropriate stages (E17.5, E18.5) were dissected and transferred to a clean petri dish containing PBS, placed on ice. Yolk sac and/or embryonic tails were used for genotyping. With clean forceps, individual embryos were picked up and placed on a tissue paper. Using a ruler, head to base of the tail of embryos were measured.

Pups were measured the same way, from head to base of the tail. Weight was measured by placing individual pups in a clean petri dish kept on a tabletop balance.

2.8.5 Retinal whole-mount staining

Asap1$^{+/+}$ and Asap1$^{GT/GT}$ pups at specified postnatal age (P3-P7) were sacrificed and their eyeballs were carefully dissected out and fixed in ice cold 100% methanol. Retinas were then isolated and blocked in 0.5% Triton X-100/1% BSA for 1h at room temperature. FITC-conjugated Isolectin B-4 antibody was used to stain the retinas for 1h at room temperature. Pictures were taken using a confocal microscope (Zeiss LSM710) and images were analyzed with Fiji, ImageJ. Relative angiogenesis was reported as stained area of the vasculature (Isolectin B-4^{+} area) compared to the total retinal area. Values obtained per animal were normalized to the mean value of the

Asap1$^{+/+}$ pups. These experiments were performed in cooperation with the laboratory of Prof. Dr. Hellmut Augustin.

2.8.6 Tumor development studies

FVB, MMTV-PyMT and FVB, MMTV-Wnt1 – wild-type and Asap1$^{GT/GT}$ were used to study tumor development. Once mice developed spontaneous mammary tumors, the tumors were measured weekly. Mice were sacrificed either when the tumor reached 2 cm in one direction or when the animals became moribund. After the animals were sacrificed by cervical dislocation, important parameters like the age, number of lesions and tumor volume (calculated using the formula, $V= 4/3 \times \pi \times r^3$) were recorded, where r denotes the average radius of the tumor. Primary mammary tumors were either snap frozen or formalin-fixed, or were utilized immediately to isolate tumor-cells.

2.8.7 Metastasis studies

Lungs from FVB, MMTV-PyMT and FVB, MMTV-Wnt1 – wild-type and Asap1$^{GT/GT}$ mice were isolated after the primary tumor characteristics were recorded, and samples from the tumor tissue were prepared. Visible metastatic foci were counted on the lung surface, from all the lung lobes. The lungs were also studied under a light microscope to check for smaller metastatic foci that could not be observed by eye. Lungs were then either snap frozen or formalin-fixed for detailed analysis.

2.8.8 Lung float analysis

Pups at P0 were sacrificed by dislocating the head from the body through cutting at the base of the skull. Lungs were isolated, carefully removed with clean forceps, and placed in a glass test tube containing PBS. A healthy inflated lung floated on the solutions whereas a defective non-inflated lung sank to the bottom of the tube.

2.9 Statistical analysis

Statistical analysis was performed using GraphPad Prism v7. Data are expressed as mean ± s.d, unless stated otherwise. Statistical significance was calculated using either two-tailed paired Student's *t*-test, ANOVA when comparing multiple groups followed by

Bonferroni's comparison, or the Mann-Whitney's U test for non-parametric data, and regression analysis for survival curves. In each case, the specific statistical test used is specified. A *p*-value of less than 0.05 was considered statistically significant, and is represented as * when $p \leq 0.05$, ** when $p \leq 0.01$ and *** when $p \leq 0.001$.

3. Results

My objectives in this study were to characterize the phenotype of *Asap1* knockout mice, and to use them to investigate the role of *Asap1* in tumor metastasis by crossing them with autochthonous murine breast cancer models

3.1 Identification of *Asap1* knockout embryos

The Asap1$^{GT/GT}$ mice do not express endogenous *Asap1* because of the loss-of-function mutation arising in the *Asap1* gene from the gene trap. They do however, display *lacZ* fusion gene activity that enables an easy and sensitive method for detecting homozygous knockout progeny. This detection method relies on the ability of the embryos to cleave a compound known as X-gal into an insoluble blue-colored product that is detectable by eye. Homozygous wild-type (Asap1$^{+/+}$) embryos appear colourless, homozygous knockout (Asap1$^{GT/GT}$) mice develop an intense blue color, while the heterozygous embryos (Asap1$^{+/GT}$) display a weak blue stain (Figure 10*)*. Yolk sac from the embryos obtained by cesarean sections was utilized for genotyping to further validate correct identification. Once *Asap1*$^{GT/GT}$ mice were generated, the next task was to determine if *Asap1* was dispensable for embryonic development of the mice and which embryonic growth processes were affected by its absence.

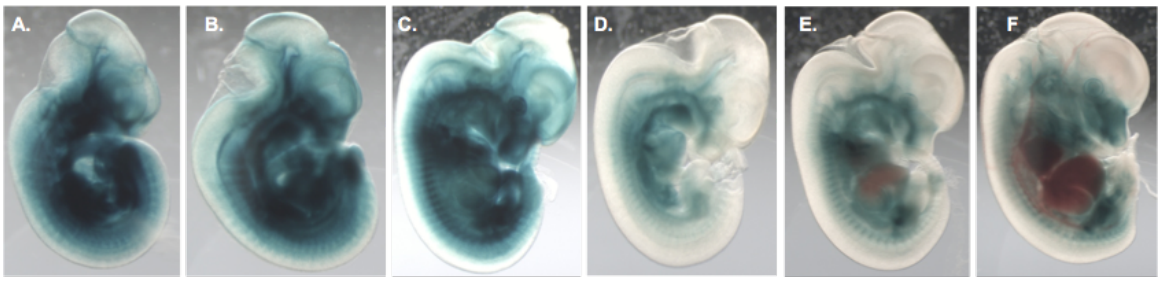

Figure 10. Identification of *Asap1* knockout embryos.
X-gal staining performed on embryos obtained at various embryonic stages like E11.5 (A, D), E12.5 (B, E) and E13.5 (C, F) reveals homozygous *Asap1* knockout (A, B, C) and heterozygous (D, E, F) embryos.

3.2 Deletion of *Asap1* is partially neonatal lethal

Adult Asap1$^{GT/GT}$ mice do not display any overt phenotypic differences when compared to wild-type mice. They are able to live to maturity and reproduce normally. The absence of a distinguishable phenotype does not however, hold true for Asap1$^{GT/GT}$ embryos and newborn pups. A careful study of 256 embryos and 176 newborn pups born from breeding heterozygous *Asap1* mice, disclosed a strong, albeit transitory phenotype. Genotyping *Asap1* embryos from various stages of gestation and on the day of their birth, P0, exhibited a disparity in the Mendelian ratio of homozygous *Asap1* knockout offspring (Figure 11 A*)*. Normally when heterozygous transgenic mice are bred, the typical ratio of resultant homozygous wild-type, heterozygous transgenic and homozygous knockout offspring is 25%, 50% and 25% respectively. The Asap1$^{GT/GT}$ mice population arising from crosses between Asap1$^{+/GT}$ mice is significantly lower than expected. I found that across all embryonic stages Asap1$^{GT/GT}$ embryos maintain the expected normal ratio, with the discrepancy in their number arising only at birth (Figure 11 B, C*)*. These data suggest that loss of *Asap1* speaks for a partially penetrant neonatal lethality.

A.	Asap1$^{+/+}$	Asap1$^{+/GT}$	Asap1$^{GT/GT}$	Asap1$^{+/+}$: Asap1$^{+/GT}$: Asap1$^{GT/GT}$
E 10.5	2	8	2	16.6% : 66.6% : 16.6%
E 11.5	2	7	2	18.1% : 63.6% : 18.1%
E 12.5	3	6	1	30% : 60% : 10%
E 13.5	6	24	10	15% : 60% : 25%
E 14.5	1	7	2	10% : 70% : 20%
E 15.5	7	10	7	29.1% : 41.6% : 29.1%
E 16.5	8	6	5	42.1% : 31.5% : 26.3%
E 17.5	15	40	18	20.5% : 54.7% : 24.6%
E 18.5	14	27	16	24.5% : 47.3% : 28%
All Embryonic Stages	59	134	63	23% : 52.3% : 24.6%
P0	56	89	31	31.8% : 50.5% : 17.6%

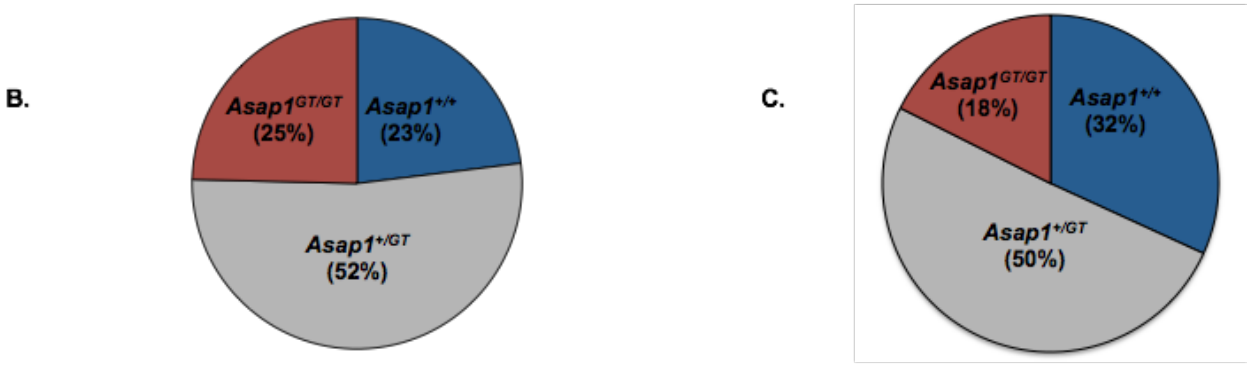

Figure 11. Partial neonatal lethality in Asap1$^{GT/GT}$ mice.
(A) Embryonic stage-wise distribution of Asap1$^{+/+}$, Asap1$^{+/GT}$ and Asap1$^{GT/GT}$ mice indicating the number of offspring of each genotype and the corresponding Mendelian ratio at that age. Pie charts show distribution of offspring resulting from breeding of heterozygous *Asap1* mice. Normal distribution of embryos (B) and abnormally reduced Asap1$^{GT/GT}$ newborn pups (C) demonstrate partially penetrant neonatal lethality.

The partial neonatal lethality warranted a detailed study of Asap1$^{GT/GT}$ newborn pups. According to the Phenotype Ontology Database resource, in a study of genotypes associated with lethality, 26% of genotypes were lethal perinatal. Hence, the time of death in these mutant mice provides an important platform on which to base further investigations. I therefore performed an extensive study on late stage Asap1$^{GT/GT}$ embryos and the newborns.

3.3 Late stage Asap1$^{GT/GT}$ embryos are smaller than wild-type embryos

In order to understand the partial *Asap1* lethal neonatal phenotype, I analyzed the perinatal Asap1$^{GT/GT}$ progeny. Embryos from E17.5 and E18.5 stages were isolated and assessed for gross morphological defects and any other apparent anomalies. Asap1$^{GT/GT}$ E17.5 embryos were smaller in size than their wild-type counterparts, although this difference was not statistically significant (Figure 12 A*)*. No visually striking differences were noted. At E18.5, Asap1$^{GT/GT}$ embryos were found to be significantly smaller than the wild-type embryos (Figure 12 B*)*. Growth retardation in the embryos immediately prior to birth may be a critical factor that could compromise their survival.

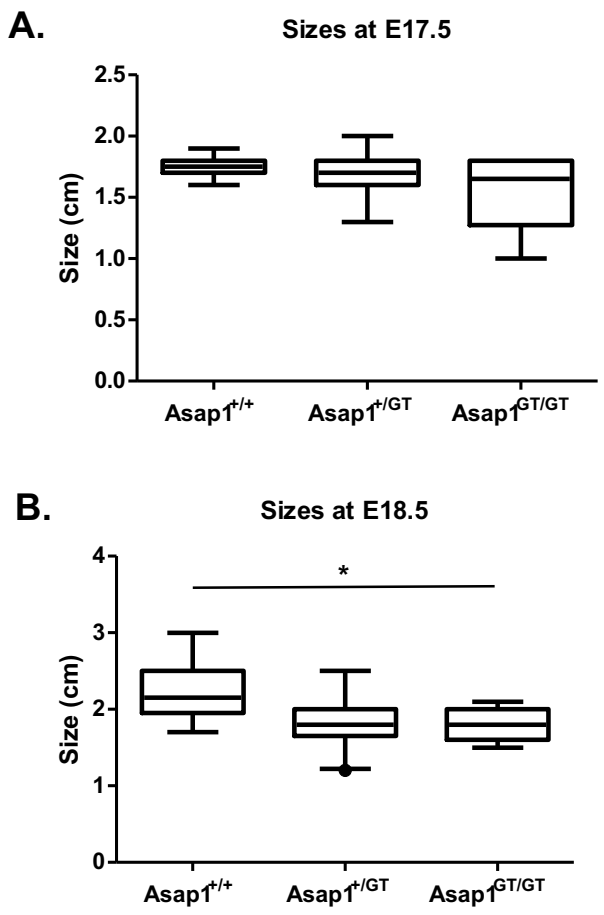

Figure 12. Size distribution of late stage Asap1$^{+/+}$, Asap1$^{+/GT}$ and Asap1$^{GT/GT}$ embryos.
(A) Smaller, though not statistically significant sizes of Asap1$^{GT/GT}$ embryos at E17.5. (n=31). (B) Statistically significant smaller Asap1$^{GT/GT}$ embryos at E18.5. (n=37, p= 0.0285). Student's unpaired t test used for p value calculation

3.4 Asap1$^{GT/GT}$ neonates display bradypnea and growth retardation

To investigate the partially penetrant death of Asap1$^{GT/GT}$ neonates, they were carefully observed for the first days following their birth. The number of neonates, their activity and general features were carefully recorded. Upon a thorough checking of the cages, many dead neonates were found, often times partially cannibalized. As expected, Asap1$^{GT/GT}$ neonates formed the majority of the dead population (56%). While Asap1$^{+/GT}$ constituted 33%, Asap1$^{+/+}$ represented only 11% of the stillborn pups. This observation explains the reduced Mendelian ratio observed in the Asap1$^{GT/GT}$ newborns. Asap1$^{GT/GT}$

pups that survived appeared normal. These pups displayed an intact, hydrated skin dismissing any possibility of loss of body fluids through broken epidermis, an important factor for survival. These pups were not subjected to abnormal nursing by the mother and they demonstrated normal suckling. Defects in suckling were discounted as there was evidence of milk in the stomach of all of the pups.

Respiratory rates of the neonatal pups were analyzed, which revealed an inability of Asap1$^{GT/GT}$ neonates to breathe normally. The breathing rates of these pups averaged 82 per minute as against 109 per minute of the wild-type pups (Figure 13 *A)*. Asap1$^{GT/GT}$ pups also demonstrated an irregular, pulsated breathing. The normal breathing rhythm in these pups was broken by bouts of respiratory apnea that was followed by a few short and rapid inhalation and exhalation attempts.

Consistent with the findings in late stage embryos, Asap1$^{GT/GT}$ pups were found to be severely growth retarded. Their size and weight were significantly lower than the wild-type pups (Figure 13 B, C*)*. While the mean size of a wild-type pup was found to be 2.68 cm, that of an Asap1$^{GT/GT}$ pup was only 2.43 cm. Similarly, the mean weight of a wild-type pup was 1.56 g as compared to 1.26 g for an Asap1$^{GT/GT}$ pup. It is important to mention here that all of the dead pups that were retrieved from the cages weighed less than 1 g. The differences in respiratory rates, size and weight of wild-type and Asap1$^{GT/GT}$ neonates were found to be statistically significant. Interestingly, the disparity in the breathing and weights of these pups was found to be gene dose-dependent, in that these defects also affected the heterozygous pups. In these pups, a single mutated allele of *Asap1* was sufficient to lower the breathing rates and weights.

Pups were monitored for six days after being born and their respiratory rates and growth parameters were routinely recorded. Once the pups had survived the initial 24 hours of birth, none of them were found dead. While the respiratory rates and sizes of the neonates varied greatly on P0, these parameters gradually became comparable by the third or fourth day after birth (Figure 14 A, B*)*. A day after birth, the breathing pattern of surviving Asap1$^{GT/GT}$ pups became regular and rhythmic, and matched those of wild-

type pups. The breathing rates increased for Asap1$^{+/+}$, Asap1$^{+/GT}$ and Asap1$^{GT/GT}$ pups comparatively, and no difference between knockout and wild-type pups was subsequently observed. All pups grew in size and weight, displaying normal growth and development, and no differences regarding the growth of Asap1$^{+/+}$, Asap1$^{+/GT}$ and Asap1$^{GT/GT}$ pups was observed (*Figure 14)*. A more detailed analysis with higher number of animals would be required to obtain a statistically robust result. However, the absence of bradypnea and growth retardation after the first day of birth strongly underlines the transient nature of this phenotype.

3.5 Lungs of Asap1$^{GT/GT}$ neonates show areas of insufficient aeration

Deletion of *Asap1* compromised not just the respiratory rates, but also the quality of breathing. The observed bradypnea in neonatal Asap1$^{GT/GT}$ pups prompted further functional analyses of lungs isolated from P0 pups to understand possible causes of this transient phenotype. Although Asap1$^{GT/GT}$ pups exhibited abnormal breathing for the first hours after birth, their survival after 24 hours was not affected by this defect. I therefore isolated lungs from early neonates and analyzed their aeration. To this end, lungs were tested for their ability to float on phosphate-buffered saline (PBS). Under these conditions, poorly aerated lungs sink, while healthy aerated lungs float. Compared to other genotypes, a significantly higher proportion of the Asap1$^{GT/GT}$ lungs sank, indicating abnormal aeration (Figure 15 A*)*. Specifically, 45% of Asap1$^{GT/GT}$ lungs displayed inability to float as compared to 18% of Asap1$^{+/+}$ and 24% of Asap1$^{+/GT}$ lungs that sank.

To further investigate this phenotype, the lungs were embedded in paraffin, sectioned and stained to study their histology. This revealed why many of the Asap1$^{GT/GT}$ lungs could not float in PBS, as instead of a well-aerated parenchyma, many areas of thick mesh-like parenchyma were observed (Figure 15 B*)*. These observations suggest that the bradypnea phenotype of Asap1$^{GT/GT}$ pups may be caused by an improperly developed lung parenchyma that limits aeration, possibly compounded by defective growth that may contribute to the severely impaired breathing in Asap1$^{GT/GT}$ pups.

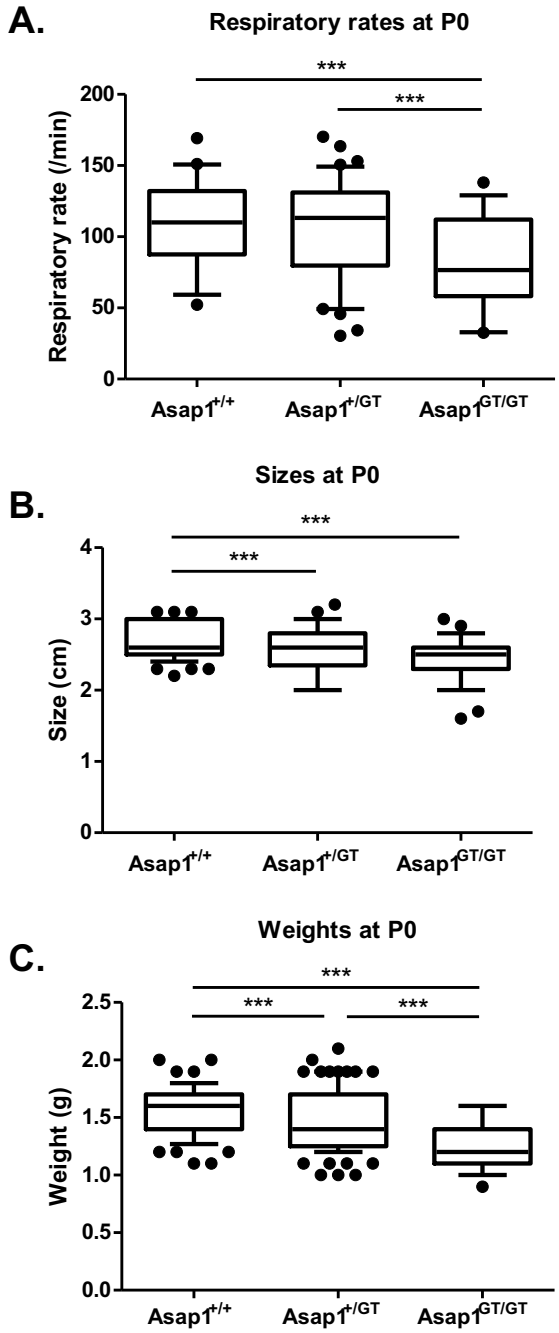

Figure 13. Respiratory rates and growth analysis of Asap1$^{+/+}$, Asap1$^{+/GT}$ and Asap1$^{GT/GT}$ pups.
Asap1$^{GT/GT}$ pups (n=31) display reduced breathing rates (A), lower sizes (B) and lower weights (C) as compared to wild-type (n=56) and heterozygous (n=89) pups. p values for respiratory rates, sizes and weights are given with following comparison between wild-type versus heterozygous, knockout versus heterozygous and wild-type versus knockout, respectively (Respiratory rates p=0.38, 0.001, 6.1x10^{-5}; Sizes p=0.01, 0.06, 9.3x10^{-5}; Weights p=0.03, 9.12x10^{-5}, 1.9x10^{-8}). Student's unpaired t test used for p value calculation.

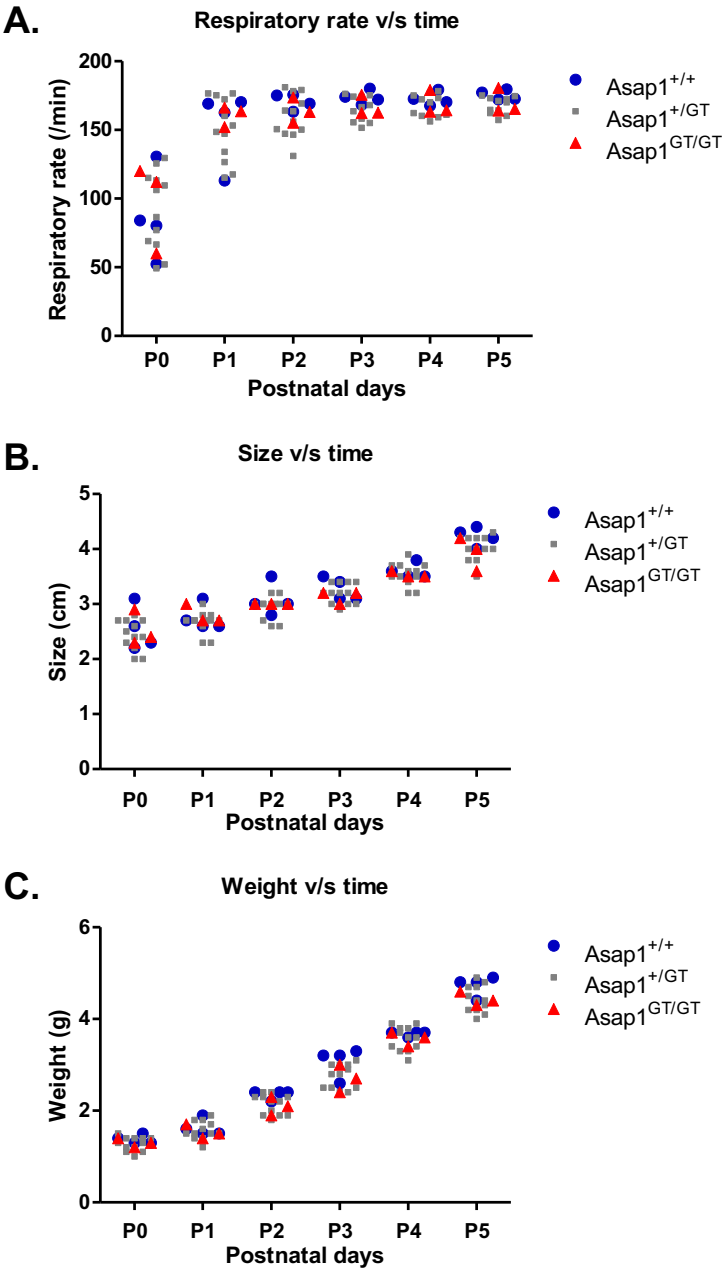

Figure 14. Time course analysis of Asap1$^{+/+}$, Asap1$^{+/GT}$ and Asap1$^{GT/GT}$ pups.
Pups were analyzed for respiratory rates (A), sizes (B) and weights (C). Values for breathing rates and growth parameters consistently increase every post-natal day and Asap1$^{GT/GT}$ pups (n=3) record values comparable to both Asap1$^{+/+}$ (n=4) and Asap1$^{+/GT}$ (n=12) pups after P0.

Of interest is also the fact that 11% of Asap1$^{+/+}$ pups were found dead at birth. Consistently, 18% of Asap1$^{+/+}$ neonatal lungs were inadequately aerated, as assessed by their inability to float in PBS. Thus wild-type pups can exhibit similar defects to Asap1$^{GT/GT}$ pups, albeit at a statistically significant lower frequency.

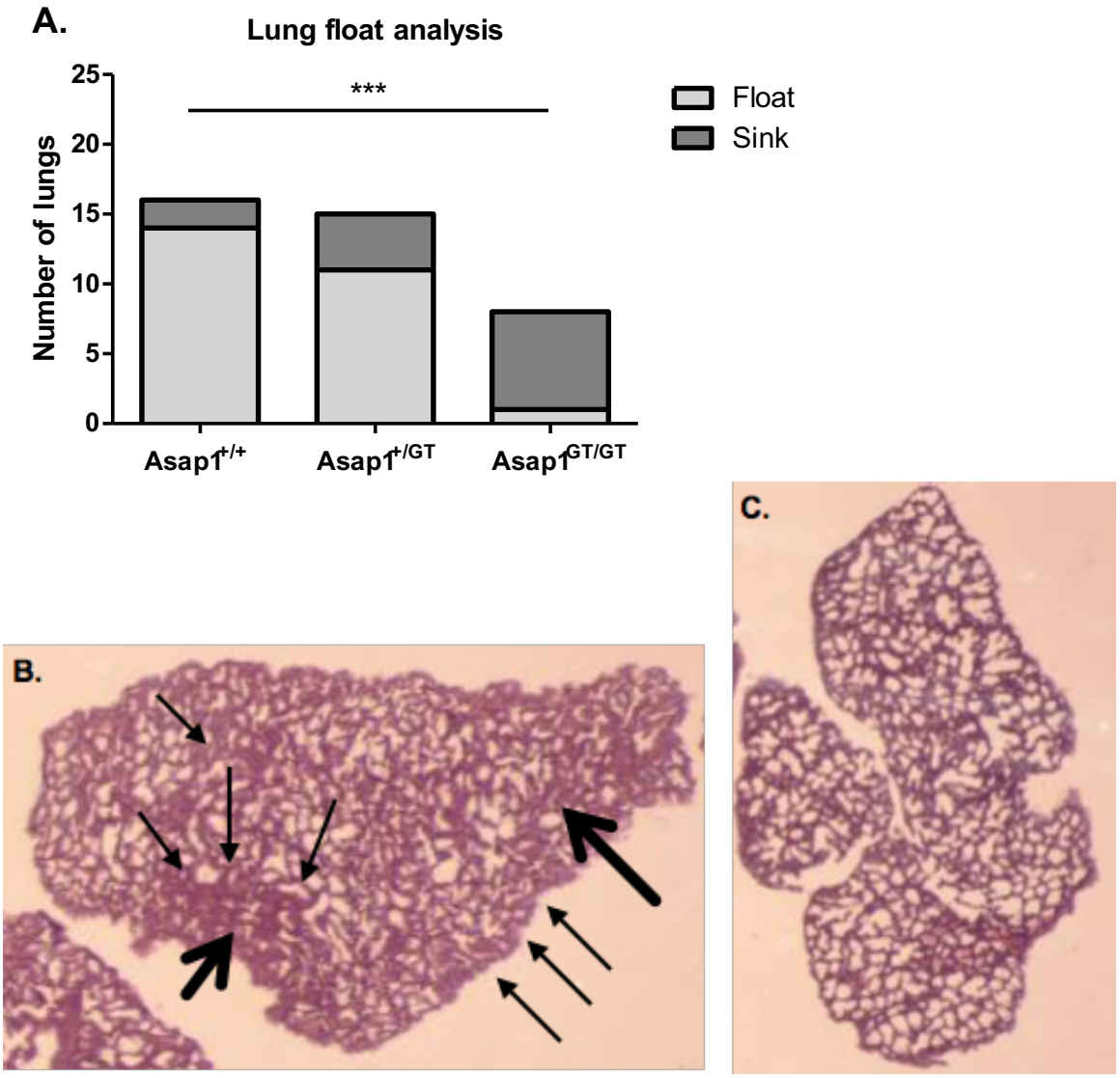

Figure 15. Functional analyses of Asap1$^{+/+}$ and Asap1$^{GT/GT}$ lungs.
Lung float test (A) shows that majority of *Asap1$^{GT/GT}$* lungs (n=8) cannot float in PBS as compared to *Asap1$^{+/GT}$* (n=15) and *Asap1$^{+/+}$* (n=16) lungs. (p=0.0007, fisher test). H&E stained *Asap1$^{GT/GT}$* (B) and *Asap1$^{+/+}$* (C) lungs showing histology. Arrows indicate poorly aerated areas of lung.

3.6 *Asap1* deficiency delays neonatal retinal angiogenesis

Endothelial cells express high levels of ASAP1, and VEGFR2 promotes angiogenesis by activating a pathway involving ASAP1 (Hashimoto et al., 2011). Furthermore, ASAP1 regulates cell motility, a key cellular process during angiogenesis. I therefore hypothesized that ASAP1 may play a role in angiogenesis. To explore this hypothesis, I investigated retinal angiogenesis in Asap1$^{+/+}$ and Asap1$^{GT/GT}$ mice. To this end, retinas of Asap1$^{+/+}$ and Asap1$^{GT/GT}$ pups were isolated at various post-natal days, starting from P3, and stained to study vascular network development. For technical reasons, it was difficult to carry out retinal angiogenesis analyses on younger pups (P0, P1 and P2) because the retinas from these pups were extremely fragile, and the outgrowth of the retina was sub-optimal for quantification. The Asap1$^{GT/GT}$ retinas showed reduced retinal angiogenesis until P5, after which they display angiogenesis comparable with that in Asap1$^{+/+}$ retinas (Figure 16*)*. The initial delay in the outgrowth of retinal vascular network in Asap1$^{GT/GT}$ retinas is transient, and only lasts until about P5, after which normal retinal angiogenesis was observed. Although the differences in the quantified retinal angiogenesis are not statistically significant, there is nevertheless a tendency of delayed retinal vascularization in the absence of *Asap1*.

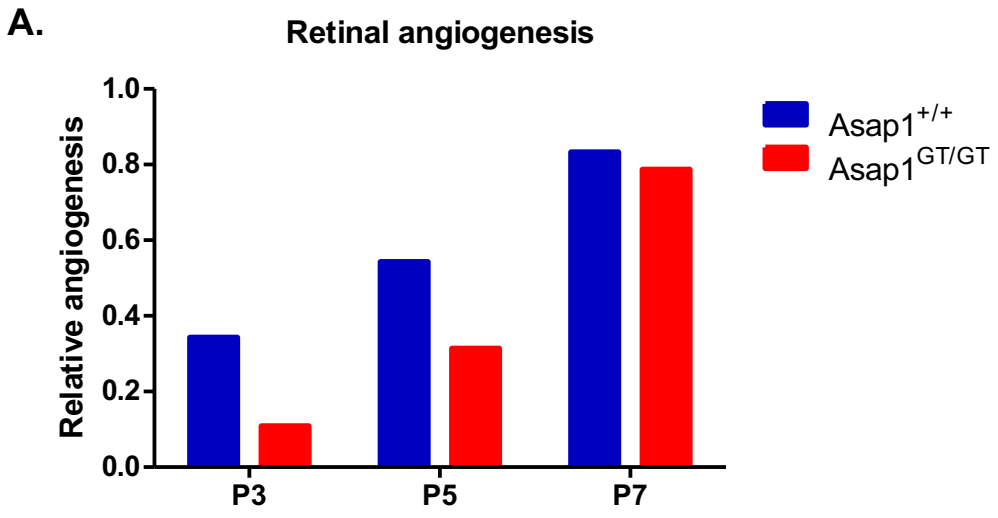

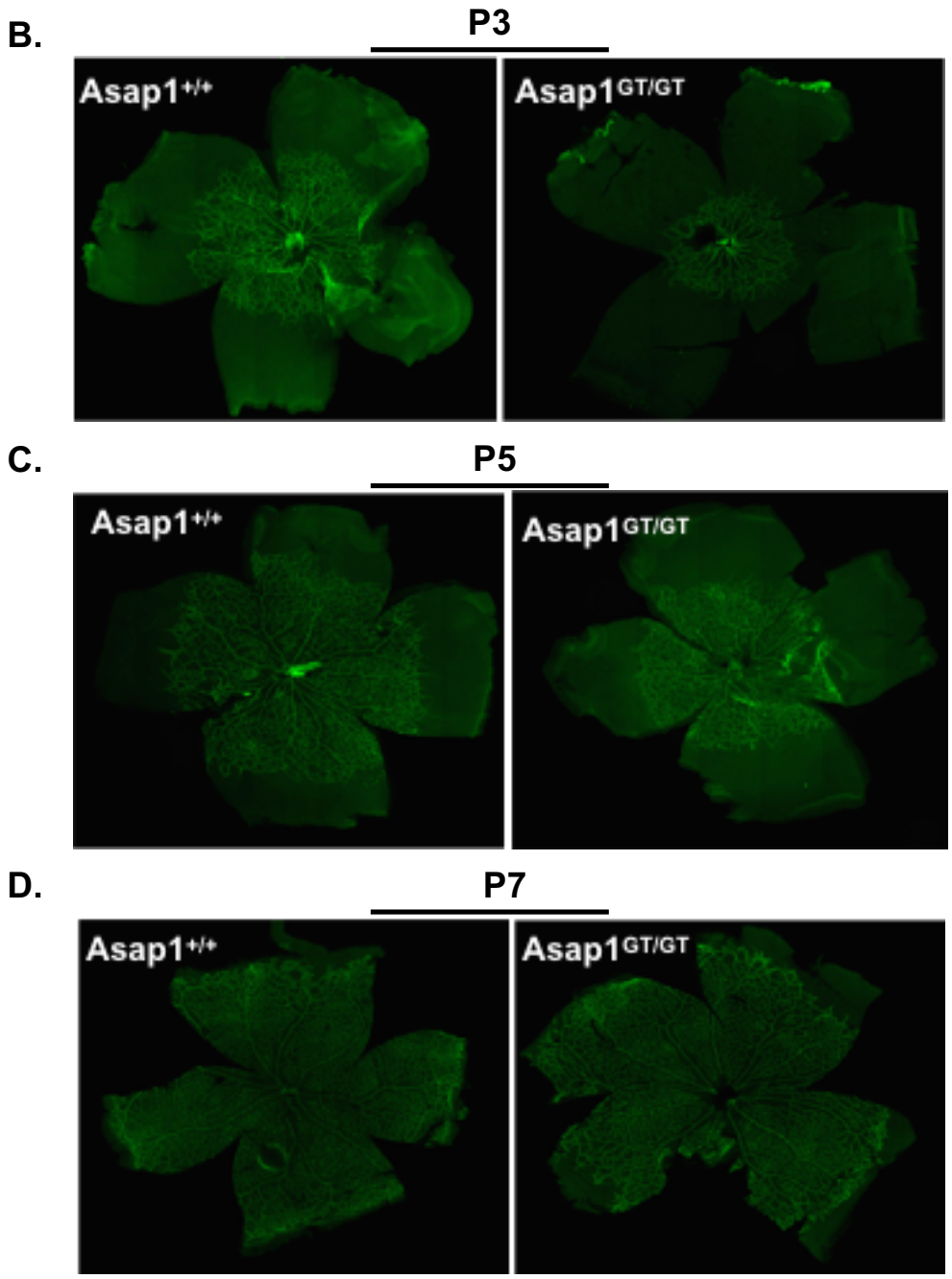

Figure 16. Retinal angiogenesis in Asap1$^{+/+}$ and Asap1$^{GT/GT}$ pups.
(A) Quantification of retinal angiogenesis through P3-P7 stages. P>0.05. A delay in retinal angiogenesis is seen in P3 and P5 stages. (B, C, D) Stained retinas of Asap1$^{+/+}$ and Asap1$^{GT/GT}$ at P3 (n=3, n=2), P5 (n=2, n=2) and P7 (n=3, n=4) are shown respectively. Experiment performed in collaboration with Dr. Claudia Korn, DKFZ, Heidelberg.

3.7 *Asap1* does not influence lymphangiogenesis

As there was a tendency for delayed development of the vasculature in retinas of Asap1$^{GT/GT}$ pups compared to Asap1$^{+/+}$ pups, we investigated whether lymphangiogenesis is also affected by loss of Asap1. Consistent with this hypothesis, the thoracic duct was found to express *Asap1* (Figure 17 A*).* Lymphatic ring assays were therefore performed with thoracic ducts isolated from 2-3 months old Asap1$^{+/+}$ and Asap1$^{GT/GT}$ mice. In these *ex-vivo* lymphangiogenesis assays, pieces of thoracic duct were embedded in collagen and the outgrowth of lymphatic vessels was assessed. No difference in lymphangiogenesis between Asap1$^{+/+}$ and Asap1$^{GT/GT}$ mice was observed*.* *Asap1* plays no apparent role in lymphangiogenesis process, suggesting that this process does not rely on *Asap1*-mediated cellular motility, or that other molecules may be compensating for ASAP1.

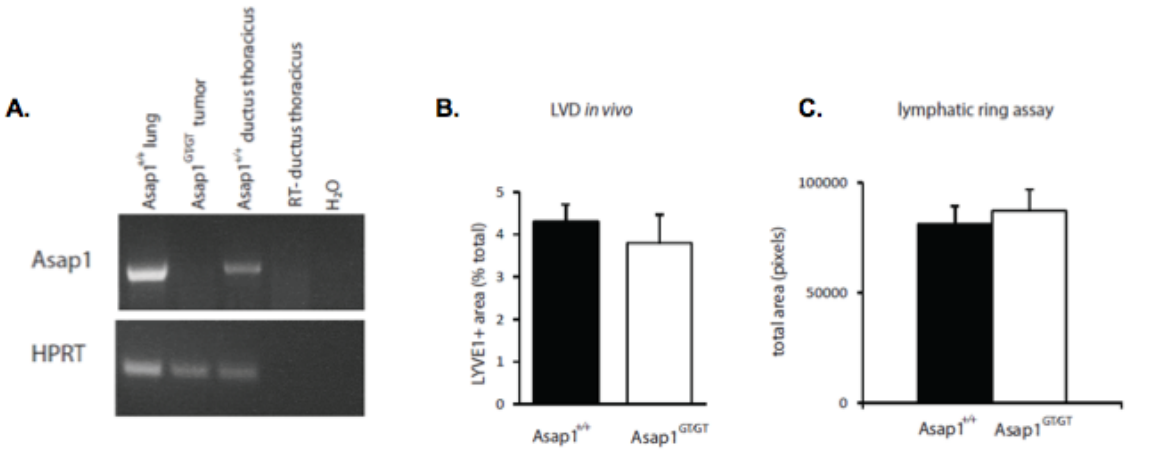

Figure 17. Lymphangiogenesis in Asap1$^{+/+}$ and Asap1$^{GT/GT}$ mice.
(A) *Asap1* expression in thoracic duct. (B) No significant difference between Asap1$^{+/+}$ and Asap1$^{GT/GT}$ is observed in lymphatic vessel density (n=6, n=6, p=0.5) and (C) also in lymphatic ring assay (n=30, n=54, p=0.7). Experiments performed by Dr. Anja Schmaus, Dr. Melanie Rothley and Dr. Diana Plaumann, KIT, Karlsruhe.

3.8 Loss of *Asap1* impairs ossification

The growth retardation in Asap1$^{GT/GT}$ neonates, prompted us next to investigate whether *Asap1* plays a role in bone development. Skeletons of E15.5 Asap1$^{+/+}$ and Asap1$^{GT/GT}$ embryos were therefore prepared and stained with Alizarin Red and Alcian Blue to visualize bone and cartilage respectively (Figure 18*)*. Clearly, Asap1$^{GT/GT}$ embryos show normal cartilage development. However, they show ossification defects. It is noteworthy that loss of *Asap1* affects both types of ossification processes – the intramembranous as well the endochondral ossification. Lack of Alizarin Red staining in the skull bone and vertebrae indicate both modes of ossification are compromised in the absence of *Asap1*. This defect in ossification could conceivably predispose Asap1$^{GT/GT}$ embryos and neonates to delayed growth development.

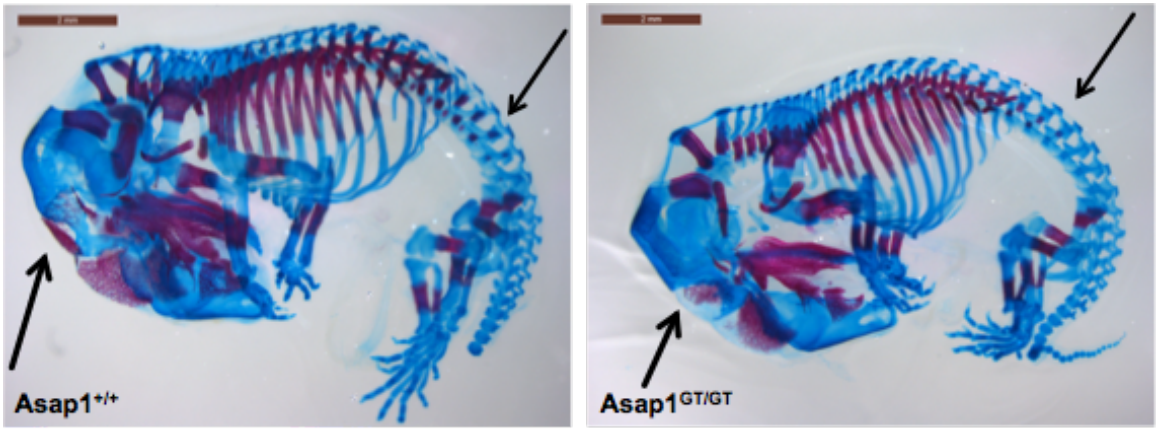

Figure 18. Impaired ossification in E15.5 Asap1$^{GT/GT}$ embryos.
Normal cartilage development as seen by Alcian Blue staining and defective ossification as seen by Alizarin Red staining. Arrows indicate differences in ossification in Asap1$^{+/+}$ and Asap1$^{GT/GT}$ embryos. Experiment performed together with Dr. Caroline Schreiber, CBTM, Mannheim.

Role of ASAP1 in breast cancer development and progression

Given our own work and that of others showing that ASAP1 expression correlates with poor prognosis in human breast and colorectal cancer patients, I investigated the role of ASAP1 in breast cancer using three autochthonous mouse models, namely MMTV-Neu, MMTV-Wnt1 and MMTV-PyMT. To this end, heterozygous *Asap1* mice were bred with these three mouse models that form spontaneous mammary tumors, and tumor development and metastasis in Asap1$^{+/+}$- and Asap1$^{GT/GT}$- tumor-bearing mice were monitored.

3.9 Tumorigenesis in MMTV-Neu Asap1$^{+/+}$ and MMTV-Neu Asap1$^{GT/GT}$ mice

It was observed that Neu Asap1$^{+/+}$ and Neu Asap1$^{GT/GT}$ mice presented with multifocal mammary tumors, formed after a long and highly varying latency period. The mice were sacrificed when the size of the tumor reached 2 cm in one dimension. The tumor burden at the time of sacrifice varied within the group, with most of the tumors being necrotic. Although the group size was too small to allow a statistical analysis, nevertheless there was no obvious difference in the size of the primary tumors from Neu Asap1$^{+/+}$ and Neu Asap1$^{GT/GT}$ mice (Figure 19). Tumor necrosis did not positively correlate with the tumor size. Even small tumors were found to be necrotic or fluid-filled, making a detailed study of the primary tumor impossible. Lungs were isolated from these mice to study surface metastases, but no metastasis was recorded in any of the mice studied. Due to these problems, this murine model of breast cancer was discontinued for the purpose of elucidating the role of *Asap1* in tumor development and metastasis.

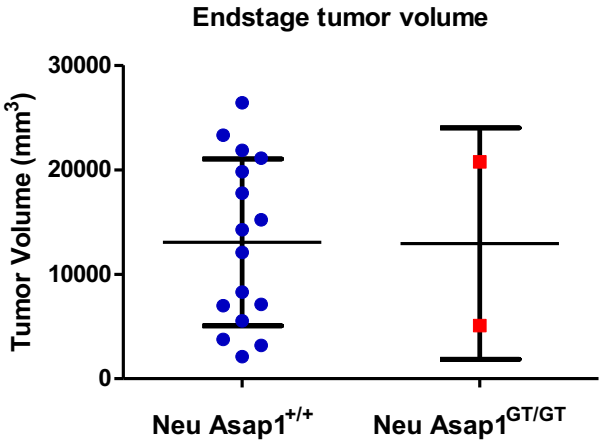

Figure 19. Tumor volumes of MMTV-Neu Asap1$^{+/+}$ and MMTV-Neu Asap1$^{GT/GT}$ mice.
The MMTV-Neu Asap1$^{+/+}$ (n=16) and MMTV-Neu Asap1$^{GT/GT}$ Mice (n=2) tumor mice display highly varying tumor burden at the time of sacrifice. Total tumor volume refers to the sum of the volumes of all the mammary tumors formed in the animal.

3.10 Tumorigenesis in MMTV-Wnt Asap1$^{+/+}$ and MMTV-Wnt Asap1$^{GT/GT}$ mice

The Wnt Asap1$^{+/+}$ and Wnt Asap1$^{GT/GT}$ mice developed tumors following a long and highly varying latency period, in that Wnt Asap1$^{+/+}$ mice developed tumors only at 14 weeks of age whereas Wnt Asap1$^{GT/GT}$ mice developed tumors at about 20 weeks of age, thus displaying a delayed tumor onset (Figure 20 A*)*. The mice rarely, if ever presented with multifocal mammary tumors. They developed tumors only in any one of the mammary glands. Once palpable, tumors were routinely measured and growth curves were generated. I found that both groups of mice exhibited heterogeneous tumor growth patterns (Figure 20 B*)*. It was thus difficult to draw conclusive remarks about the role of *Asap1* in delaying tumor onset in this model of breast cancer as the tumors developed at varying ages, and no statistically significant difference in the age was found at the time of palpable tumor formation. The mice were sacrificed when the tumor reached 2 cm in one dimension. At the time of sacrifice, both groups of mice displayed comparable average tumor burden (Figure 20 C*)* and lungs were isolated from them to study metastases. However, I found no incidence of lung metastasis in any of the mice.

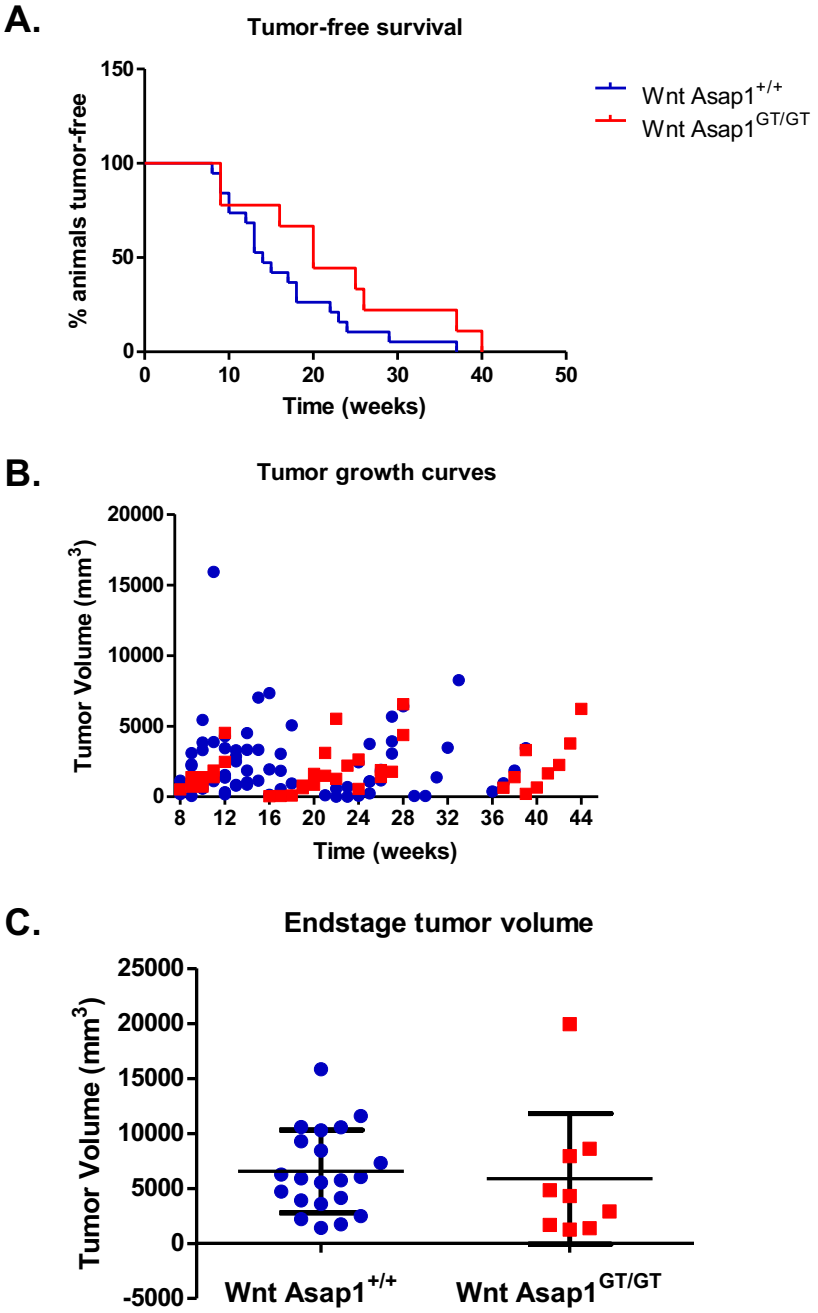

Figure 20. Tumor growth characteristics of MMTV-Wnt Asap1$^{+/+}$ and MMTV-Wnt Asap1$^{GT/GT}$ Mice. (A) Tumor-free survival curves showing that MMTV-Wnt Asap1$^{+/+}$ mice (n=19) develop tumors earlier than MMTV-Wnt Asap1$^{GT/GT}$ mice (n=9) at 14 weeks as compared to 20 weeks. P>0.05. (B) Tumor growth curves showing highly variable growth characteristics of tumors formed in MMTV-Wnt Asap1$^{+/+}$ and MMTV-Wnt Asap1$^{GT/GT}$ mice. P>0.05. (C) The total tumor volume at the time of sacrifice is comparable in MMTV-Wnt Asap1$^{+/+}$ and MMTV-Wnt Asap1$^{GT/GT}$ mice. Total tumor volume refers to the sum of the volumes of all the mammary tumors formed in the animal. P>0.05.

3.11 MMTV-PyMT Asap1$^{GT/GT}$ mice show early tumor onset and increased metastasis to lungs compared to MMTV-PyMT Asap1$^{+/+}$ mice

MMTV-PyMT Asap1$^{+/+}$ and MMTV-PyMT Asap1$^{GT/GT}$ mice, like the two previously described mouse models, were studied for tumor growth and lung metastases. PyMT mice were analyzed either by me or by Dr. Caroline Schreiber. Analysis was matched/ aligned. It was found that PyMT Asap1$^{GT/GT}$ mice displayed a shorter tumor-free survival as compared to the wild-type mice, indicative of an early tumor onset in these mice (Figure 21 A*)*. The median tumor-free survival for PyMT Asap1$^{+/+}$ mice was 60 days whereas that for PyMT Asap1$^{GT/GT}$ mice was 52.5 days. The mice were sacrificed when the tumor reached 2 cm in one dimension. These mice developed multifocal mammary tumors and upon comparison of tumor volumes in the two groups of mice, it was found that PyMT Asap1$^{GT/GT}$ mice displayed significantly higher tumor volumes in the weeks immediately prior to their sacrifice. Hence, the tumors in the *Asap1* knockout mice grew faster and more aggressively than the tumors in the PyMT Asap1$^{+/+}$ mice (Figure 21 B*)*.

At weeks 10, 11 and 12 after palpable tumors were detected in PyMT Asap1$^{+/+}$ and PyMT Asap1$^{GT/GT}$ mice, there was a significantly higher tumor burden in the PyMT Asap1$^{GT/GT}$ mice. However, between week 12 and 13, the tumors in PyMT Asap1$^{+/+}$ mice grew in size such that the tumor burden in the two groups of mice became comparable.

When the tumor volumes of PyMT Asap1$^{+/+}$ tumors in the penultimate and final week before sacrifice (86-96 days) were plotted against time and linear regression analysis was performed, it was found that these tumors displayed a positive slope, indicating that tumor size positively correlated with age and that tumors increasingly grow in size (Figure 21 C*),* suggesting they are still in the exponential phase of growth. On the other hand, *Asap1* knockout tumors displayed a negative slope when a similar analysis was performed, indicating that tumors have reached a plateau and tumor sizes no more positively correlate with age (Figure 21 D*)*. This implies that Asap1$^{GT/GT}$ tumors grew faster and more aggressively, thereby reaching a plateau by roughly 90 days after the first palpable tumors were detected, whereas Asap1$^{+/+}$ tumors grew more slowly,

exhibiting significantly lower tumor volumes than Asap1$^{GT/GT}$ tumors, and were still found to be growing exponentially at roughly 90 days when Asap1$^{GT/GT}$ tumors had already reached a plateau phase. Taken together, this means that deletion of *Asap1* results in faster growing tumors in the PyMT mouse model.

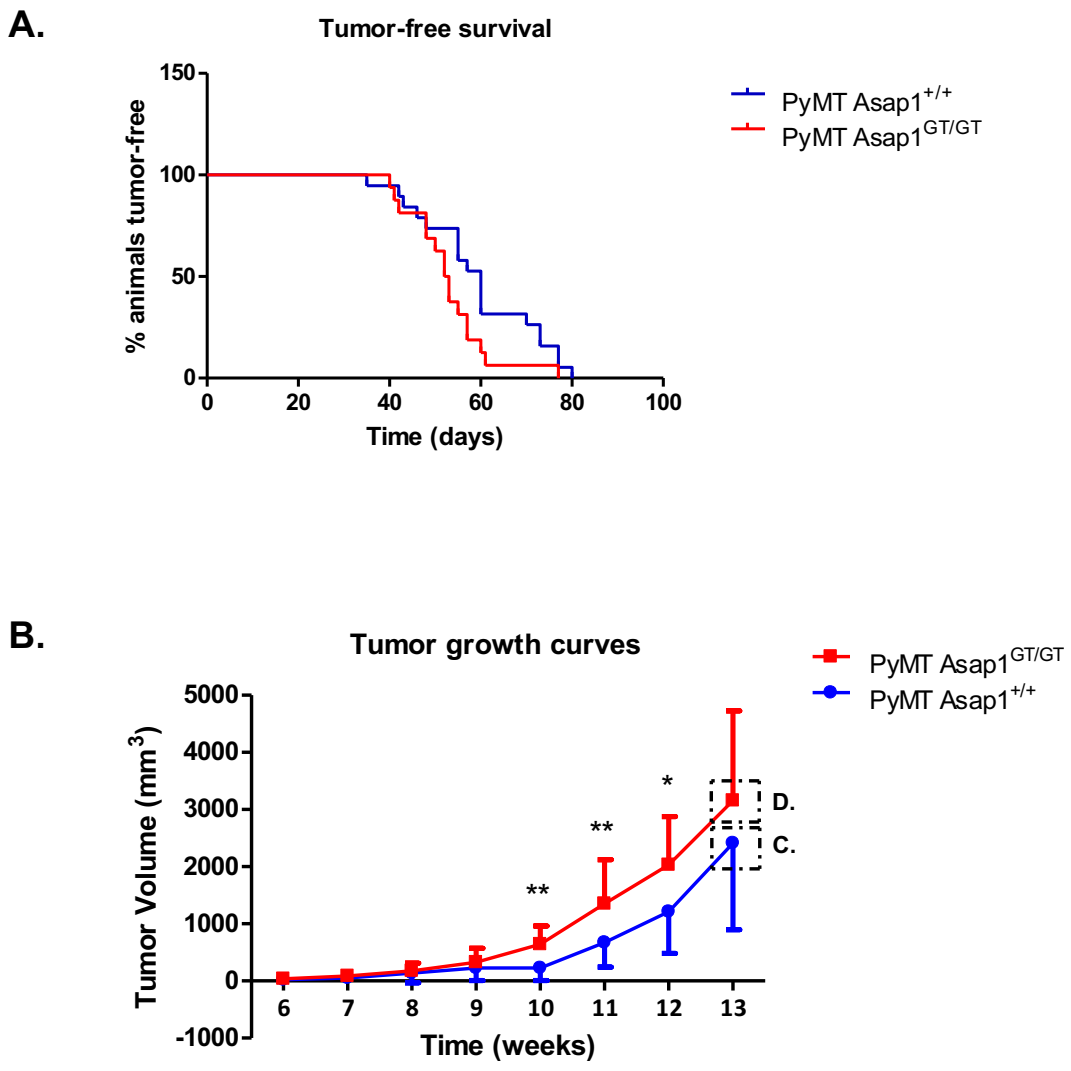

C.

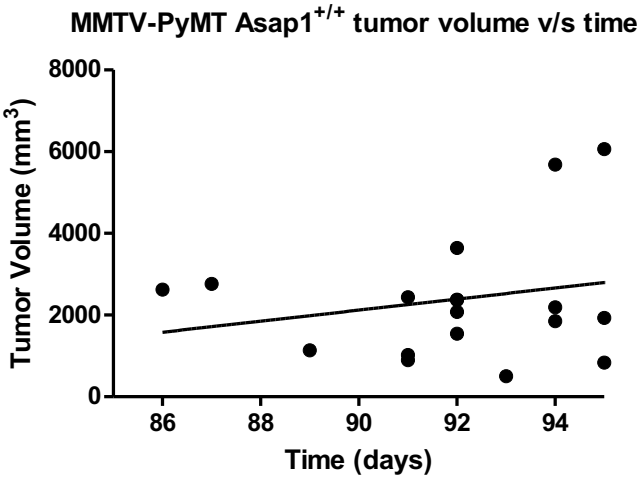

D.

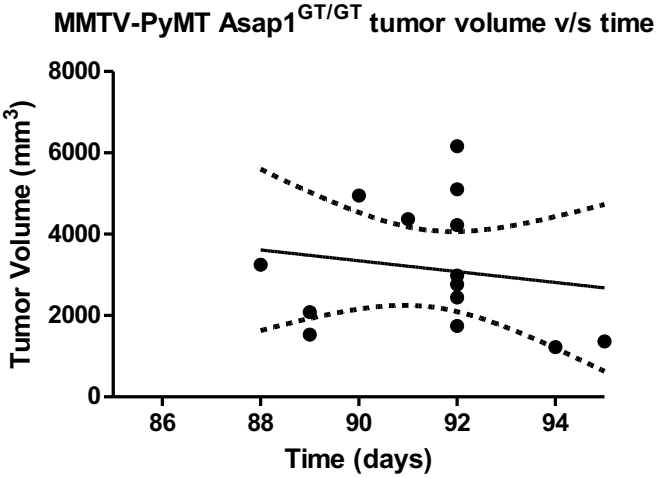

Figure 21. Tumor growth characteristics of MMTV-PyMT Asap1$^{+/+}$ and MMTV-PyMT Asap1$^{GT/GT}$ Mice. (A) Tumor-free survival curves showing that MMTV-PyMT Asap1$^{GT/GT}$ mice (n=19) develop tumors earlier than MMTV-PyMT Asap1$^{+/+}$ mice (n=16) at 52.5 days as compared to 60 days. P>0.05. (B) Tumor growth curves showing that PyMT Asap1$^{GT/GT}$ mice bear significantly higher volumes of tumor at week 10 (p=0.0061), week 11 (0.0036) and week 12 (0.0133) as compared to PyMT Asap1$^{+/+}$ mice. The dotted boxes at week 13 display tumor growth as depicted by linear regression analysis that reveals exponential growth phase of PyMT Asap1$^{+/+}$ tumors (C) and plateau phase of PyMT Asap1$^{GT/GT}$ tumors (D).

The PyMT Asap1$^{+/+}$ and PyMT Asap1$^{GT/GT}$ mice formed tumors with short latency periods and high penetrance. Nevertheless, they exhibited a comparable mean tumor burden when lungs were isolated from them for the purpose of analysing metastasis formation (Figure 22 A*)*. It was found that PyMT Asap1$^{GT/GT}$ lungs contained significantly higher number of superficial metastatic foci on the lung surface as compared to PyMT Asap1$^{+/+}$lungs (Figure 22 B*)*. Lungs from these mice were embedded in paraffin, sectioned and stained using hematoxylin and eosin to study micrometastases. A total of 10 sections (5 μm thick), 100 μm apart were selected. The number of deep metastatic lesions was counted and it was found that PyMT Asap1$^{GT/GT}$ lungs again showed higher number of metastases (Figure 22 C*)* and larger metastatic foci size (Figure 22 D*)*. Although this difference was not found to be statistically significant, the trend is similar to the surface metastasis count.

Given that PyMT Asap1$^{GT/GT}$ mice formed tumors earlier than PyMT Asap1$^{+/+}$ mice, it is reasonable to argue that *Asap1* knockout tumors can colonize the lung earlier than Asap1$^{+/+}$ tumors. Furthermore, the metastatic foci formed by Asap1$^{+/+}$ tumors were fewer in number and smaller in size than those formed by Asap1$^{GT/GT}$ tumors. Together the data from the metastasis study shows that absence of *Asap1* confers an enhanced metastatic potential on the primary mammary tumor in the PyMT model of breast cancer.

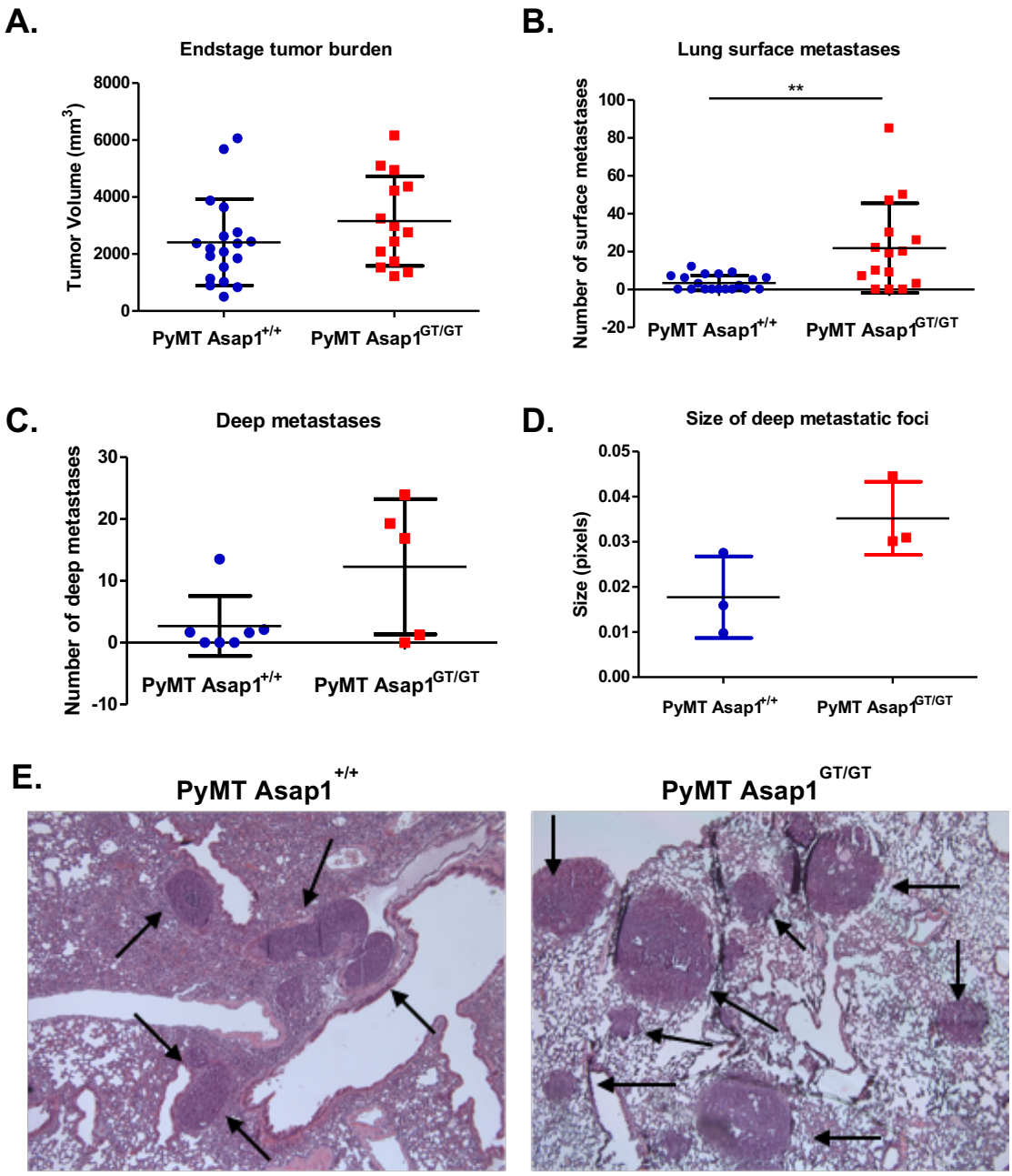

Figure 22. Metastasis study in MMTV-PyMT Asap1 $^{+/+}$ and MMTV-PyMT Asap1$^{GT/GT}$ mice. (A) PyMT Asap1$^{+/+}$ and PyMT Asap1$^{GT/GT}$ mice display comparable total tumor volumes when lungs were isolated from them for metastasis studies. Total tumor volume refers to the sum of the volumes of all the mammary tumors formed in the animal. (B) Surface metastases as counted on the lung lobes of the mice show that PyMT Asap1$^{GT/GT}$ mice have significantly higher metastases (p=0.0021) as compared to PyMT Asap1$^{+/+}$ mice. Deep metastasis count as obtained from sectioning the lungs and counting the metastasis reveals a similar trend as that of surface metastasis and shows that PyMT Asap1$^{GT/GT}$ mice have more number (C) and bigger (D) metastasis than PyMT Asap1$^{+/+}$ mice, although the difference was not statistically significant. (E) shows H&E stained images of PyMT Asap1$^{+/+}$ and PyMT Asap1$^{GT/GT}$ lungs. Arrows indicate metastatic foci.

3.12 Morphological and molecular analysis of tumors from MMTV-PyMT Asap1$^{GT/GT}$ and MMTV-PyMT Asap1$^{+/+}$ mice

To determine whether deletion of *Asap1* leads to modification of tumor subtype, tissue of cancer origin, or other characteristics of the primary and metastatic tumors, tumors from PyMT Asap1$^{+/+}$ and PyMT Asap1$^{GT/GT}$ mice were isolated and formalin-fixed. Sections were stained with hematoxylin and eosin, and also used for immunohistochemistry. As normal breast tissue is composed of three types of cells – luminal, basal and myoepithelial – antibodies against markers of these cell types were used. Luminal cells express cytokeratins (CK) 7, 8, 18, 19, estrogen receptor (ER) and progesterone receptor (PR). Basal cells express CK 5/6, 14, 17. Myoepithelial cells express basal cell-type CKs and other markers like smooth muscle actin ((Böcker et al., 1992). The tumor sections obtained from PyMT Asap1$^{+/+}$ and PyMT Asap1$^{GT/GT}$ mice were therefore stained with antibodies against luminal (CK18), basal (CK14) and myoepithelial (smooth muscle actin) markers. The staining revealed that tumors from both PyMT Asap1$^{+/+}$ and the PyMT Asap1$^{GT/GT}$ mice stained for luminal cytokeratin as well as basal cytokeratin. The staining confirmed the epithelial origin of the tumors.

In the normal breast, the interstitial fibroblasts do not express α-smooth muscle actin (SMA) whereas peritumoral stromal myofibroblasts in breast carcinoma have been shown to express this protein ((Rønnov-Jessen et al., 1995). SMA staining is therefore used as a marker for activated stromal fibroblasts. It was found that PyMT Asap1$^{GT/GT}$ mice displayed a more intense SMA staining (Figure 23*)*, suggesting that differences exist in the tumor stroma in PyMT Asap1$^{GT/GT}$ mammary tumors compared to PyMT Asap1$^{+/+}$ tumors.

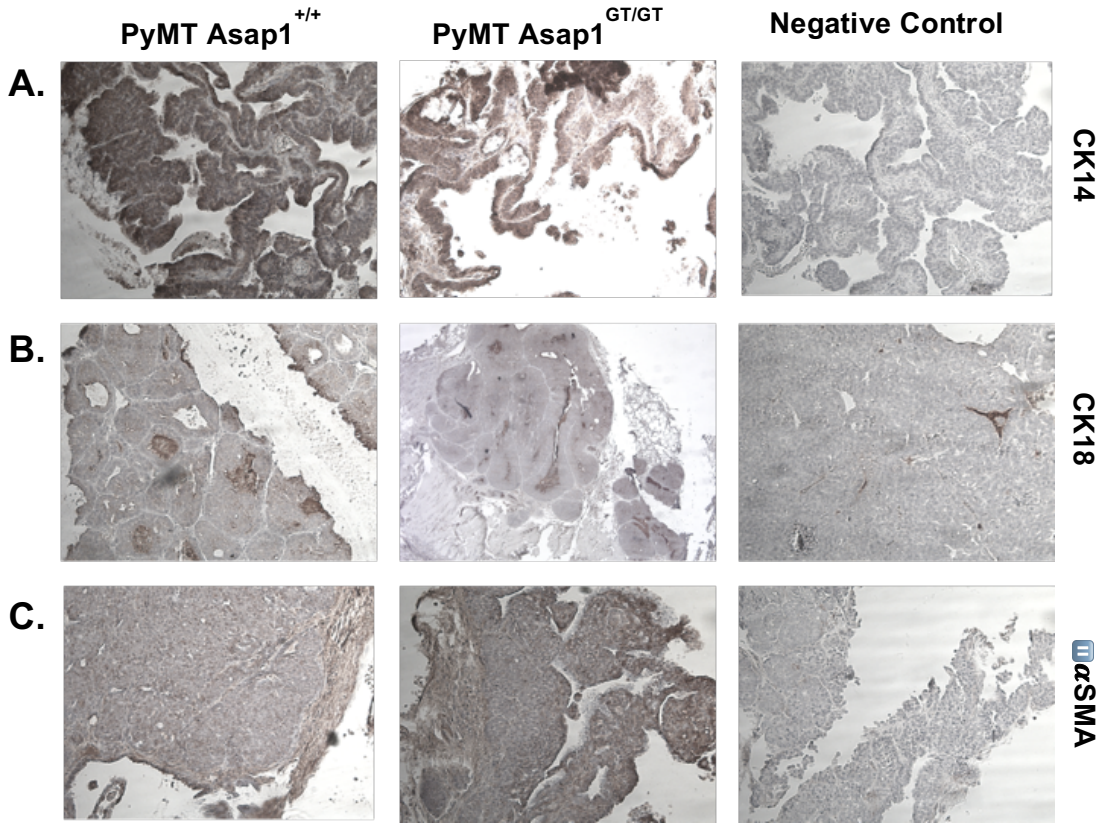

Figure 23. Immunohistochemistry of PyMT Asap1$^{+/+}$ and PyMT Asap1$^{GT/GT}$ tumors showing the epithelial nature of the mammary tumors. Cytokeratin staining (CK14) reveals a concomitant expression of basal subtype (A) and a luminal (CK18) subtype (B) of breast tumor. SMA staining (C) reveals a reactive stroma in PyMT Asap1$^{GT/GT}$ tumors. Immunostaining was achieved using specified antibodies and NovaRed (red/brown color) and tissues were counterstained with hematoxylin (blue color).

3.13 Properties of tumor cells derived from tumors of MMTV-PyMT Asap1$^{GT/GT}$ and MMTV-PyMT Asap1$^{+/+}$ mice

3.13.1 Cell migration and adhesion assays

To investigate in more detail how loss of ASAP1 modified tumor growth and metastasis, I isolated tumor cells from PyMT Asap1$^{+/+}$ and PyMT Asap1$^{GT/GT}$ tumors and established them in culture. I also isolated embryonic fibroblasts from Asap1$^{+/+}$ and Asap1$^{GT/GT}$

mice, and used these cells as positive controls to study the processes of cell migration and adhesion.

As ASAP1 has been implicated in regulating cell migration, wound-healing migration assays were performed, in which cultured monolayers of Asap1$^{+/+}$and Asap1$^{GT/GT}$ fibroblasts and PyMT Asap1$^{+/+}$and Asap1$^{GT/GT}$ tumor cells were wounded and allowed to heal over a period of time. In comparison to Asap1$^{+/+}$ fibroblasts, Asap1$^{GT/GT}$ fibroblasts showed significantly reduced cell migration 6,12 and 18 hours after monolayer wounding. This effect was quantified as percent wound-healing. Whereas Asap1$^{+/+}$ fibroblasts display complete wound closure at 18 hours, Asap1$^{GT//GT}$ fibroblasts are only able to close 46.9% of the wound area at this time-point (Figure 24 A, B*).* In contrast, PyMT Asap1$^{+/+}$ and PyMT Asap1$^{GT/GT}$ tumor cells displayed comparable cell migration, as PyMT Asap1$^{+/+}$ tumor cells closed 55% and PyMT Asap1$^{GT/GT}$ tumor cells closed 65% of the wounded area 24 hours after creation of the wound (Figure 24 C, D).

To study adhesion defects, a spreading assay was performed in which cells were seeded on a fibronectin-coated plate and fixed at certain time intervals. The percentage of attached cells was determined. At 40 minutes post seeding, it was found that 66.25% Asap1$^{+/+}$ fibroblasts attached to the substratum as compared to 57.52% Asap1$^{GT//GT}$ fibroblasts (Figure 24 E, F*).* No statistically significant adhesion differences were observed between PyMT Asap1$^{+/+}$ and PyMT Asap1$^{GT/GT}$ tumor cells as comparable percentage of cells from wild-type and *Asap1* knockout tumors – 57.75% and 54.75%, respectively, were found to attach to fibronectin-coated plates at 1 hour of seeding (Figure 24 G, H).

A.

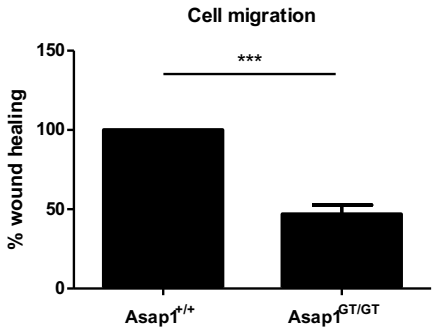
Cell migration
***
% wound healing
150
100
50
0
Asap1+/+
Asap1GT/GT

B.

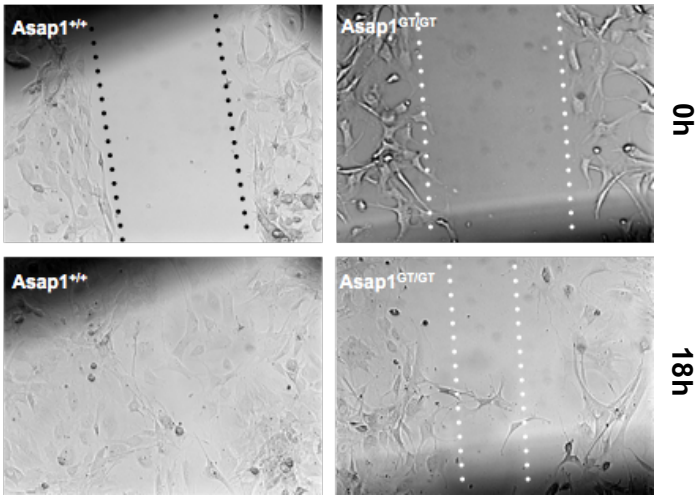
Asap1+/+
Asap1GT/GT
0h
Asap1+/+
Asap1GT/GT
18h

C.

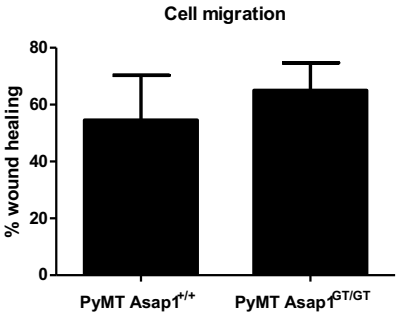
Cell migration
% wound healing
80
60
40
20
0
PyMT Asap1+/+
PyMT Asap1GT/GT

D.

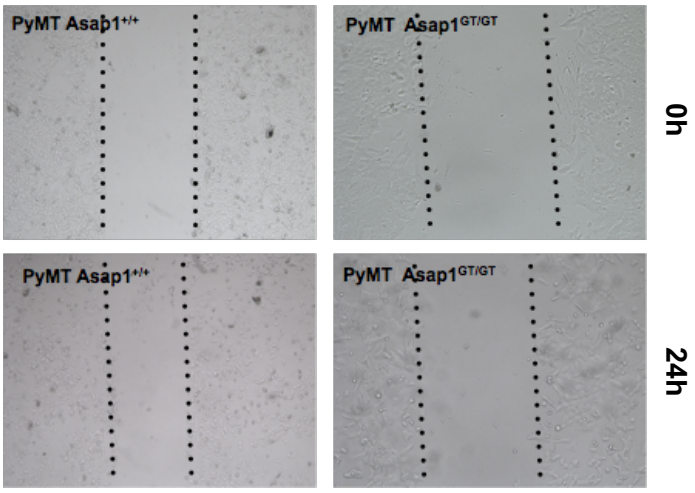
PyMT Asap1+/+
PyMT Asap1GT/GT
0h
PyMT Asap1+/+
PyMT Asap1GT/GT
24h

E.

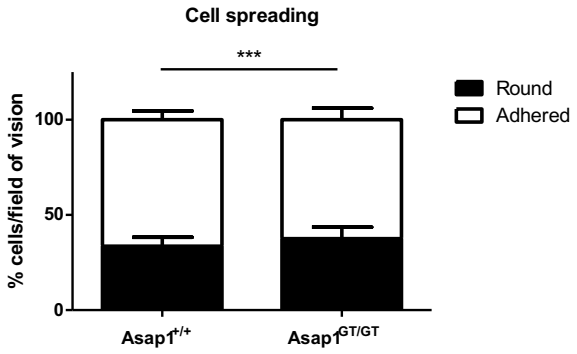
Cell spreading
***
% cells/field of vision
100
50
0
Asap1+/+
Asap1GT/GT
Round
Adhered

F.

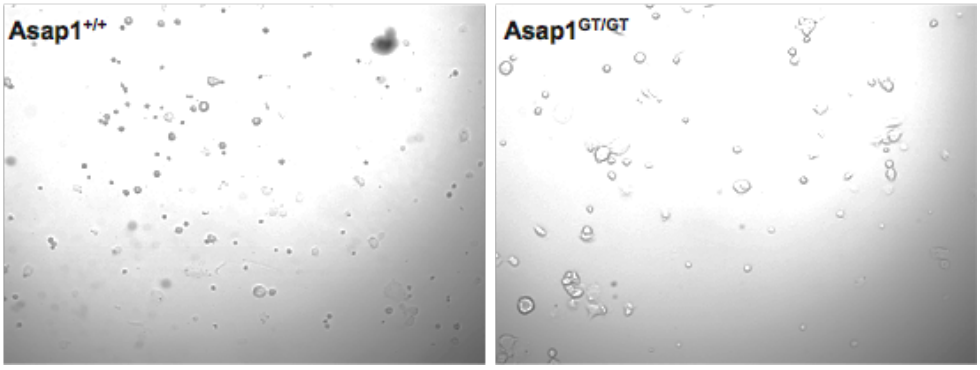
Asap1+/+
Asap1GT/GT

G.

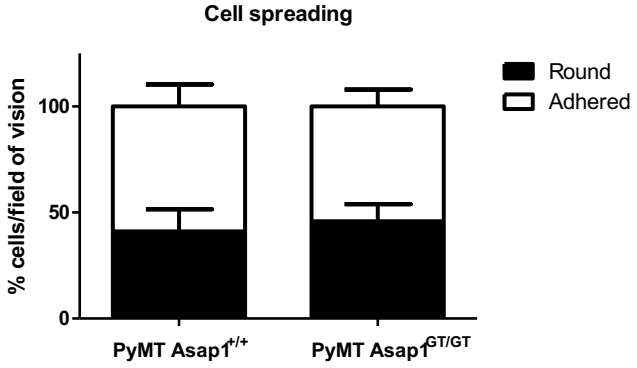
Cell spreading
% cells/field of vision
100
50
0
PyMT Asap1+/+
PyMT Asap1GT/GT
Round
Adhered

H.

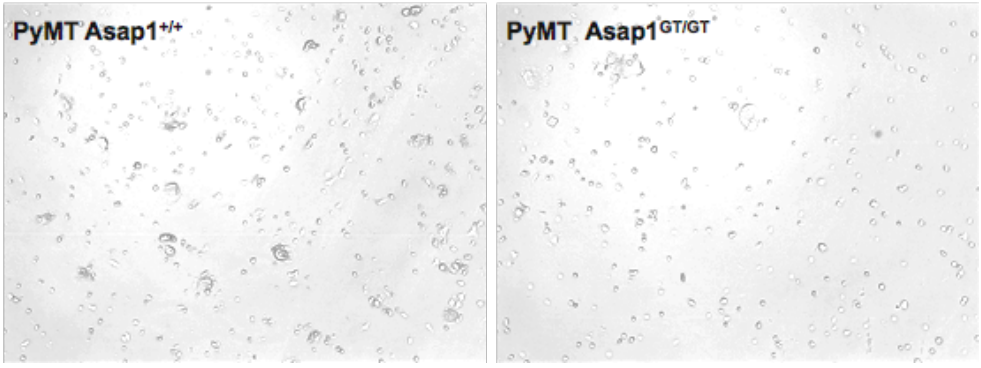
PyMT Asap1+/+
PyMT Asap1GT/GT

Figure 24. Cell migration and spreading assay in Asap1$^{+/+}$ and Asap1$^{GT/GT}$ fibroblasts and PyMT Asap1$^{+/+}$and Asap1$^{GT/GT}$ tumor cells. Asap1$^{GT/GT}$ fibroblasts show significantly reduced cell migration ($p<0.001$) as compared to Asap1$^{+/+}$ fibroblasts (A). Images of fibroblasts at 0h and 18h are shown (B). PyMT Asap1$^{+/+}$ and PyMT Asap1$^{GT/GT}$ tumor cells display comparable migration behavior (C). Images at 0h and 24h are shown (D). Asap1$^{GT/GT}$ fibroblasts show significantly reduced cell adhesion on fibronectin at 40 minutes after plating ($p<0.001$) (E). Images for Asap1$^{+/+}$ and Asap1$^{GT/GT}$ fibroblasts at this time point are shown (F). PyMT Asap1$^{+/+}$and Asap1$^{GT/GT}$ tumor cells do not display any cell adhesion differences (G). Images at 1h are shown for tumor cells.

3.13.2 Studying the actin cytoskeleton

Specific cellular machineries are known to be involved in enabling motility. Having observed migration and adhesion defects in Asap1$^{GT/GT}$ fibroblasts, I next investigated whether proteins associated with motility-enabling structures were affected by the absence of ASAP1. When stained for ASAP1, Asap1$^{GT/GT}$ fibroblasts and PyMT Asap1$^{GT/GT}$ tumor cells showed no expression of ASAP1, thus confirming the deletion of *Asap1* (Figure 25 B, D). In Asap1$^{+/+}$ fibroblasts and PyMT Asap1$^{+/+}$ tumor cells, ASAP1 showed cytoplasmic and perinuclear localization (Figure 25 A, C*).* Actin fibers did not exhibit any striking visual difference in the absence of ASAP1.

ASAP1 has previously been shown to colocalize with several focal adhesion markers such as β1 integrin, paxillin, FAK and vinculin. Hence, I hypothesized that focal adhesion assembly may be perturbed in the absence of *Asap1*. To test this possibility, I stained Asap1$^{+/+}$ and Asap1$^{GT/GT}$ fibroblasts and PyMT Asap1$^{+/+}$and Asap1$^{GT/GT}$ tumor cells with vinculin and actin so as to analyze focal adhesions and actin fibers in these cells. Asap1$^{+/+}$ fibroblasts showed a more intense vinculin staining as compared to Asap1$^{GT/GT}$ fibroblasts (Figure 26 A, C*)*. Stress fiber formation was not affected by the loss of *Asap1*, as visually no differences were observed in the actin stress fibers formed by Asap1$^{+/+}$ and Asap1$^{GT/GT}$ fibroblasts (Figure 25 A, B and Figure 26 A, C*)*. PyMT Asap1$^{+/+}$ cells showed very specific vinculin staining at the periphery so that distinct focal adhesions were visible at the cell edge. In contrast, PyMT Asap1$^{GT/GT}$ cells showed an increased, yet random arrangement of focal adhesions throughout the

cytoplasm and little staining at the periphery, implying a less efficient ability to organize and/or traffic cytoskeletal and focal adhesion proteins (Figure 26 E, G).

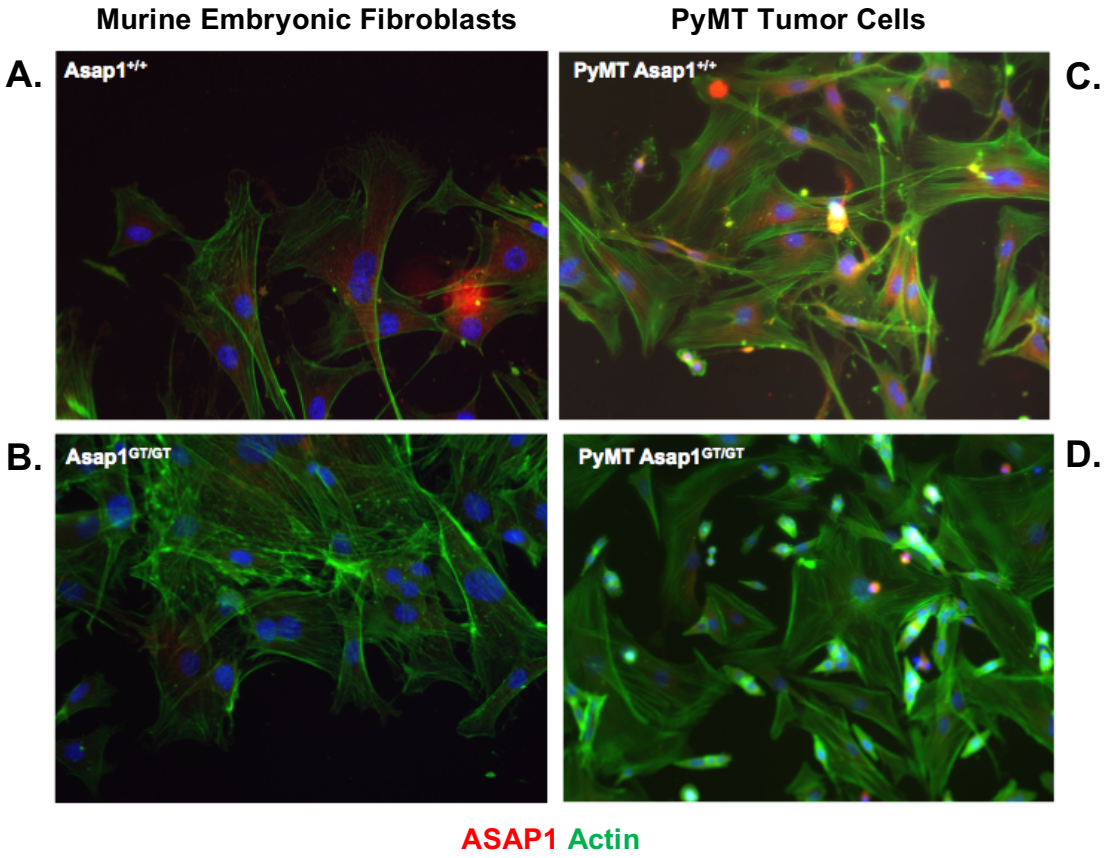

Figure 25. Actin cytoskeleton in Asap1$^{+/+}$ and Asap1$^{GT/GT}$ fibroblasts and PyMT Asap1$^{+/+}$and Asap1$^{GT/GT}$ tumor cells. Loss of *Asap1* does not affect actin framework in fibroblasts and tumor cells derived from PyMT mice. ASAP1 staining confirms its cytoplasmic and perinuclear localization (A, C). No ASAP1 staining was observed in Asap1$^{GT/GT}$ fibroblasts (B) and PyMT Asap1$^{GT/GT}$ tumor cells (D), showing deletion of *Asap1* in these cells.

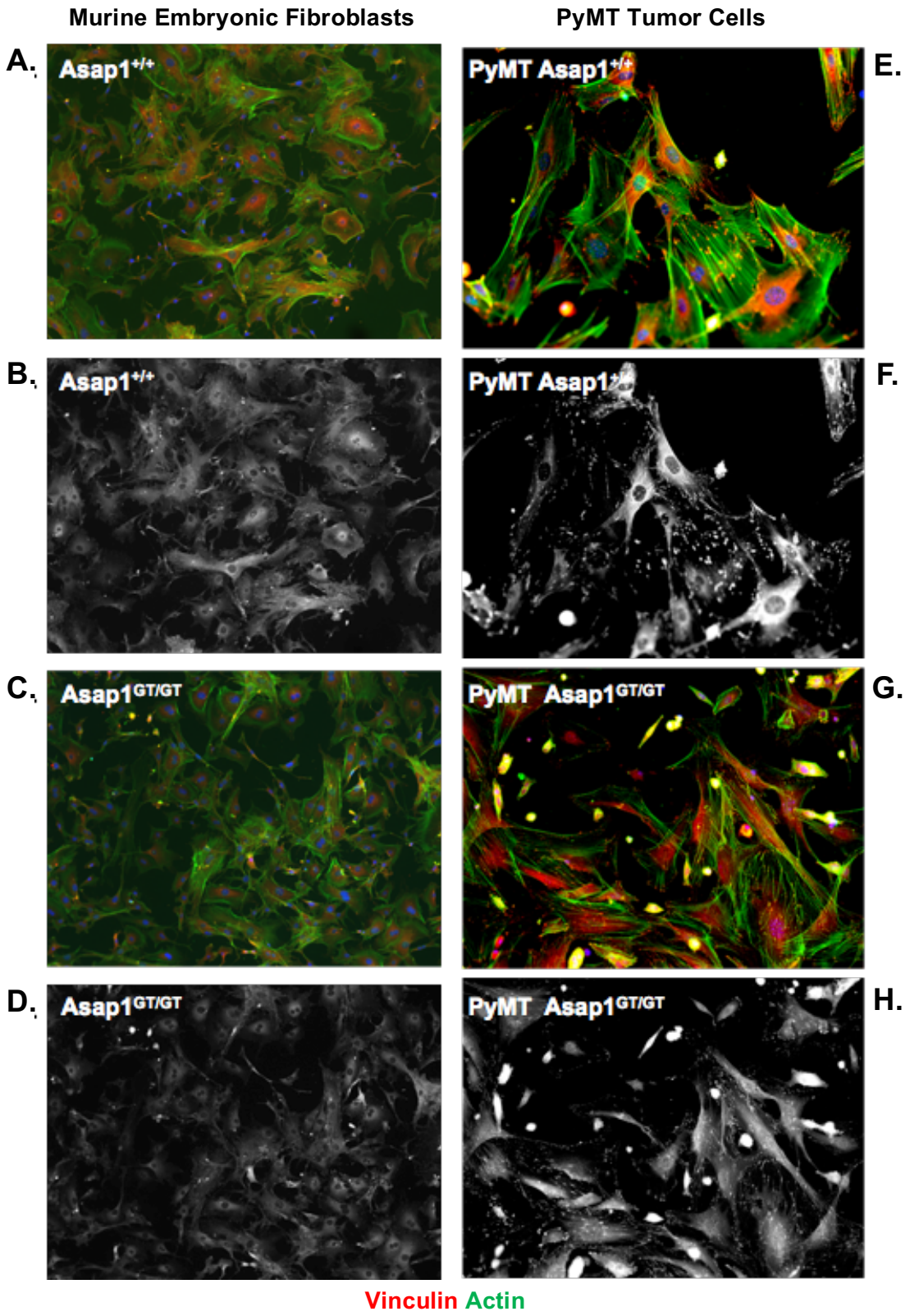
Murine Embryonic Fibroblasts
PyMT Tumor Cells
A.
Asap1+/+
E.
PyMT Asap1+/+
B.
Asap1+/+
F.
PyMT Asap1+/+
C.
Asap1GT/GT
G.
PyMT Asap1GT/GT
D.
Asap1GT/GT
H.
PyMT Asap1GT/GT
Vinculin Actin

Figure 26. Inefficient focal adhesion assembly in Asap1$^{GT/GT}$ fibroblasts and PyMT Asap1$^{GT/GT}$ tumor cells. Asap1$^{+/+}$ fibroblasts display a more intense staining for vinculin, a focal adhesion marker (A, B) as compared to Asap1$^{GT/GT}$ fibroblasts (C, D) and PyMT Asap1$^{+/+}$ tumor cells show extremely specific vinculin staining that display organized peripheral focal adhesions (E, F) as against PyMT Asap1$^{GT/GT}$ tumor cells that exhibit an increased, yet randomly arranged focal adhesions (G, H). These results demonstrate defective focal adhesion assembly in the absence of *Asap1*. Black and white images (B, F, D, and H) show intense and specific vinculin staining.

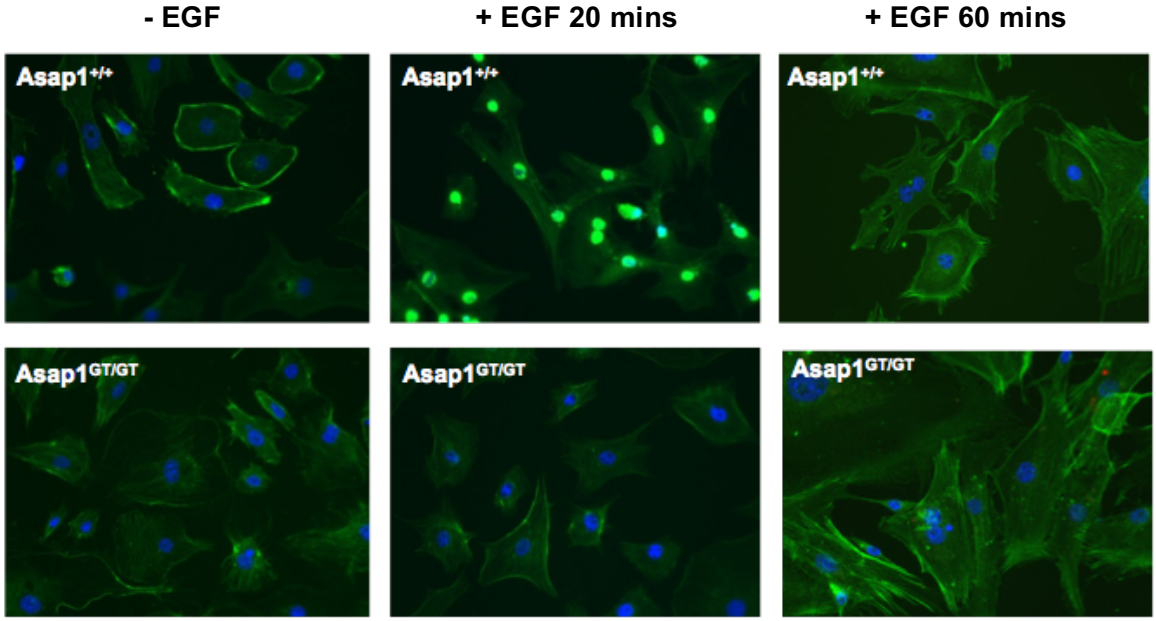

Figure 27. Inefficient remodeling of actin in Asap1$^{GT/GT}$ fibroblasts upon EGF stimulation. The resting phenotype of fibroblasts undergoes a change when the cells are stimulated to move, in response to EGF. Asap1$^{+/+}$ fibroblasts display a strong expression of nuclear actin after 20 minutes of EGF treatment thus showing that they are able to remodel their actin framework as opposed to Asap1$^{GT/GT}$ fibroblasts, which do not change their resting phenotype after addition of EGF. The expression of nuclear actin is temporary, after cells return to their original resting states.

The results obtained are indicative of a perturbed actin cytoskeleton in Asap1$^{GT/GT}$ fibroblasts, as demonstrated by their reduced cell migration, reduced cell spreading and disorganized focal adhesion assembly. Next, I therefore decided to study the cytoskeleton of these cells in response to a migratory stimulus, namely epidermal growth factor (EGF). When cells were treated with EGF and monitored over the

specified time periods, it was found that Asap1$^{+/+}$ fibroblasts exhibited an accumulation of actin in their nuclei. The nuclear actin was visible 20 minutes after the addition of EGF to the cells and remained until about 50 minutes after EGF addition, after which the resting phenotype of the cell was restored. In the case of Asap1$^{GT/GT}$ fibroblasts, no such remodeling of actin was observed until much later time points (data for later time-points not shown), indicating that actin remodeling is impaired in *Asap1* deficient fibroblasts (Figure 27*).*

3.14 Studying the effects of ASAP1-SLK interactions

In line with the observations pertaining to the role of *Asap1* in regulating the actin cytoskeleton, certain interaction partners of ASAP1, like c-src, SLK and cortactin have been documented to functionally contribute towards podosome formation and adhesion structures that are typically formed in migrating cells that facilitate processes of invasion and matrix remodeling ((Brown et al., 1998; Onodera et al., 2005; Wagner et al., 2002). One of these interaction partners, Ste20-like kinase (SLK) was shown to co-immunoprecipitate with ASAP1 ((Müller et al., 2010) and I chose to study how the interaction of ASAP1 with SLK might influence the actin cytoskeleton. For this, I stimulated the Asap1$^{+/+}$ and Asap1$^{GT/GT}$ fibroblasts to move by wounding cell monolayers, and then stained these cells for specific markers of cytoskeletal proteins and focal adhesions. In mouse fibroblasts, SLK has been shown to colocalize with the microtubule network and peripheral focal adhesions as reflected by α-tubulin and vinculin staining ((Wagner et al., 2002). I therefore investigated whether the interaction of SLK with the cytoskeleton and focal adhesions is influenced by ASAP1. After monolayer wounding and subsequent healing, Asap1$^{+/+}$ and Asap1$^{GT/GT}$ fibroblasts were stained with SLK and actin antibodies. SLK did not co-localize with actin, irrespective of ASAP1 expression (Figure 28 A, D and G, J).

An increase in tubulin staining was observed in Asap1$^{+/+}$ fibroblasts, 12 hours post-wounding. In Asap1$^{GT/GT}$ fibroblasts, however, tubulin expression remained unchanged (Figure 28 B, E and H, K*)*. Vinculin expression increased in Asap1$^{+/+}$ fibroblasts 12

hours after cells were stimulated to move by wounding their monolayer. In contrast, Asap1$^{GT/GT}$ fibroblasts displayed unchanged vinculin expression (Figure 28 C, F and I, L).

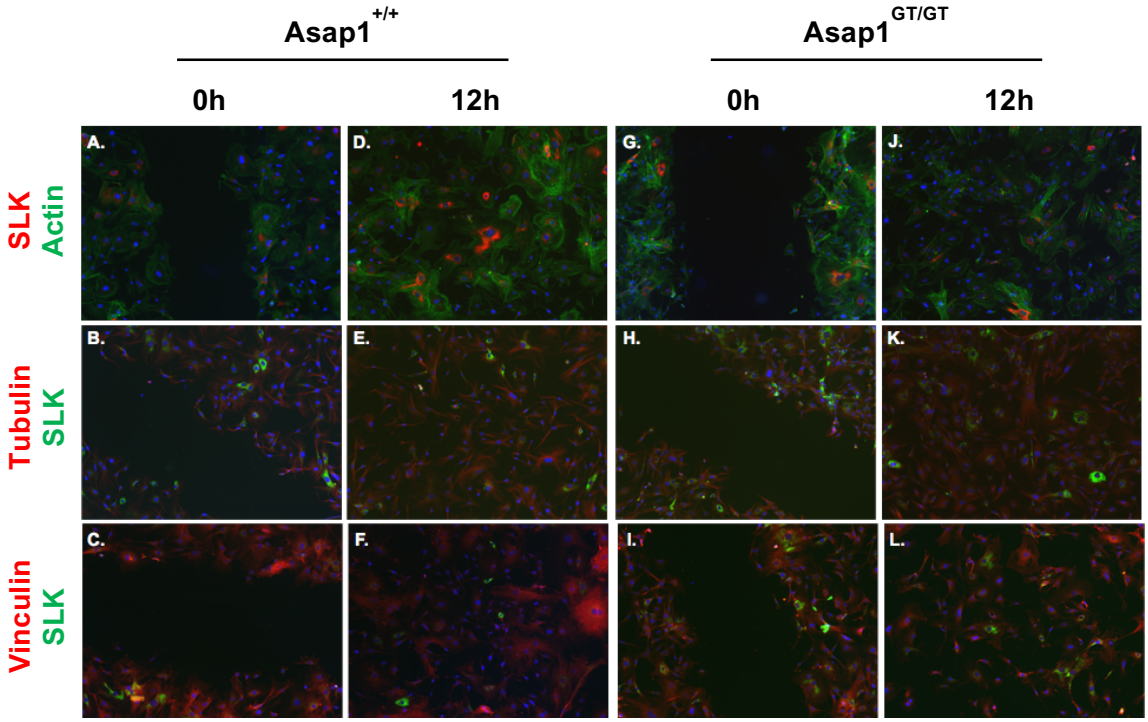

Figure 28. Effects of SLK on cytoskeleton and focal adhesion in Asap1$^{+/+}$ and Asap1$^{GT/GT}$ fibroblasts. When the cells were stimulated to move, by wounding their monolayers and letting them heal, SLK did not colocalize with actin (A, D, G, J); tubulin expression increased in Asap1$^{+/+}$ fibroblasts (E) but not in Asap1$^{GT/GT}$ fibroblasts (K); increased vinculin expression observed in Asap1$^{+/+}$ fibroblasts (F) but not in Asap1$^{GT/GT}$ fibroblasts (L). Respective control images at 0h are also shown (A, B, C, G, H, I).

After having studied the role of SLK on the expression of tubulin and vinculin, I next explored whether ASAP1 affected the expression of SLK, and for this Asap1$^{+/+}$ and Asap1$^{GT/GT}$ fibroblasts were stained with SLK. It was observed that Asap1$^{GT/GT}$ fibroblasts exhibited reduced SLK staining as compared to Asap1$^{+/+}$ fibroblasts (Figure 29 A). This effect was quantified and indeed, SLK expression was found to be significantly reduced in Asap1$^{GT/GT}$ fibroblasts (Figure 29 B). The decline in SLK expression was also assessed by immunoblotting and I observed that SLK expression

was drastically reduced in Asap1$^{GT/GT}$ fibroblasts (Figure 29 C*)*. In another experiment (performed by Katharina Fibi, data not shown), it was found that SLK transcript levels were not altered in Asap1$^{+/+}$ and Asap1$^{GT/GT}$ fibroblasts. This implies that Asap1$^{+/+}$ and Asap1$^{GT/GT}$ fibroblasts express similar levels of SLK mRNA, however there is a significant reduction in the protein levels of SLK in Asap1$^{GT/GT}$ fibroblasts, suggesting a role for ASAP1 in stabilizing the SLK protein.

Next, I checked whether ASAP1 colocalizes with SLK, with which it also co-immunoprecipitates. However, I found that these two proteins exhibit distinct subcellular localizations and do not colocalize (Figure 29 D*)*. I studied the expression of SLK in the tumors obtained from PyMT Asap1$^{+/+}$ and PyMT Asap1$^{GT/GT}$ mice, and found that the reduction of SLK expression in the absence of ASAP1 was also reflected in the tumors, and that PyMT Asap1$^{GT/GT}$ tumors displayed reduced SLK staining as compared to PyMT Asap1$^{+/+}$ tumors (Figure 29 E*)*.

Taken together, the data suggest that in the absence of ASAP1, mouse fibroblasts have an impaired ability to reorganize actin cytoskeleton and focal adhesion assembly, leading to reduced cell migration and spreading on fibronectin. Protein expression of SLK, but not SLK mRNA, was also severely reduced in the absence of ASAP1, implying that ASAP1 is an important factor to maintain the stability of SLK.

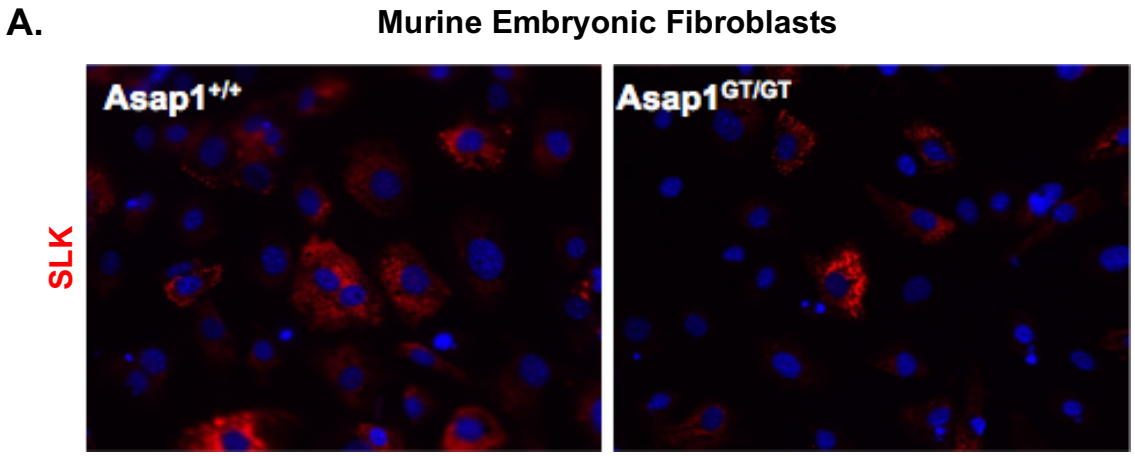

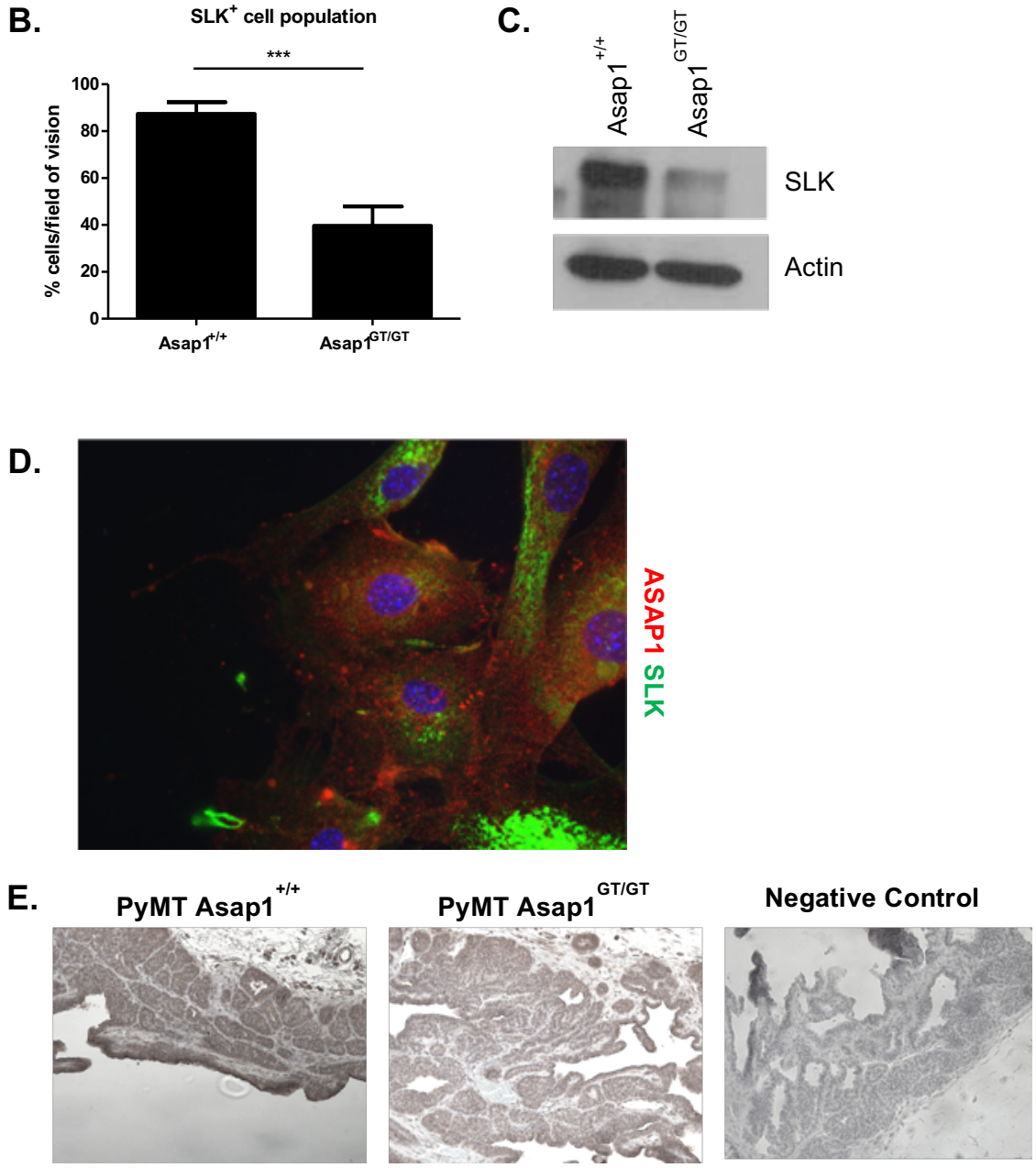

Figure 29. ASAP1-SLK interactions. Reduced SLK expression in Asap1$^{GT/GT}$ fibroblasts (A) and quantification of this effect (B) that shows significant reduction ($p<0.001$) of SLK^{+} cells in *Asap1* deficient fibroblasts. SLK protein levels, as seen by immunoblotting, are also reduced in Asap1$^{GT/GT}$ fibroblasts (C). ASAP1 (red) and SLK (green) do not colocalize (D). Tumors obtained from PyMT Asap1$^{+/+}$ and PyMT Asap1$^{GT/GT}$ mice, stained for SLK show decreased SLK expression in PyMT Asap1$^{GT/GT}$ tumors (E). Tissues were stained with SLK antibody and NovaRed (red/brown color) and counterstained with hematoxylin (blue color).

4. Discussion

Previous work in the Sleeman lab has shown that *Asap1* is functionally involved in the process of metastasis, and consistently is correlated with poor prognosis of colorectal cancer patients. During my thesis work, my aim was to decipher normal physiological roles for *Asap1* as well as to understand its function in the cancer context. To this end, I worked with mice with targeted deletion of *Asap1*. Deletion of *Asap1* results in partially penetrant neonatal lethality. The surviving pups manifest *Asap1* deficiency in the form of severe growth retardation and respiratory distress. Angiogenesis is reduced in the absence of *Asap1*. Using autochthonous models of breast cancer, I studied breast tumor development and metastasis in mice harboring global deletion of *Asap1*. The phenotype associated with the loss of *Asap1* in murine models of breast cancer is a shorter tumor-free survival, more aggressive tumor growth and higher numbers of metastases.

4.1 Mouse phenotype in the absence of *Asap1*

4.1.1 Growth retardation and respiratory distress

Adult Asap1$^{GT/GT}$ mice do not display any overt phenotype and are morphologically undistinguishable from wildtype mice. However, Asap1$^{GT/GT}$ mice display a disparity in the Mendelian ratio of offspring born from *Asap*$^{+/GT}$ mice breeding, in that, the number of homozygous *Asap1* knockout survivors is drastically reduced at birth. Two prominent features pertaining to Asap1$^{GT/GT}$ neonates are revealed upon their birth. First, many Asap1$^{GT/GT}$ neonates are found dead at birth, and secondly, the surviving neonates are growth retarded and display significantly reduced breathing rates, a phenomenon known as bradypnea. For a newborn pup, the first extrauterine challenge is to be able to breathe, and defects in multiple physiological systems could work to interfere with normal breathing (Turgeon and Meloche, 2009). *Wnt7b* promotes mesenchymal proliferation and supports vascular development in the lung. *Wnt7b* deficient mice die within 10 minutes of being born and their small and collapsed lungs exhibit vascular

defects that results in vessel rupture and hemorrhage at birth (Shu et al., 2002). Another important regulator of the lung mesenchyme is *Fgf9*, in the absence of which, mice display reduced branching complexity that leads to abnormally small lungs, and this results in neonatal lethality in these mice (Colvin et al., 2001). In contrast, *Asap1* mutants do not exhibit collapsed, hemorrhagic lungs. Rather, functional analyses revealed differences in lung aeration areas, with Asap1$^{GT/GT}$ lungs displaying many areas of thick mesh-like parenchyma as opposed to the well-aerated parenchyma in Asap1$^{+/+}$ lungs.

Surfactant production and clearance of the liquid from the lung are required to attain normal respiration after birth. Failure to achieve this could lead to neonatal death shortly after birth and respiratory distress in the living pups, similar to the phenotype observed in *Asap1* mutant mice. Surfactant protein B coding gene *Sftpb* deletion results in production of aberrant surfactant lipids that disrupt lung inflation, leading to cyanosis and death of pups within a few minutes (Clark et al., 1995). Further studies on understanding bradypnea in Asap1$^{GT/GT}$ pups could benefit from exploring whether absence of *Asap1* affects biosynthesis of surfactants.

A number of non-cell-autonomous factors could also conceivably affect breathing in Asap1$^{GT/GT}$ pups, and these may include endocrinal defects that affect lung development. Corticotropin-releasing hormone (CRH) deficient mice show dependency on glucocorticoid for lung maturation in fetal lungs. CRH deficient mice grow up normally and are fertile, with no overt phenotype, indicating a role of glucocorticoids during fetal rather than postnatal life (Muglia et al., 1995). Prostaglandins have been shown to be important players in the closure of ductus arteriosus, required for the transition from the fetal (placental) circulation to respiratory circulation (increased blood flow to the lung). Accordingly, mice deficient in prostaglandin E_2 receptor gene die between 24-48 hours after birth due to lung edema and congestive heart failure (Segi et al., 1998). *Kif1b* deficient mice that no longer have the ability to produce a microtubule motor protein necessary for axonal transport, die due to failure in lung expansion (Zhao et al., 2001). Targeted deletion of muscle regulatory factor myogenin is responsible for

cyanosis and death in neonates arising due to insufficient respiration from a defective diaphragm (Nabeshima et al., 1993). It will therefore be interesting in future work to explore whether these factors play a role in the breathing defect observed in ASAP1 deficient mice

4.1.2 Ossification defects

Through careful perinatal analysis, it was revealed that Asap1$^{GT/GT}$ embryos and neonates both exhibited significantly smaller sizes and weights as compared to their wildtype counterparts. This stunted growth in the absence of *Asap1* may be critical for breathing and overall survival of Asap1$^{GT/GT}$ neonates. The skeleton spans throughout the body, and is comprised of two distinct tissues, cartilage and bone (Karsenty and Wagner, 2002). Osteogenesis encompasses two major processes of bone formation, namely intramembranous and endochondral ossification, both involving transformation of pre-existing mesenchymal tissue into bone tissue. Intramembranous ossification occurs when the pre-existing mesenchymal tissue converts directly into bone, like the bones of the skull. The other mode of bone formation, known as endochondral ossification occurs when the mesenchymal tissue is converted into cartilage and then to bone, like all the bones in the body other than those of skull and clavicle (Gilbert, 2000). Asap1$^{GT/GT}$ embryos display defective ossification, and interestingly, the absence of *Asap1* results in defects in both intramembranous as well as endochondral ossification. Such defects may work to predispose the growing embryo to growth retardation, in the absence of *Asap1.* Mice deficient for *Runx2* die shortly after birth due to lack of breathing. Maturational arrest of osteoblasts in these mice leads to complete blockage of intramembranous and endochondral ossification (Komori et al., 1997). Abnormal respiration could also result from either a complete absence or a smaller rib cage associated with inefficient lung inflation, as seen in *Myf5* knockout mice and *Tbx18* null mice, respectively (Braun et al., 1992; Bussen et al., 2004). *Asap1$^{GT/GT}$* neonates have a developed rib cage, ribs and sternum, however size of the thoracic cavity remains to be studied in these pups.

Many chromosomes harbor regions that contain clusters of genes that may have similar functions, and mutations in these regions often lead to similar disease phenotypes. It is interesting to note that chromosome 8 contains at least two distinct gene clusters – genes involved in epilepsies, on the long arm, and presumptive tumor suppressor genes on the short arm. There are some genes present in proximity to *Asap1* that may be of interest. These include CCAL1 (chondrocalcinosis) at 8q, NBS1 (Nijmegen breakage syndrome 1) at 8q21, and PLEC1 (plectin 1) and TNFRSF11B (tumor necrosis factor receptor superfamily 11b) both at 8q24. Mutations in these genes lead to abnormalities of the bone and muscle, for example, CCAL1 is implicated in chondrocalcinosis with early-onset osteoarthritis, NBS results in growth retardation, immunodeficiency and predisposition to cancers, PLEC1 mutations are associated with muscular dystrophy, and mutated TNFRSF11B causes juvenile Paget's disease that affects bone growth (Carney et al., 1998; Hilton and Wells, 2001). It is not unprecedented that targeted mouse mutations may result in up- or down- regulation of neighboring genes (West et al., 2016). In the case of *Asap1*, such mutations in the neighboring gene may produce phenotypes that exhibit growth retardation, muscular dystrophy or bone defects. This is however unlikely, given the strong phenotype that correlates well with the absence of *Asap1.*

The regulation of the process of cartilage formation is crucial to embryonic bone development and postnatal bone growth. Upon exiting from the cell cycle, hypertrophic chondrocytes undergo apoptosis so as to be replaced by bone (Ye et al., 2005). In the context of chondrocytes, the absence of *Asap1* may orchestrate generation of multinucleate cells following cytokinesis failure, which may lead to increased apoptosis. In *Drosophila*, Asap regulates cleavage furrow biosynthesis by recycling Arf1 to the Golgi from post-Golgi membranes thereby organizing Golgi and providing optimal Golgi output (Rodrigues et al., 2016). Upon cytokinesis failure, cells either undergo apoptosis or cell cycle arrest and senescence, and the presence of multinucleate cells positively correlates with apoptosis (Mason and Bessler, 2011). Thus the absence of *Asap1* in the Asap-Arf1-Golgi pathway for biosynthesis of cleavage furrow may orchestrate the generation of multinucleate cells following cytokinesis failure, which may lead to

increased apoptosis. Could then, the delayed ossification as observed in Asap1$^{GT/GT}$ embryos correspond to specific time points where increased chondrocyte apoptosis does not match with osteoblast formation? In view of this possibility it would be worthwhile to explore the status of expression of various apoptotic genes such as caspases, Bcl-2 etc., in Asap1$^{GT/GT}$ embryonic cells to understand further the defective ossification phenotype of Asap1$^{GT/GT}$ embryos.

The literature does not provide evidence of *in vivo* chondrocyte motility as yet, and chondrocyte migration has been so far studied only in *in vitro* model systems. It has however, been established that these cells possess a primary cilium, in addition to other finger-like processes. The primary cilium has been proposed to be involved in mechanotransduction (McGlashan et al., 2008). The primary cilia have been demonstrated to be critical for endochondral bone formation during limb development (Haycraft et al., 2007). It is known that ASAP1 is an important scaffold protein that links Arf4 to the Rab GTPases involved in the ciliiogenesis cascade (Wang et al., 2012). ASAP1 controls cargo progression and the direction of ciliary traffic and may also control actin polymerization in the periciliary region so as to facilitate ciliary trafficking (Wang and Deretic, 2015). It is reasonable to argue that loss of *Asap1* may lead to defective cilia formation, restricting chondrocyte movement within the matrix of cartilage, and hence affecting cartilage development as observed in Asap1$^{GT/GT}$ embryos.

4.1.3 The transient nature of the Asap1$^{GT/GT}$ phenotype

Bradypnea and growth retardation are prominent phenotypes of Asap1$^{GT/GT}$ neonates at P0. However, these differences between Asap1$^{+/+}$ and Asap1$^{GT/GT}$ embryos last for only the initial 24 hours after birth. These differences gradually diminish over the next few days, and pups belonging to both genotypes display comparable values for breathing rates and growth. These data show that *Asap1* is largely dispensable for mouse embryonic development. The transient nature of the physiological phenotype associated with loss of *Asap1* may be attributed to a genetic or functional compensation mechanism. Paralogous gene redundancy is often regarded as a mechanism for lack of

a knockout phenotype. Two genes, *MyoD* and *Myf5* that are implicated in skeletal muscle development, do not have an overt phenotype when either of them are knocked out. However, mice deficient for both these genes are completely devoid of skeletal muscle (Rudnicki et al., 1993). *MyoD*-null mice show delayed limb and brachial arch muscle development, and *Myf5*-null mice have abnormal rib development, and thus these two genes display partial redundancy (Kablar et al., 1997). There also exists a possibility of an unequal genetic redundancy in paralogous genes, as in the case of knockout mice of various caspases. *Casp8* and *Casp9* knockout result in pre- and perinatal lethality, respectively whereas knockout mice of *Casp1* and *Casp12* have no detectable phenotype (Barbaric et al., 2007; Kuida et al., 1995, 1998; Varfolomeev et al., 1998). It is imperative that gene expression profiling be conducted on Asap1$^{GT/GT}$ embryos as it will enable identification of genes performing similar functions or genes belonging to signaling pathways of similar processes as regulated by *Asap1*. This could potentially lead to identification of new, previously undescribed phenotype in multiple gene knockout mice involving *Asap1* deletion, and thus divulge novel roles of this gene.

Previous studies on the other two members of ASAP family, namely ASAP2 and ASAP3, do not report their cellular expression pattern. Future work will describe tissue/organ-specific expression of ASAP1 isoforms to answer the intriguing question of whether functional diversity exists within the ASAP family. The present study provides the first look at the global pattern of ASAP1 expression in mouse tissue. With this knowledge, it is now possible to focus on specific physiological processes that may be regulated by ASAP1 and its isoforms, either in combination or independently. There is also a possibility that a shift in the expression of isoforms occurs during embryonic development, and this may also be revealed by studies on mice harboring deletion of these isoforms. It has previously been reported that two ARF-GAP GIT family members, GIT1 and GIT2 display differential expression in mice tissue. Mice deficient for GIT1 and GIT2 show a broad distribution of GIT2, whereas GIT1 expression was found to be restricted to certain cell populations. A developmental shift in the expression of these genes occurs in testis, where GIT2 is expressed by spermatogonia and mature spermatids express GIT1 (Schmalzigaug et al., 2007). Studies exploring expression

pattern of ASAP1 isoforms in the *Asap1* knockout mouse model generated in our lab, coupled with studies on individually knocked out *Asap2* and *Asap3* will contribute immensely to our current understanding of the role of *Asap1* in embryonic development.

4.2 Does *Asap1* affect angiogenesis?

The developing embryo engages in many physiological events at different stages of gestation. Certain critical physiological processes prepare the embryo for its post-partum life, like angiogenesis (Adams and Alitalo, 2007). In mice, intraretinal vasculature development takes place postnatally, in a distinct spatiotemporal manner that can be monitored (Dorrell and Friedlander, 2006). This development is strain-specific and varies within a margin of a few days for different strains of mice (Stahl et al., 2010). I used the FVB strain of mice in my studies. The most commonly utilized mouse strain to study the time course of normal vascular development is C57Bl/6 mice, and in these mice vessels grow radially from the optic nerve into the periphery seven days after birth, thus forming the superficial vascular plexus. Vertical outgrowth of superficial capillaries forms at first the deep plexus and then the intermediate vascular plexus after eight post-natal days. After about 12 days of birth, the deep plexus grows and reaches retinal periphery, followed shortly by the intermediate plexus. It takes approximately three weeks after birth for all the three vascular layers to completely develop and for the many vessels between these layers to interconnect them (Stahl et al., 2010). One of the major regulators of blood vessel formation and function is VEGF. Specialized endothelial cells present at the tips of vascular sprouts respond to VEGF regulated angiogenic sprouting by guided migration (Gerhardt et al., 2003). Endothelial cells express high levels of ASAP1, which has been shown to be a part of a signaling cascade employed for angiogenesis activities. The GEP100-Arf6-ASAP1-cortactin pathway is activated by VEGFR2 (Hashimoto et al., 2011). It is known from the present study, and also from other research groups, that ASAP1 is involved in regulating cellular motility. Fibroblasts deficient in ASAP1 exhibit significantly reduced motility, as is evident from wound healing assay performed on embryonic fibroblasts obtained from $Asap1^{+/+}$ and $Asap1^{GT/GT}$ mice. Taking into account the expression of ASAP1 in

endothelial cells and its role in cellular motility, a presumptive role of ASAP1 in angiogenesis emerges. The hypothesis that absence of ASAP1 in the retinas of Asap1$^{GT/GT}$ mice may lead to a delay in the outgrowth of retinal vasculature, was tested by staining retinas of Asap1$^{+/+}$ and Asap1$^{GT/GT}$ pups isolated at various post-natal days. Retinal angiogenesis was observed to be reduced in P3-P5 Asap1$^{GT/GT}$ retinas as compared to Asap1$^{+/+}$ retinas. At P7 retinas from both Asap1$^{+/+}$ and Asap1$^{GT/GT}$ mice showed comparable angiogenesis. The number of animals at P3 and P5 were not sufficient to make a statistically significant argument, although a trend is evident. So that the involvement of ASAP1 in retinal angiogenesis can be underscored, it is highly desirable that this study is conducted on a larger cohort of animals and statistically robust data is obtained.

The shared radial orientation of blood vessels and ganglion cell axons and the precise alignment of planar capillary plexuses with horizontal neural and astrocytic laminae, point towards an association between retinal vascular structures and neural structures (Gariano and Gardner, 2005). Astrocyte precursors enter the retina via the optic nerve and radiate towards the periphery to form an astrocytic meshwork that serves as a template for subsequent vascularization. Endothelial cell present at the tip of the growing retinal vessel extend along the processes of the underlying glial cells (Dorrell et al., 2002). In the case of Asap1$^{GT/GT}$ mice that display an initial delayed retinal vascular outgrowth, it will be interesting to investigate if the glial outgrowth also exhibits a similar phenotype and if so, can that be accounted for the delayed retinal angiogenesis in these mice.

Angiogenesis is important in bone morphogenesis. During endochondral ossification, bone replaces avascular cartilage. Blood vessel invasion is required for formation of secondary ossification centers and subsequent bone formation (Gerber and Ferrara, 2000). The delayed ossification seen in Asap1$^{GT/GT}$ mice could possibly be attributed to delayed angiogenesis in them. To confirm this, blood vessel invasion in the epiphyses of Asap1$^{GT/GT}$ mice should be checked.

The various possible inter-regulation that exists among different physiological systems, that may work together to lead to the mouse phenotype in the absence of *Asap1* is presented along with the important findings from Asap1$^{GT/GT}$ mice (Figure 30, Figure 31*)*.

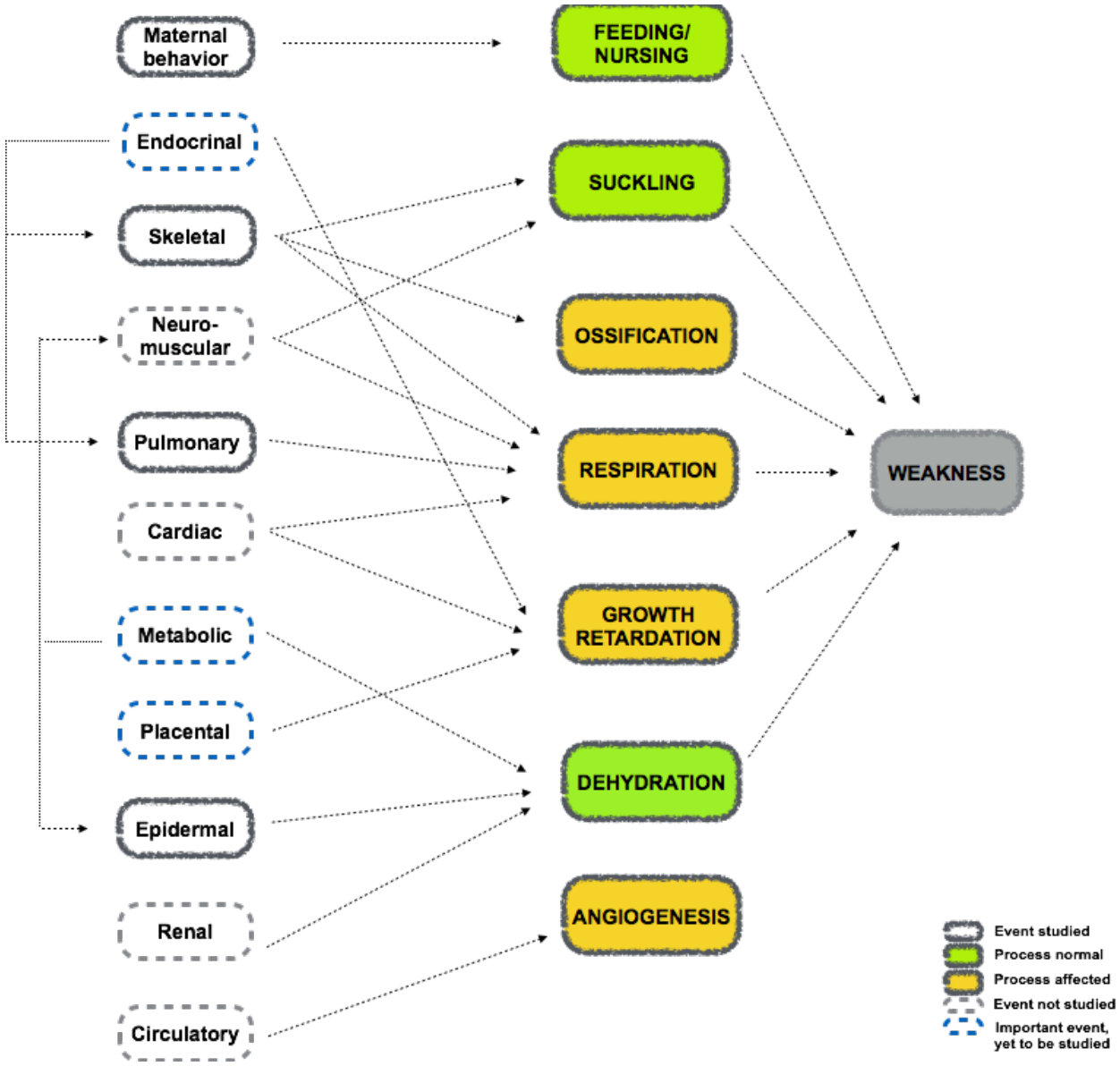

Figure 30. Physiological systems regulating *Asap1* knockout mouse phenotype.
Schematic of multiple physiological systems that work together to dictate the mouse phenotype in the absence of *Asap1*. Asap1$^{GT/GT}$ mice are fed and nursed normally and they display normal suckling and skin hydration (indicated in green boxes). They however, show defective

ossification, bradypnea and severe growth retardation and delayed angiogenesis (indicated in yellow boxes). The physiological systems that may regulate these phenotypes are shown.

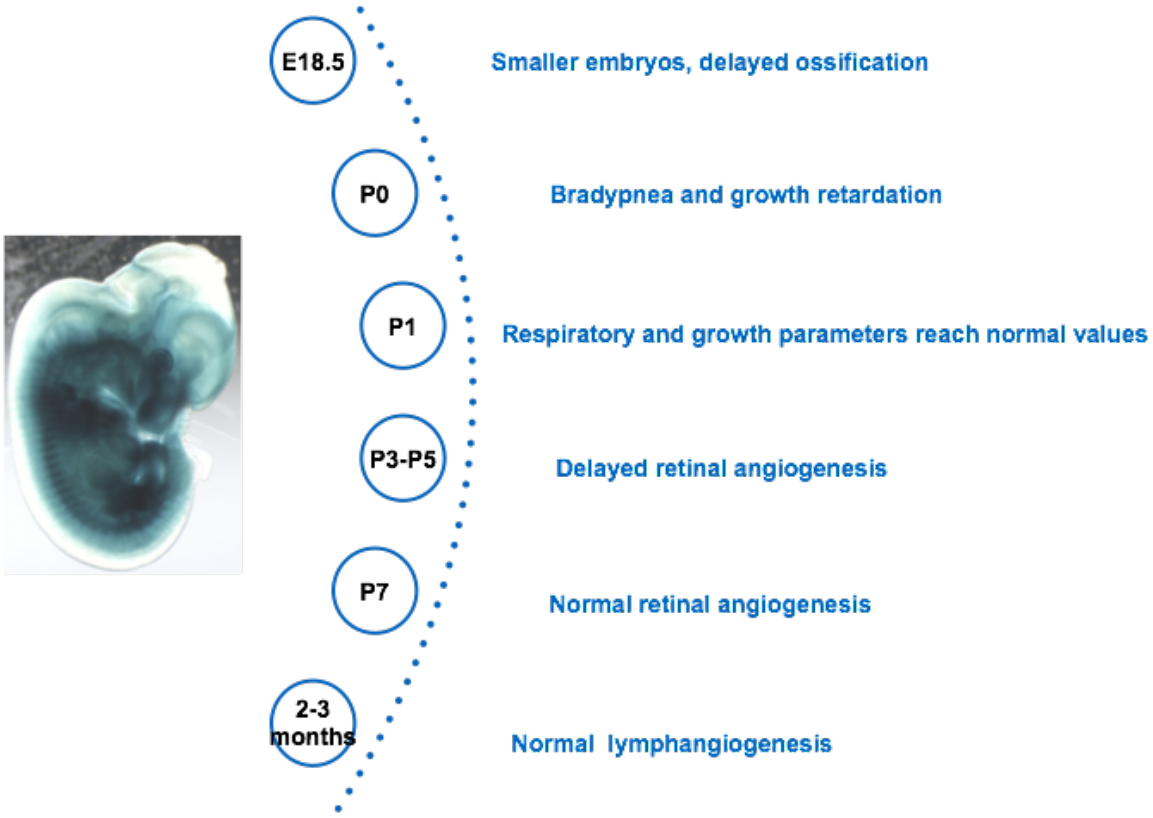

Figure 31. Notable findings from the Asap1$^{GT/GT}$ mice.
Schematic highlighting the most important findings from Asap1$^{GT/GT}$ mice at various stages of gestation to adulthood. The transient delayed phenotype of reduced breathing and growth defects, along with defective ossification and delayed angiogenesis is observed in the Asap1$^{GT/GT}$ neonates. These physiological functions are restored in the adult Asap1$^{GT/GT}$ mice.

4.3 How does *Asap1* affect breast tumor development and metastasis?

PyMT Asap1$^{+/+}$ and PyMT Asap1$^{GT/GT}$ mice presented with multifocal mammary tumors, with PyMT Asap1$^{GT/GT}$ mice displaying an early onset of tumor formation, evident in their shorter tumor-free survival. The higher tumor burden in PyMT Asap1$^{GT/GT}$ mice in the

weeks immediately before their sacrifice indicated that the absence of *Asap1* in the PyMT transgenic mice led to accelerated and more aggressive tumor growth. Lungs of PyMT Asap1$^{GT/GT}$ mice exhibited higher numbers and larger metastatic foci.

To understand the phenotype of tumors developed in the Asap1$^{GT/GT}$ background in PyMT-driven breast tumors, tumor cells were isolated, and critical cellular processes were studied. It is known that ASAP1, via its GAP activity, enhances general motility of cells (Furman et al., 2002). Fibroblasts from Asap1$^{+/+}$ and Asap1$^{GT/GT}$ mice were also isolated and used as positive controls to study cellular migration in PyMT Asap1$^{+/+}$ and PyMT Asap1$^{GT/GT}$ tumor cells. Whereas Asap1$^{GT/GT}$ fibroblasts displayed significantly reduced motility in comparison to Asap1$^{+/+}$ fibroblasts, PyMT Asap1$^{GT/GT}$ cells showed no differences in motility behavior as compared to PyMT Asap1$^{+/+}$ cells. Thus the ability of ASAP1 to regulate motility appears to be cell type dependent. ASAP1 clearly regulates the motility of fibroblasts, but its loss did not affect the motility of the breast cancer cells.

Cell migration is a multi-step process that requires coordinated effects of formation of new adhesions at the leading edge and breaking of adhesions at the trailing edge of a cell. Such processes involve extensive cytoskeletal remodeling in which ASAP1 plays a role (Kassis et al., 2001; Lambrechts et al., 2004). Cell spreading assays were performed to assess changes in actin cytoskeleton and understand the reduced migration phenotype of Asap1$^{GT/GT}$ fibroblasts, and also to explore if any adhesion defects existed in PyMT Asap1$^{+/+}$ and PyMT Asap1$^{GT/GT}$ cells. Asap1$^{GT/GT}$ fibroblasts exhibited prominent attachment defects as compared to Asap1$^{+/+}$ fibroblasts. Tumor cells obtained from PyMT Asap1$^{+/+}$ and PyMT Asap1$^{GT/GT}$ mice showed no differences in attachment to fibronectin-coated plates. When fibroblasts and tumor cells of both genotypes were stained for actin, to check whether inefficient actin remodeling was responsible for migration and adhesion defects, it was found that the cells did not show any differences in their actin expression. Taken together, these data suggest that the ability of ASAP1 to stimulate metastasis formation by tumor cells may not be connected to its role in regulating motility.

Upon a migratory stimulus, Asap1$^{+/+}$ fibroblasts showed a strong, transient nuclear actin expression that could possibly reflect cytoskeletal remodeling, absent in Asap1$^{GT/GT}$ fibroblasts. Nuclear actin is known to negatively regulate key cytoskeletal and adhesion genes and thus inhibit migration, and exclusion of actin from the nucleus has been shown to enhance cell migration (Sharili et al., 2016). Since the nuclear actin expression observed in Asap1$^{+/+}$ fibroblasts was a transient effect, lasting between 20-50 minutes of EGF addition, it is plausible that this does not affect overall cell motility as assessed in a period of 24 hours.

Early tumor onset in PyMT Asap1$^{GT/GT}$ mice may be paralleled by early metastasis formation. It would therefore be worthwhile to study the lungs of these mice a few weeks earlier than when the mice were sacrificed in my study. PyMT Asap1$^{GT/GT}$ mice show significantly higher tumor burden in weeks 10, 11 and 12, after first palpable tumors develop in them. In the absence of any migration and adhesion defects in PyMT Asap1$^{GT/GT}$ cells as compared to PyMT Asap1$^{+/+}$ cells, it would be interesting to find out whether tumor cells isolated from earlier stages of tumor development exhibit differences in motility and adhesion.

The question that arises from these observations is – how do PyMT Asap1$^{GT/GT}$ mice display enhanced metastatic potential when PyMT Asap1$^{GT/GT}$ cells do not exhibit features of highly motile cells that are capable of increased metastasis formation? There can be two possible explanations for this. One, *Asap1* has recently been shown to regulate mammary progenitor cells. In primary mouse mammary stem cells, *Asap1* knockdown resulted in an increased repopulating frequency of these cells, indicating that *Asap1* negatively regulates either mammary stem cell activity or number (Sheridan et al., 2015). Previous studies have demonstrated that cancer stem cells may exist in human breast cancer (Al-Hajj et al., 2003). To confirm whether this is the case, tumors and metastasis-bearing lungs from PyMT Asap1$^{+/+}$ and PyMT Asap1$^{GT/GT}$ mice can be stained with established progenitor/stem cell markers like BCRP-1 (breast cancer resistance protein-1) and Sca-1 (stem cell antigen-1).

The second possible answer to the above mentioned question could be that this effect may not be entirely tumor cell-autonomous. The involvement of stroma in cancer progression and metastasis has been extensively studied. Many studies report active contribution of stroma in cancer progression, and there are also studies that highlight how the microenvironment of a tumor acts to restrict its growth (Özdemir et al., 2014; Rhim et al., 2014). Normal murine fibroblasts have been shown to restrain the growth of transformed baby hamster kidney cells (Stoker et al., 1966). It is possible that deletion of *Asap1* results in the disruption of certain stromal components that are no longer able to exercise restrictive control on tumor growth and metastasis in PyMT Asap1$^{GT/GT}$ mice, thus leading to faster, more aggressive tumors that bear enhanced metastatic potential. *Asap1* knockout mice used in this study bear global deletion of the gene. Hence, to understand the role of stroma in tumor progression in these mice it is required that PyMT Asap1$^{GT/GT}$ tumors be transplanted in a wild-type background, and PyMT Asap1$^{+/+}$ tumors transplanted in PyMT Asap1$^{GT/GT}$ mice. Tumor development and metastasis formation arising from these transplanted tumors would divulge important information as to the involvement of stromal compartment in breast tumor progression in the absence of *Asap1.*

The notion that ASAP1 expression and function in stromal cells may be decisive for the tumor development and metastasis is supported by the observation that compared to PyMT Asap1$^{+/+}$ tumors, PyMT Asap1$^{GT/GT}$ tumors displayed a very strong α-SMA expression, highlighting the presence of a reactive stroma. Peritumoral stromal cells in breast cancer express α-SMA, and its expression can be used as a surrogate marker for the presence of a reactive stroma. Resident normal fibroblasts, in a reactive tissue, convert into α-SMA expressing myofibroblasts, and the cells closest in proximity to tumor cells show strongest conversion. This is explainable by a concentration gradient of growth factors, like transforming growth factor-β (TGF-β), originating from the tumor cells (Rønnov-Jessen et al., 1995). Future experiments that would aim to quantify the stromal contribution in PyMT Asap1$^{+/+}$ and PyMT Asap1$^{GT/GT}$ tumors, by way of establishing a reactive stroma index, would add to the understanding the role of stroma

in tumor progression in these mice. Reactive stroma index would assess stromal percentage to tumor mass.

Other data suggest that ASAP1 in tumor cells themselves plays a decisive role in determining tumor growth and dissemination. Thus, ectopic expression of ASAP1 in pancreatic carcinoma cells sufficed to promote their metastasis in vivo (Müller et al., 2010). Furthermore, I also studied the effect of *Asap1* on Neu- and Wnt- driven tumorigenesis. Both Neu- and Wnt- driven tumors in Asap1$^{+/+}$ and Asap1$^{GT/GT}$ mice displayed long and highly variable latency periods in tumor formation and a complete lack of observable metastases in the lungs. However, no difference was observed between wildtype and Asap1$^{GT/GT}$ mice. As ASAP1 was also lacking in the stroma of these tumors in the same way as in the PyMT model, this suggests a decisive role for ASAP1 in the PyMT tumor cells themselves, rather than a purely stromal defect as a consequence of ASAP1 deficiency. Taken together, these observations suggest that ASAP1 likely plays important roles in both the tumor cells themselves and in the stromal cells of the tumor, and that the differences in tumor development and metastasis observed in PyMT Asap1$^{+/+}$ and PyMT Asap1$^{GT/GT}$ is probably due to a combination of these effects.

Breast cancer is a heterogeneous disease comprising various subtypes. It has been previously argued that the subtypes depend on the oncogene and the cell of origin being transformed, hence MMTV-PyMT tumors have been shown to resemble luminal subtype of human breast cancer since MMTV promoter is known to be active in luminal epithelial cells (Vargo-Gogola and Rosen, 2007; Wagner et al., 2001; William Petersen et al., 2001). PyMT Asap1$^{+/+}$ and PyMT Asap1$^{GT/GT}$ tumors express CK18, which is a luminal marker, and interestingly, they also express CK14, a basal marker. Such a concomitant expression of luminal and basal markers has been earlier reported in a luminal breast cancer model that employs MMTV to drive oncogenic expression of mutant PIK3CA H1047R leading to the formation of tumors that recapitulate heterogeneity of human tumors (Meyer et al., 2011). Recent studies demonstrate that both subtypes of breast cancer arise from the luminal epithelial lineage, and so as to

become malignant, differentiated luminal cells must acquire basal-like traits (Horwitz et al., 2008; Lim et al., 2009; Molyneux et al., 2010). Although PyMT Asap1$^{+/+}$ and PyMT Asap1$^{GT/GT}$ tumors co-express luminal and basal cytokeratins, PyMT Asap1$^{GT/GT}$ tumors exhibit a stronger CK14 expression. This may possibly reveal the plasticity in the luminal compartment of PyMT Asap1$^{GT/GT}$ tumors that is responsible for recapitulating the heterogeneity observed in human breast tumors.

To understand how closely ASAP1 might be involved in breast tumor progression in PyMT-driven mouse models, mammary glands of PyMT Asap1$^{+/+}$ mice at specific time points during tumor growth can be stained for ASAP1 expression and compared. This spatio-temporal expression analysis of PyMT Asap1$^{+/+}$ mammary glands can reveal hyperplasia-associated changes in the breast and whether ASAP1 regulates any stage-specific aspect of breast tumor progression. Since elevated expression of ASAP1 in various cancer entities has been strongly evidenced, it is desirable that tumors and lungs obtained from PyMT Asap1$^{+/+}$ mice be assessed for ASAP1 expression. It will reveal whether primary and metastatic tumors obtained from spontaneous murine mammary models reflect the observations made in the clinics with respect to ASAP1 expression. The importance of finding out breast cancer subtypes in which ASAP1 expression is clinically relevant is revealed by a retrospective study that analyzed 479 patients treated with breast conservation therapy (BCT). Out of these, 20 patients developed local recurrence, and clinicopathological factors like margin-status, node-positivity and hormone receptor-status did not correlate with the rapidity of recurrence whereas concomitant expression of ASAP1 and GEP100 significantly associated with the rapidity (Kinoshita et al., 2013). Neither the individual expression of ASAP1 and GEP100, nor the individual status of ER and PR showed any statistical significance for the rapidity of recurrence. Moreover, owing to a small sample size, this study was unable to establish whether simultaneous expression of ER, PR, HER2, ASAP1 and GEP100, could correlate with local recurrence. Under these circumstances, it is imperative that human breast tumors are stratified on the basis of different subtypes and the relevance of ASAP1 expression in each of the subtype be determined.

4.4 Conclusion

This is the first study that has examined the involvement of ASAP1 in murine embryonic development, normal physiology and breast tumor metastasis in autochthonous models harboring global deletion of *Asap1.* Key findings are (i) the observed transient reduction in the expected number of homozygous knockout offspring at birth, likely caused by growth retardation and respiratory distress in the Asap1$^{GT/GT}$ pups; (ii) MMTV-PyMT Asap1$^{GT/GT}$ mice have an earlier tumor onset, faster tumor growth and increased metastasis to the lungs, in contrast to previous cell line-based studies, which together with other observations suggests that ASAP1 exerts both tumor cell autonomous and non-autonomous effects; (iii) While fibroblasts taken from Asap1$^{+/+}$ and Asap1$^{GT/GT}$ mice showed marked differences in motility and adhesion, no such differences were observed in Asap1$^{+/+}$ and Asap1$^{GT/GT}$ breast cancer cells. Future work will focus on understanding in more detail how ASAP1 regulates tumor growth and metastasis.

List of figures and tables

List of abbreviations

ASAP1	Arf-GAP with SH3-domains, Ankyrin-repeats and PH-domains
ARF	ADP-ribosylation factor
ARFL	ARF-like
$Asap1^{+/+}$	Wild-type
$Asap1^{+/GT}$	Asap1 heterozygous
$Asap1^{GT/GT}$	Asap1 knockout
BAR	Bin–Amphiphysin–Rvs
BCA	Bicinchoninic acid
BCRP-1	Breast cancer resistance protein 1
bFGF2	basic fibroblast growth factor 2
BM	Basement membrane
BMDC	Bone marrow-derived cells
BSA	Bovine serum albumin
CAF	Cancer associated fibroblasts
CCAL1	Chondrocalcinosis 1
CDR	Central dorsal ruffles
CIS	Carcinoma *in situ*
CK	Cytokeratin
CRH	Corticotropin releasing hormone
CrkL	Crk ligand
CTC	Circulating tumor cells
DMSO	Dimethyl sulfoxide
DTC	Disseminated tumor cells
ECM	Extra-cellular matrix
EGFR	Epidermal growth factor receptor
ER	Estrogen receptor
ERGIC	ER-Golgi intermediate compartment
ES cells	Embryonic stem cells
F-actin	Filamentous actin
FA	Focal adhesion
FAK	Focal adhesion kinase
FCS	Fetal calf serum
FFPE	Formalin-fixed paraffin embedded
FIP3	Rab11-family interacting protein 3
GAP	GTPase activating protein
GEF	Guanine nucleotide exchange factor
GEMM	Genetically engineered mouse model

GTPase	Guanosine triphosphatase
H&E	Haematoxylin and eosin
HER2	Human epidermal growth factor 2
HNSCC	Head and neck squamous cell carcinoma
HRP	Horseradish peroxidase
IGF-1	Insulin-like growth factor-1
IHC	Immunohistochemistry
MDSC	Myeloid cell-derived suppressor cells
MEF	Murine embryonic fibroblasts
MMP	Matrix metalloproteinase
MMTV	Mouse mammary tumor virus
MSC	Mesenchymal stem cells
N-WASP	Neural-Wiskott Aldrich syndrome protein
NBS1	Nijmegen breakage syndrome 1
NK	Natural killer cells
PBS	Phosphate-buffered saline
PCR	Polymerase chain reaction
PDGF	Platelet-derived growth factor
PFA	Paraformaldehyde
PH	Pleckstrin homology
PI3K	Phosphatidylinositol 3-kinase
PIP_2	Phosphatidylinositol 4,5- bisphospate
PLEC1	Plectin 1
PR	Progesterone receptor
PyMT	Polyoma middle T antigen
PZA	PH-Zinc finger-Ankyrin
qRT-PCR	quantitative reverse transcriptase polymerase chain reaction
RalBP	Ral binding protein
RS	Recurrence score
Sca-1	Stem cell antigen-1
SDF-1	Stroma-derived factor-1
SH3	Src homology 3
SLK	Ste-20-like kinase
SPF	Specific pathogen-free
SSH	Suppression subtractive hybridization
TAM	Tumor associated macrophages
TGF-ß	Transforming growth factor-ß
TNF	Tumor necrosis factor
TNFRSF11B	Tumor necrosis factor receptor superfamily 11B
TNM	Tumor node metastasis

VEGF	Vascular endothelial growth factor
VEGFR1	Vascular endothelial growth factor receptor 1

References

Adams, R.H., and Alitalo, K. (2007). Molecular regulation of angiogenesis and lymphangiogenesis. Nat. Rev. Mol. Cell Biol. *8*, 464–478.

Aguirre-Ghiso, J.A. (2007). Models, mechanisms and clinical evidence for cancer dormancy. Nat. Rev. Cancer *7*, 834–846.

Aird, W.C. (2007). Vascular bed-specific thrombosis. J. Thromb. Haemost. *5 Suppl 1*, 283–291.

Albiges-Rizo, C., Destaing, O., Fourcade, B., Planus, E., and Block, M.R. (2009a). Actin machinery and mechanosensitivity in invadopodia, podosomes and focal adhesions. J Cell Sci *122*, 3037–3049.

Albiges-Rizo, C., Destaing, O., Fourcade, B., Planus, E., and Block, M.R. (2009b). Actin machinery and mechanosensitivity in invadopodia, podosomes and focal adhesions. J Cell Sci *122*, 3037–3049.

Al-Hajj, M., Wicha, M.S., Benito-Hernandez, A., Morrison, S.J., and Clarke, M.F. (2003). Prospective identification of tumorigenic breast cancer cells. PNAS *100*, 3983–3988.

Allemani, C., Weir, H.K., Carreira, H., Harewood, R., Spika, D., Wang, X.-S., Bannon, F., Ahn, J.V., Johnson, C.J., Bonaventure, A., et al. (2015). Global surveillance of cancer survival 1995–2009: analysis of individual data for 25 676 887 patients from 279 population-based registries in 67 countries (CONCORD-2). The Lancet *385*, 977–1010.

Al-Mehdi, A.B., Tozawa, K., Fisher, A.B., Shientag, L., Lee, A., and Muschel, R.J. (2000). Intravascular origin of metastasis from the proliferation of endothelium-attached tumor cells: a new model for metastasis. Nat. Med. *6*, 100–102.

Andreev, J., Simon, J.P., Sabatini, D.D., Kam, J., Plowman, G., Randazzo, P.A., and Schlessinger, J. (1999). Identification of a new Pyk2 target protein with Arf-GAP activity. Mol. Cell. Biol. *19*, 2338–2350.

Artym, V.V., Zhang, Y., Seillier-Moiseiwitsch, F., Yamada, K.M., and Mueller, S.C. (2006). Dynamic interactions of cortactin and membrane type 1 matrix metalloproteinase at invadopodia: defining the stages of invadopodia formation and function. Cancer Res. *66*, 3034–3043.

Autier, P., Boniol, M., LaVecchia, C., Vatten, L., Gavin, A., Héry, C., and Heanue, M. (2010). Disparities in breast cancer mortality trends between 30 European countries: retrospective trend analysis of WHO mortality database. BMJ *341*, c3620.

Bani, D., Riva, A., Bigazzi, M., and Bani Sacchi, T. (1994). Differentiation of breast cancer cells in vitro is promoted by the concurrent influence of myoepithelial cells and relaxin. Br. J. Cancer *70*, 900–904.

Barbaric, I., Miller, G., and Dear, T.N. (2007). Appearances can be deceiving: phenotypes of knockout mice. Brief Funct Genomics *6*, 91–103.

Barcellos-Hoff, M.H., Lyden, D., and Wang, T.C. (2013). The evolution of the cancer niche during multistage carcinogenesis. Nat Rev Cancer *13*, 511–518.

Bargmann, C.I., and Weinberg, R.A. (1988a). Increased tyrosine kinase activity associated with the protein encoded by the activated neu oncogene. Proc Natl Acad Sci U S A *85*, 5394–5398.

Bargmann, C.I., and Weinberg, R.A. (1988b). Increased tyrosine kinase activity associated with the protein encoded by the activated neu oncogene. Proc Natl Acad Sci U S A *85*, 5394–5398.

Bar-Sagi, D., and Hall, A. (2000). Ras and Rho GTPases: a family reunion. Cell *103*, 227–238.

Beck, R., Rawet, M., Ravet, M., Wieland, F.T., and Cassel, D. (2009). The COPI system: molecular mechanisms and function. FEBS Lett. *583*, 2701–2709.

Bharti, S., Inoue, H., Bharti, K., Hirsch, D.S., Nie, Z., Yoon, H.-Y., Artym, V., Yamada, K.M., Mueller, S.C., Barr, V.A., et al. (2007). Src-dependent phosphorylation of ASAP1 regulates podosomes. Mol. Cell. Biol. *27*, 8271–8283.

Biswas, S.K., and Mantovani, A. (2010). Macrophage plasticity and interaction with lymphocyte subsets: cancer as a paradigm. Nat. Immunol. *11*, 889–896.

Böcker, W., Bier, B., Freytag, G., Brömmelkamp, B., Jarasch, E.D., Edel, G., Dockhorn-Dworniczak, B., and Schmid, K.W. (1992). An immunohistochemical study of the breast using antibodies to basal and luminal keratins, alpha-smooth muscle actin, vimentin, collagen IV and laminin. Part I: Normal breast and benign proliferative lesions. Virchows Arch A Pathol Anat Histopathol *421*, 315–322.

Bowden, E.T., Barth, M., Thomas, D., Glazer, R.I., and Mueller, S.C. (1999). An invasion-related complex of cortactin, paxillin and PKCmu associates with invadopodia at sites of extracellular matrix degradation. Oncogene *18*, 4440–4449.

Boyd, N.F., Dite, G.S., Stone, J., Gunasekara, A., English, D.R., McCredie, M.R.E., Giles, G.G., Tritchler, D., Chiarelli, A., Yaffe, M.J., et al. (2002). Heritability of Mammographic Density, a Risk Factor for Breast Cancer. New England Journal of Medicine *347*, 886–894.

Braun, T., Rudnicki, M.A., Arnold, H.H., and Jaenisch, R. (1992). Targeted inactivation of the muscle regulatory gene Myf-5 results in abnormal rib development and perinatal death. Cell *71*, 369–382.

Brown, M.T., Andrade, J., Radhakrishna, H., Donaldson, J.G., Cooper, J.A., and Randazzo, P.A. (1998). ASAP1, a phospholipid-dependent arf GTPase-activating

protein that associates with and is phosphorylated by Src. Mol. Cell. Biol. *18*, 7038–7051.

Bryce, N.S., Clark, E.S., Leysath, J.L., Currie, J.D., Webb, D.J., and Weaver, A.M. (2005). Cortactin promotes cell motility by enhancing lamellipodial persistence. Curr. Biol. *15*, 1276–1285.

Buccione, R., Orth, J.D., and McNiven, M.A. (2004). Foot and mouth: podosomes, invadopodia and circular dorsal ruffles. Nat Rev Mol Cell Biol *5*, 647–657.

Budczies, J., Bockmayr, M., Denkert, C., Klauschen, F., Lennerz, J.K., Györffy, B., Dietel, M., Loibl, S., Weichert, W., and Stenzinger, A. (2015a). Classical pathology and mutational load of breast cancer - integration of two worlds. J Pathol Clin Res *1*, 225–238.

Budczies, J., von Winterfeld, M., Klauschen, F., Bockmayr, M., Lennerz, J.K., Denkert, C., Wolf, T., Warth, A., Dietel, M., Anagnostopoulos, I., et al. (2015b). The landscape of metastatic progression patterns across major human cancers. Oncotarget *6*, 570–583.

Buffart, T.E., Coffa, J., Hermsen, M. a. J.A., Carvalho, B., van der Sijp, J.R.M., Ylstra, B., Pals, G., Schouten, J.P., and Meijer, G.A. (2005). DNA copy number changes at 8q11-24 in metastasized colorectal cancer. Cell. Oncol. *27*, 57–65.

Bussen, M., Petry, M., Schuster-Gossler, K., Leitges, M., Gossler, A., and Kispert, A. (2004). The T-box transcription factor Tbx18 maintains the separation of anterior and posterior somite compartments. Genes Dev. *18*, 1209–1221.

Campa, F., and Randazzo, P.A. (2008). Arf GTPase-activating proteins and their potential role in cell migration and invasion. Cell Adh Migr *2*, 258–262.

Candia, P. de, Solit, D.B., Giri, D., Brogi, E., Siegel, P.M., Olshen, A.B., Muller, W.J., Rosen, N., and Benezra, R. (2003). Angiogenesis impairment in Id-deficient mice cooperates with an Hsp90 inhibitor to completely suppress HER2/neu-dependent breast tumors. PNAS *100*, 12337–12342.

Carman, C.V., Sage, P.T., Sciuto, T.E., de la Fuente, M.A., Geha, R.S., Ochs, H.D., Dvorak, H.F., Dvorak, A.M., and Springer, T.A. (2007). Transcellular diapedesis is initiated by invasive podosomes. Immunity *26*, 784–797.

Carney, J.P., Maser, R.S., Olivares, H., Davis, E.M., Le Beau, M., Yates III, J.R., Hays, L., Morgan, W.F., and Petrini, J.H.J. (1998). The hMre11/hRad50 Protein Complex and Nijmegen Breakage Syndrome: Linkage of Double-Strand Break Repair to the Cellular DNA Damage Response. Cell *93*, 477–486.

Chambers, A.F., Groom, A.C., and MacDonald, I.C. (2002a). Dissemination and growth of cancer cells in metastatic sites. Nat. Rev. Cancer *2*, 563–572.

Chambers, A.F., Groom, A.C., and MacDonald, I.C. (2002b). Dissemination and growth

of cancer cells in metastatic sites. Nat. Rev. Cancer *2*, 563–572.

Chardin, P., Paris, S., Antonny, B., Robineau, S., Béraud-Dufour, S., Jackson, C.L., and Chabre, M. (1996). A human exchange factor for ARF contains Sec7- and pleckstrin-homology domains. Nature *384*, 481–484.

Che, M.M., Nie, Z., and Randazzo, P.A. (2005a). Assays and properties of the Arf GAPs AGAP1, ASAP1, and Arf GAP1. Meth. Enzymol. *404*, 147–163.

Che, M.M., Boja, E.S., Yoon, H.-Y., Gruschus, J., Jaffe, H., Stauffer, S., Schuck, P., Fales, H.M., and Randazzo, P.A. (2005b). Regulation of ASAP1 by phospholipids is dependent on the interface between the PH and Arf GAP domains. Cell. Signal. *17*, 1276–1288.

Chia, S.K., Bramwell, V.H., Tu, D., Shepherd, L.E., Jiang, S., Vickery, T., Mardis, E., Leung, S., Ung, K., Pritchard, K.I., et al. (2012). A 50-gene intrinsic subtype classifier for prognosis and prediction of benefit from adjuvant tamoxifen. Clin. Cancer Res. *18*, 4465–4472.

Chun, J., Shapovalova, Z., Dejgaard, S.Y., Presley, J.F., and Melançon, P. (2008). Characterization of class I and II ADP-ribosylation factors (Arfs) in live cells: GDP-bound class II Arfs associate with the ER-Golgi intermediate compartment independently of GBF1. Mol. Biol. Cell *19*, 3488–3500.

Cirri, P., and Chiarugi, P. (2011). Cancer associated fibroblasts: the dark side of the coin. Am J Cancer Res *1*, 482–497.

Clark, E.S., Whigham, A.S., Yarbrough, W.G., and Weaver, A.M. (2007). Cortactin is an essential regulator of matrix metalloproteinase secretion and extracellular matrix degradation in invadopodia. Cancer Res. *67*, 4227–4235.

Clark, J.C., Wert, S.E., Bachurski, C.J., Stahlman, M.T., Stripp, B.R., Weaver, T.E., and Whitsett, J.A. (1995). Targeted disruption of the surfactant protein B gene disrupts surfactant homeostasis, causing respiratory failure in newborn mice. PNAS *92*, 7794–7798.

Colvin, J.S., White, A.C., Pratt, S.J., and Ornitz, D.M. (2001). Lung hypoplasia and neonatal death in Fgf9-null mice identify this gene as an essential regulator of lung mesenchyme. Development *128*, 2095–2106.

Condeelis, J., and Pollard, J.W. (2006). Macrophages: obligate partners for tumor cell migration, invasion, and metastasis. Cell *124*, 263–266.

Condeelis, J., and Segall, J.E. (2003). Intravital imaging of cell movement in tumours. Nat. Rev. Cancer *3*, 921–930.

Conklin, M.W., and Keely, P.J. (2012). Why the stroma matters in breast cancer: insights into breast cancer patient outcomes through the examination of stromal

biomarkers. Cell Adh Migr *6*, 249–260.

Cougoule, C., Carréno, S., Castandet, J., Labrousse, A., Astarie-Dequeker, C., Poincloux, R., Le Cabec, V., and Maridonneau-Parini, I. (2005). Activation of the lysosome-associated p61Hck isoform triggers the biogenesis of podosomes. Traffic *6*, 682–694.

Cukierman, E., Huber, I., Rotman, M., and Cassel, D. (1995). The ARF1 GTPase-activating protein: zinc finger motif and Golgi complex localization. Science *270*, 1999–2002.

D'Angelo, A., Garzia, L., André, A., Carotenuto, P., Aglio, V., Guardiola, O., Arrigoni, G., Cossu, A., Palmieri, G., Aravind, L., et al. (2004). Prune cAMP phosphodiesterase binds nm23-H1 and promotes cancer metastasis. Cancer Cell *5*, 137–149.

DeMali, K.A., Barlow, C.A., and Burridge, K. (2002). Recruitment of the Arp2/3 complex to vinculin. J Cell Biol *159*, 881–891.

Denève, E., Riethdorf, S., Ramos, J., Nocca, D., Coffy, A., Daurès, J.-P., Maudelonde, T., Fabre, J.-M., Pantel, K., and Alix-Panabières, C. (2013). Capture of viable circulating tumor cells in the liver of colorectal cancer patients. Clin. Chem. *59*, 1384–1392.

Desai, B., Ma, T., and Chellaiah, M.A. (2008). Invadopodia and Matrix Degradation, a New Property of Prostate Cancer Cells during Migration and Invasion. J Biol Chem *283*, 13856–13866.

Diop-Frimpong, B., Chauhan, V.P., Krane, S., Boucher, Y., and Jain, R.K. (2011). Losartan inhibits collagen I synthesis and improves the distribution and efficacy of nanotherapeutics in tumors. Proc. Natl. Acad. Sci. U.S.A. *108*, 2909–2914.

Donaldson, J.G., and Jackson, C.L. (2011). ARF family G proteins and their regulators: roles in membrane transport, development and disease. Nat Rev Mol Cell Biol *12*, 362–375.

Dorrell, M.I., and Friedlander, M. (2006). Mechanisms of endothelial cell guidance and vascular patterning in the developing mouse retina. Prog Retin Eye Res *25*, 277–295.

Dorrell, M.I., Aguilar, E., and Friedlander, M. (2002). Retinal vascular development is mediated by endothelial filopodia, a preexisting astrocytic template and specific R-cadherin adhesion. Invest. Ophthalmol. Vis. Sci. *43*, 3500–3510.

D'Souza-Schorey, C., and Chavrier, P. (2006). ARF proteins: roles in membrane traffic and beyond. Nat Rev Mol Cell Biol *7*, 347–358.

Duijsings, D., Lanke, K.H.W., van Dooren, S.H.J., van Dommelen, M.M.T., Wetzels, R., de Mattia, F., Wessels, E., and van Kuppeveld, F.J.M. (2009). Differential membrane association properties and regulation of class I and class II Arfs. Traffic *10*, 316–323.

Dumont, N., Liu, B., Defilippis, R.A., Chang, H., Rabban, J.T., Karnezis, A.N., Tjoe, J.A., Marx, J., Parvin, B., and Tlsty, T.D. (2013). Breast fibroblasts modulate early dissemination, tumorigenesis, and metastasis through alteration of extracellular matrix characteristics. Neoplasia *15*, 249–262.

Dvorak, H.F. (1986). Tumors: wounds that do not heal. Similarities between tumor stroma generation and wound healing. N. Engl. J. Med. *315*, 1650–1659.

Ehlers, J.P., Worley, L., Onken, M.D., and Harbour, J.W. (2005). DDEF1 is located in an amplified region of chromosome 8q and is overexpressed in uveal melanoma. Clin. Cancer Res. *11*, 3609–3613.

Elenbaas, B., Spirio, L., Koerner, F., Fleming, M.D., Zimonjic, D.B., Donaher, J.L., Popescu, N.C., Hahn, W.C., and Weinberg, R.A. (2001). Human breast cancer cells generated by oncogenic transformation of primary mammary epithelial cells. Genes Dev. *15*, 50–65.

Erler, J.T., Bennewith, K.L., Nicolau, M., Dornhöfer, N., Kong, C., Le, Q.-T., Chi, J.-T.A., Jeffrey, S.S., and Giaccia, A.J. (2006). Lysyl oxidase is essential for hypoxia-induced metastasis. Nature *440*, 1222–1226.

Escribese, M.M., Casas, M., and Corbí, A.L. (2012). Influence of low oxygen tensions on macrophage polarization. Immunobiology *217*, 1233–1240.

Farmer, P., Bonnefoi, H., Anderle, P., Cameron, D., Wirapati, P., Becette, V., André, S., Piccart, M., Campone, M., Brain, E., et al. (2009). A stroma-related gene signature predicts resistance to neoadjuvant chemotherapy in breast cancer. Nat Med *15*, 68–74.

Farsad, K., Ringstad, N., Takei, K., Floyd, S.R., Rose, K., and De Camilli, P. (2001a). Generation of high curvature membranes mediated by direct endophilin bilayer interactions. J. Cell Biol. *155*, 193–200.

Farsad, K., Ringstad, N., Takei, K., Floyd, S.R., Rose, K., and De Camilli, P. (2001b). Generation of high curvature membranes mediated by direct endophilin bilayer interactions. J. Cell Biol. *155*, 193–200.

Farsad, K., Ringstad, N., Takei, K., Floyd, S.R., Rose, K., and De Camilli, P. (2001c). Generation of high curvature membranes mediated by direct endophilin bilayer interactions. J. Cell Biol. *155*, 193–200.

Ferlay, J., Steliarova-Foucher, E., Lortet-Tieulent, J., Rosso, S., Coebergh, J.W.W., Comber, H., Forman, D., and Bray, F. (2013). Cancer incidence and mortality patterns in Europe: estimates for 40 countries in 2012. Eur. J. Cancer *49*, 1374–1403.

Fidler, I.J. (1970). Metastasis: Quantitative Analysis of Distribution and Fate of Tumor Emboli Labeled With 125I-5-Iodo-2′ -deoxyuridine. JNCI J Natl Cancer Inst *45*, 773–782.

Fidler, I.J. (2003). The pathogenesis of cancer metastasis: the “seed and soil” hypothesis revisited. Nat. Rev. Cancer *3*, 453–458.

Finak, G., Bertos, N., Pepin, F., Sadekova, S., Souleimanova, M., Zhao, H., Chen, H., Omeroglu, G., Meterissian, S., Omeroglu, A., et al. (2008). Stromal gene expression predicts clinical outcome in breast cancer. Nat. Med. *14*, 518–527.

Folkman, J. (1971). Tumor angiogenesis: therapeutic implications. N. Engl. J. Med. *285*, 1182–1186.

Folkman, J., Klagsbrun, M., Sasse, J., Wadzinski, M., Ingber, D., and Vlodavsky, I. (1988). A heparin-binding angiogenic protein--basic fibroblast growth factor--is stored within basement membrane. Am J Pathol *130*, 393–400.

Folkman, J., Watson, K., Ingber, D., and Hanahan, D. (1989). Induction of angiogenesis during the transition from hyperplasia to neoplasia. Nature *339*, 58–61.

Forsberg, K., Valyi-Nagy, I., Heldin, C.H., Herlyn, M., and Westermark, B. (1993). Platelet-derived growth factor (PDGF) in oncogenesis: development of a vascular connective tissue stroma in xenotransplanted human melanoma producing PDGF-BB. PNAS *90*, 393–397.

Frame, M.C. (2004). Newest findings on the oldest oncogene; how activated src does it. J. Cell. Sci. *117*, 989–998.

Frese, K.K., and Tuveson, D.A. (2007). Maximizing mouse cancer models. Nat. Rev. Cancer *7*, 645–658.

Friedl, P., and Gilmour, D. (2009). Collective cell migration in morphogenesis, regeneration and cancer. Nat. Rev. Mol. Cell Biol. *10*, 445–457.

Friedl, P., and Wolf, K. (2003). Tumour-cell invasion and migration: diversity and escape mechanisms. Nat. Rev. Cancer *3*, 362–374.

Fujiwara, T., Bandi, M., Nitta, M., Ivanova, E.V., Bronson, R.T., and Pellman, D. (2005). Cytokinesis failure generating tetraploids promotes tumorigenesis in p53-null cells. Nature *437*, 1043–1047.

Fukumura, D., Xavier, R., Sugiura, T., Chen, Y., Park, E.C., Lu, N., Selig, M., Nielsen, G., Taksir, T., Jain, R.K., et al. (1998). Tumor induction of VEGF promoter activity in stromal cells. Cell *94*, 715–725.

Furman, C., Short, S.M., Subramanian, R.R., Zetter, B.R., and Roberts, T.M. (2002). DEF-1/ASAP1 is a GTPase-activating protein (GAP) for ARF1 that enhances cell motility through a GAP-dependent mechanism. J. Biol. Chem. *277*, 7962–7969.

Gariano, R.F., and Gardner, T.W. (2005). Retinal angiogenesis in development and disease. Nature *438*, 960–966.

Geiger, B., Spatz, J.P., and Bershadsky, A.D. (2009). Environmental sensing through focal adhesions. Nat Rev Mol Cell Biol *10*, 21–33.

Gerber, H.P., and Ferrara, N. (2000). Angiogenesis and bone growth. Trends Cardiovasc. Med. *10*, 223–228.

Gerhardt, H., Golding, M., Fruttiger, M., Ruhrberg, C., Lundkvist, A., Abramsson, A., Jeltsch, M., Mitchell, C., Alitalo, K., Shima, D., et al. (2003). VEGF guides angiogenic sprouting utilizing endothelial tip cell filopodia. J. Cell Biol. *161*, 1163–1177.

Gilbert, S.F. (2000a). Developmental Biology (Sinauer Associates).

Gilbert, S.F. (2000b). Developmental Biology (Sinauer Associates).

Gillingham, A.K., and Munro, S. (2007). The small G proteins of the Arf family and their regulators. Annu. Rev. Cell Dev. Biol. *23*, 579–611.

Gimona, M., Kaverina, I., Resch, G.P., Vignal, E., and Burgstaller, G. (2003). Calponin Repeats Regulate Actin Filament Stability and Formation of Podosomes in Smooth Muscle Cells. Mol Biol Cell *14*, 2482–2491.

Gossler, A., Joyner, A.L., Rossant, J., and Skarnes, W.C. (1989). Mouse embryonic stem cells and reporter constructs to detect developmentally regulated genes. Science *244*, 463–465.

Grivennikov, S.I., Greten, F.R., and Karin, M. (2010). Immunity, inflammation, and cancer. Cell *140*, 883–899.

Grobstein, C. (1967). Mechanisms of organogenetic tissue interaction. Natl Cancer Inst Monogr *26*, 279–299.

Gudmundsson, J., Sulem, P., Manolescu, A., Amundadottir, L.T., Gudbjartsson, D., Helgason, A., Rafnar, T., Bergthorsson, J.T., Agnarsson, B.A., Baker, A., et al. (2007). Genome-wide association study identifies a second prostate cancer susceptibility variant at 8q24. Nat. Genet. *39*, 631–637.

Gusterson, B.A., Warburton, M.J., Mitchell, D., Ellison, M., Neville, A.M., and Rudland, P.S. (1982). Distribution of myoepithelial cells and basement membrane proteins in the normal breast and in benign and malignant breast diseases. Cancer Res. *42*, 4763–4770.

Guy, C.T., Webster, M.A., Schaller, M., Parsons, T.J., Cardiff, R.D., and Muller, W.J. (1992a). Expression of the neu protooncogene in the mammary epithelium of transgenic mice induces metastatic disease. Proc Natl Acad Sci U S A *89*, 10578–10582.

Guy, C.T., Cardiff, R.D., and Muller, W.J. (1992b). Induction of mammary tumors by expression of polyomavirus middle T oncogene: a transgenic mouse model for metastatic disease. Mol Cell Biol *12*, 954–961.

Guy, C.T., Cardiff, R.D., and Muller, W.J. (1992c). Induction of mammary tumors by expression of polyomavirus middle T oncogene: a transgenic mouse model for metastatic disease. Mol Cell Biol *12*, 954–961.

Ha, V.L., Bharti, S., Inoue, H., Vass, W.C., Campa, F., Nie, Z., de Gramont, A., Ward, Y., and Randazzo, P.A. (2008a). ASAP3 is a focal adhesion-associated Arf GAP that functions in cell migration and invasion. J. Biol. Chem. *283*, 14915–14926.

Ha, V.L., Luo, R., Nie, Z., and Randazzo, P.A. (2008b). Contribution of AZAP-Type Arf GAPs to cancer cell migration and invasion. Adv. Cancer Res. *101*, 1–28.

Hansen, R.K., and Bissell, M.J. (2000). Tissue architecture and breast cancer: the role of extracellular matrix and steroid hormones. Endocr. Relat. Cancer *7*, 95–113.

Hashimoto, A., Hashimoto, S., Ando, R., Noda, K., Ogawa, E., Kotani, H., Hirose, M., Menju, T., Morishige, M., Manabe, T., et al. (2011). GEP100-Arf6-AMAP1-cortactin pathway frequently used in cancer invasion is activated by VEGFR2 to promote angiogenesis. PLoS ONE *6*, e23359.

Hashimoto, S., Onodera, Y., Hashimoto, A., Tanaka, M., Hamaguchi, M., Yamada, A., and Sabe, H. (2004). Requirement for Arf6 in breast cancer invasive activities. PNAS *101*, 6647–6652.

Hashimoto, S., Hashimoto, A., Yamada, A., Onodera, Y., and Sabe, H. (2005). Assays and properties of the ArfGAPs, AMAP1 and AMAP2, in Arf6 function. Meth. Enzymol. *404*, 216–231.

Hashimoto, S., Hirose, M., Hashimoto, A., Morishige, M., Yamada, A., Hosaka, H., Akagi, K., Ogawa, E., Oneyama, C., Agatsuma, T., et al. (2006). Targeting AMAP1 and cortactin binding bearing an atypical src homology 3/proline interface for prevention of breast cancer invasion and metastasis. Proc. Natl. Acad. Sci. U.S.A. *103*, 7036–7041.

Haycraft, C.J., Zhang, Q., Song, B., Jackson, W.S., Detloff, P.J., Serra, R., and Yoder, B.K. (2007). Intraflagellar transport is essential for endochondral bone formation. Development *134*, 307–316.

Hilton, M.J., and Wells, D.E. (2001a). Chromosome 8. In eLS, (John Wiley & Sons, Ltd), p.

Hilton, M.J., and Wells, D.E. (2001b). Chromosome 8. In eLS, (John Wiley & Sons, Ltd), p.

Hiratsuka, S., Watanabe, A., Aburatani, H., and Maru, Y. (2006). Tumour-mediated upregulation of chemoattractants and recruitment of myeloid cells predetermines lung metastasis. Nat Cell Biol *8*, 1369–1375.

Holmgren, L., O'Reilly, M.S., and Folkman, J. (1995). Dormancy of micrometastases: balanced proliferation and apoptosis in the presence of angiogenesis suppression. Nat.

Med. *1*, 149–153.

Hong, J.X., Lee, F.J., Patton, W.A., Lin, C.Y., Moss, J., and Vaughan, M. (1998). Phospholipid- and GTP-dependent activation of cholera toxin and phospholipase D by human ADP-ribosylation factor-like protein 1 (HARL1). J. Biol. Chem. *273*, 15872–15876.

Horwitz, K.B., Dye, W.W., Harrell, J.C., Kabos, P., and Sartorius, C.A. (2008). Rare steroid receptor-negative basal-like tumorigenic cells in luminal subtype human breast cancer xenografts. PNAS *105*, 5774–5779.

Hou, T., Yang, C., Tong, C., Zhang, H., Xiao, J., and Li, J. (2014). Overexpression of ASAP1 is associated with poor prognosis in epithelial ovarian cancer. Int J Clin Exp Pathol *7*, 280–287.

Hu, Z., Fan, C., Oh, D.S., Marron, J., He, X., Qaqish, B.F., Livasy, C., Carey, L.A., Reynolds, E., Dressler, L., et al. (2006). The molecular portraits of breast tumors are conserved across microarray platforms. BMC Genomics *7*, 96.

Hurst, J., Maniar, N., Tombarkiewicz, J., Lucas, F., Roberson, C., Steplewski, Z., James, W., and Perras, J. (1993). A novel model of a metastatic human breast tumour xenograft line. Br. J. Cancer *68*, 274–276.

Ikeda, W., Nakanishi, H., Tanaka, Y., Tachibana, K., and Takai, Y. (2001). Cooperation of Cdc42 small G protein-activating and actin filament-binding activities of frabin in microspike formation. Oncogene *20*, 3457–3463.

Inoue, H., and Randazzo, P.A. (2007a). Arf GAPs and their interacting proteins. Traffic *8*, 1465–1475.

Inoue, H., and Randazzo, P.A. (2007b). Arf GAPs and Their Interacting Proteins. Traffic *8*, 1465–1475.

Inoue, H., Ha, V.L., Prekeris, R., and Randazzo, P.A. (2008). Arf GTPase-activating Protein ASAP1 Interacts with Rab11 Effector FIP3 and Regulates Pericentrosomal Localization of Transferrin Receptor–positive Recycling Endosome. Mol. Biol. Cell *19*, 4224–4237.

Isaacs, J.T., Isaacs, W.B., Feitz, W.F., and Scheres, J. (1986). Establishment and characterization of seven Dunning rat prostatic cancer cell lines and their use in developing methods for predicting metastatic abilities of prostatic cancers. Prostate *9*, 261–281.

Jackson, T.R., Kearns, B.G., and Theibert, A.B. (2000). Cytohesins and centaurins: mediators of PI 3-kinase-regulated Arf signaling. Trends Biochem. Sci. *25*, 489–495.

Jian, X., Brown, P., Schuck, P., Gruschus, J.M., Balbo, A., Hinshaw, J.E., and Randazzo, P.A. (2009). Autoinhibition of Arf GTPase-activating Protein Activity by the

BAR Domain in ASAP1. J Biol Chem *284*, 1652–1663.

Joyce, J.A., and Pollard, J.W. (2009). Microenvironmental regulation of metastasis. Nat. Rev. Cancer *9*, 239–252.

Kablar, B., Krastel, K., Ying, C., Asakura, A., Tapscott, S.J., and Rudnicki, M.A. (1997). MyoD and Myf-5 differentially regulate the development of limb versus trunk skeletal muscle. Development *124*, 4729–4738.

Kahn, R.A., Bruford, E., Inoue, H., Logsdon, J.M., Nie, Z., Premont, R.T., Randazzo, P.A., Satake, M., Theibert, A.B., Zapp, M.L., et al. (2008). Consensus nomenclature for the human ArfGAP domain-containing proteins. The Journal of Cell Biology *182*, 1039–1044.

Kam, J.L., Miura, K., Jackson, T.R., Gruschus, J., Roller, P., Stauffer, S., Clark, J., Aneja, R., and Randazzo, P.A. (2000). Phosphoinositide-dependent Activation of the ADP-ribosylation Factor GTPase-activating Protein ASAP1 EVIDENCE FOR THE PLECKSTRIN HOMOLOGY DOMAIN FUNCTIONING AS AN ALLOSTERIC SITE. J. Biol. Chem. *275*, 9653–9663.

Kaplan, R.N., Riba, R.D., Zacharoulis, S., Bramley, A.H., Vincent, L., Costa, C., MacDonald, D.D., Jin, D.K., Shido, K., Kerns, S.A., et al. (2005). VEGFR1-positive haematopoietic bone marrow progenitors initiate the pre-metastatic niche. Nature *438*, 820–827.

Karsenty, G., and Wagner, E.F. (2002). Reaching a genetic and molecular understanding of skeletal development. Dev. Cell *2*, 389–406.

Kassis, J., Lauffenburger, D.A., Turner, T., and Wells, A. (2001). Tumor invasion as dysregulated cell motility. Semin. Cancer Biol. *11*, 105–117.

Kennecke, H., Yerushalmi, R., Woods, R., Cheang, M.C.U., Voduc, D., Speers, C.H., Nielsen, T.O., and Gelmon, K. (2010). Metastatic Behavior of Breast Cancer Subtypes. JCO *28*, 3271–3277.

Kienast, Y., von Baumgarten, L., Fuhrmann, M., Klinkert, W.E.F., Goldbrunner, R., Herms, J., and Winkler, F. (2010). Real-time imaging reveals the single steps of brain metastasis formation. Nat Med *16*, 116–122.

Kim, L.S., Huang, S., Lu, W., Lev, D.C., and Price, J.E. (2004). Vascular endothelial growth factor expression promotes the growth of breast cancer brain metastases in nude mice. Clin. Exp. Metastasis *21*, 107–118.

Kim, Y.C., Clark, R.J., Ranheim, E.A., and Alexander, C.M. (2008). Wnt1 expression induces short-range and long-range cell recruitments that modify mammary tumor development and are not induced by a cell-autonomous beta-catenin effector. Cancer Res. *68*, 10145–10153.

King, C.R., Kraus, M.H., and Aaronson, S.A. (1985). Amplification of a novel v-erbB-related gene in a human mammary carcinoma. Science *229*, 974–976.

King, F.J., Hu, E., Harris, D.F., Sarraf, P., Spiegelman, B.M., and Roberts, T.M. (1999). DEF-1, a novel Src SH3 binding protein that promotes adipogenesis in fibroblastic cell lines. Mol. Cell. Biol. *19*, 2330–2337.

Kinoshita, R., Nam, J.-M., Ito, Y.M., Hatanaka, K.C., Hashimoto, A., Handa, H., Otsuka, Y., Hashimoto, S., Onodera, Y., Hosoda, M., et al. (2013). Co-Overexpression of GEP100 and AMAP1 Proteins Correlates with Rapid Local Recurrence after Breast Conservative Therapy. PLOS ONE *8*, e76791.

Kittaneh, M., and Glück, S. (2011a). Adjuvant Therapy for Early Breast Cancer.

Kittaneh, M., and Glück, S. (2011b). Exemestane in the adjuvant treatment of breast cancer in postmenopausal women. Breast Cancer (Auckl) *5*, 209–226.

Kittaneh, M., Montero, A.J., and Glück, S. (2013). Molecular profiling for breast cancer: a comprehensive review. Biomark Cancer *5*, 61–70.

Komori, T., Yagi, H., Nomura, S., Yamaguchi, A., Sasaki, K., Deguchi, K., Shimizu, Y., Bronson, R.T., Gao, Y.H., Inada, M., et al. (1997). Targeted disruption of Cbfa1 results in a complete lack of bone formation owing to maturational arrest of osteoblasts. Cell *89*, 755–764.

Kowanetz, K., Husnjak, K., Höller, D., Kowanetz, M., Soubeyran, P., Hirsch, D., Schmidt, M.H.., Pavelic, K., De Camilli, P., Randazzo, P.A., et al. (2004). CIN85 Associates with Multiple Effectors Controlling Intracellular Trafficking of Epidermal Growth Factor Receptors. Mol Biol Cell *15*, 3155–3166.

Kruljac-Letunic, A., Moelleken, J., Kallin, A., Wieland, F., and Blaukat, A. (2003). The tyrosine kinase Pyk2 regulates Arf1 activity by phosphorylation and inhibition of the Arf-GTPase-activating protein ASAP1. J. Biol. Chem. *278*, 29560–29570.

Kuida, K., Lippke, J.A., Ku, G., Harding, M.W., Livingston, D.J., Su, M.S., and Flavell, R.A. (1995). Altered cytokine export and apoptosis in mice deficient in interleukin-1 beta converting enzyme. Science *267*, 2000–2003.

Kuida, K., Haydar, T.F., Kuan, C.Y., Gu, Y., Taya, C., Karasuyama, H., Su, M.S., Rakic, P., and Flavell, R.A. (1998). Reduced apoptosis and cytochrome c-mediated caspase activation in mice lacking caspase 9. Cell *94*, 325–337.

Kuperwasser, C., Dessain, S., Bierbaum, B.E., Garnet, D., Sperandio, K., Gauvin, G.P., Naber, S.P., Weinberg, R.A., and Rosenblatt, M. (2005). A mouse model of human breast cancer metastasis to human bone. Cancer Res. *65*, 6130–6138.

Labelle, M., Begum, S., and Hynes, R.O. (2011). Direct signaling between platelets and cancer cells induces an epithelial-mesenchymal-like transition and promotes

metastasis. Cancer Cell *20*, 576–590.

Lambrechts, A., Van Troys, M., and Ampe, C. (2004). The actin cytoskeleton in normal and pathological cell motility. Int. J. Biochem. Cell Biol. *36*, 1890–1909.

Le Gal, K., Ibrahim, M.X., Wiel, C., Sayin, V.I., Akula, M.K., Karlsson, C., Dalin, M.G., Akyürek, L.M., Lindahl, P., Nilsson, J., et al. (2015). Antioxidants can increase melanoma metastasis in mice. Sci Transl Med *7*, 308re8.

Levental, K.R., Yu, H., Kass, L., Lakins, J.N., Egeblad, M., Erler, J.T., Fong, S.F.T., Csiszar, K., Giaccia, A., Weninger, W., et al. (2009). Matrix crosslinking forces tumor progression by enhancing integrin signaling. Cell *139*, 891–906.

Lewis, C., and Murdoch, C. (2005). Macrophage responses to hypoxia: implications for tumor progression and anti-cancer therapies. Am. J. Pathol. *167*, 627–635.

Li, M., Tian, L., Yao, H., Lu, J., Ge, J., Guo, Y., Liu, M., and Xiao, H. (2014). ASAP1 mediates the invasive phenotype of human laryngeal squamous cell carcinoma to affect survival prognosis. Oncol. Rep. *31*, 2676–2682.

Li, Y., Hively, W.P., and Varmus, H.E. (2000). Use of MMTV-Wnt-1 transgenic mice for studying the genetic basis of breast cancer. Oncogene *19*, 1002–1009.

Li, Y., Kelly, W.G., Logsdon, J.M., Schurko, A.M., Harfe, B.D., Hill-Harfe, K.L., and Kahn, R.A. (2004). Functional genomic analysis of the ADP-ribosylation factor family of GTPases: phylogeny among diverse eukaryotes and function in C. elegans. FASEB J. *18*, 1834–1850.

Lim, E., Vaillant, F., Wu, D., Forrest, N.C., Pal, B., Hart, A.H., Asselin-Labat, M.-L., Gyorki, D.E., Ward, T., Partanen, A., et al. (2009). Aberrant luminal progenitors as the candidate target population for basal tumor development in BRCA1 mutation carriers. Nat Med *15*, 907–913.

Lin, D., Watahiki, A., Bayani, J., Zhang, F., Liu, L., Ling, V., Sadar, M.D., English, J., Fazli, L., So, A., et al. (2008). ASAP1, a gene at 8q24, is associated with prostate cancer metastasis. Cancer Res. *68*, 4352–4359.

Linder, S., and Aepfelbacher, M. (2003). Podosomes: adhesion hot-spots of invasive cells. Trends Cell Biol. *13*, 376–385.

Liu, Q.Y., Niranjan, B., Gomes, P., Gomm, J.J., Davies, D., Coombes, R.C., and Buluwela, L. (1996). Inhibitory Effects of Activin on the Growth and Morphogenesis of Primary and Transformed Mammary Epithelial Cells. Cancer Res *56*, 1155–1163.

Liu, Y., Loijens, J.C., Martin, K.H., Karginov, A.V., and Parsons, J.T. (2002). The Association of ASAP1, an ADP Ribosylation Factor-GTPase Activating Protein, with Focal Adhesion Kinase Contributes to the Process of Focal Adhesion Assembly. Mol. Biol. Cell *13*, 2147–2156.

Liu, Y., Yerushalmi, G.M., Grigera, P.R., and Parsons, J.T. (2005). Mislocalization or reduced expression of Arf GTPase-activating protein ASAP1 inhibits cell spreading and migration by influencing Arf1 GTPase cycling. J. Biol. Chem. *280*, 8884–8892.

Lochter, A., Galosy, S., Muschler, J., Freedman, N., Werb, Z., and Bissell, M.J. (1997). Matrix Metalloproteinase Stromelysin-1 Triggers a Cascade of Molecular Alterations That Leads to Stable Epithelial-to-Mesenchymal Conversion and a Premalignant Phenotype in Mammary Epithelial Cells. The Journal of Cell Biology *139*, 1861–1872.

Lombardi, R., and Riezman, H. (2001a). Rvs161p and Rvs167p, the Two Yeast Amphiphysin Homologs, Function Together in Vivo. J. Biol. Chem. *276*, 6016–6022.

Lombardi, R., and Riezman, H. (2001b). Rvs161p and Rvs167p, the Two Yeast Amphiphysin Homologs, Function Together in Vivo. J. Biol. Chem. *276*, 6016–6022.

Luo, R., Jacques, K., Ahvazi, B., Stauffer, S., Premont, R.T., and Randazzo, P.A. (2005). Mutational analysis of the Arf1*GTP/Arf GAP interface reveals an Arf1 mutant that selectively affects the Arf GAP ASAP1. Curr. Biol. *15*, 2164–2169.

Luo, R., Miller Jenkins, L.M., Randazzo, P.A., and Gruschus, J. (2008). Dynamic interaction between Arf GAP and PH domains of ASAP1 in the regulation of GAP activity. Cell. Signal. *20*, 1968–1977.

Ma, X.-J., Dahiya, S., Richardson, E., Erlander, M., and Sgroi, D.C. (2009). Gene expression profiling of the tumor microenvironment during breast cancer progression. Breast Cancer Res. *11*, R7.

Maffini, M.V., Soto, A.M., Calabro, J.M., Ucci, A.A., and Sonnenschein, C. (2004). The stroma as a crucial target in rat mammary gland carcinogenesis. J. Cell. Sci. *117*, 1495–1502.

Mahmoud, S.M.A., Lee, A.H.S., Paish, E.C., Macmillan, R.D., Ellis, I.O., and Green, A.R. (2012). Tumour-infiltrating macrophages and clinical outcome in breast cancer. J. Clin. Pathol. *65*, 159–163.

Mansour, S.L., Thomas, K.R., and Capecchi, M.R. (1988). Disruption of the proto-oncogene int-2 in mouse embryo-derived stem cells: a general strategy for targeting mutations to non-selectable genes. Nature *336*, 348–352.

Marino, N., and Zollo, M. (2007). Understanding h-prune biology in the fight against cancer. Clin. Exp. Metastasis *24*, 637–645.

Martin, L.J., and Boyd, N.F. (2008). Mammographic density. Potential mechanisms of breast cancer risk associated with mammographic density: hypotheses based on epidemiological evidence. Breast Cancer Research *10*, 201.

Martin, R.K., and Jackson, T.R. (2005). Centaurin β4 in cancer. Biochemical Society Transactions *33*, 1282–1284.

Mason, P.J., and Bessler, M. (2011). Cytokinesis failure and attenuation: new findings in Fanconi anemia. J Clin Invest *121*, 27–30.

Massagué, J., and Obenauf, A.C. (2016). Metastatic colonization by circulating tumour cells. Nature *529*, 298–306.

Masterson, J., and O'Dea, S. (2007). Posttranslational truncation of E-cadherin and significance for tumour progression. Cells Tissues Organs (Print) *185*, 175–179.

Mayer, B.J. (2001). SH3 domains: complexity in moderation. J. Cell. Sci. *114*, 1253–1263.

McAllister, S.S., Gifford, A.M., Greiner, A.L., Kelleher, S.P., Saelzler, M.P., Ince, T.A., Reinhardt, F., Harris, L.N., Hylander, B.L., Repasky, E.A., et al. (2008). Systemic endocrine instigation of indolent tumor growth requires osteopontin. Cell *133*, 994–1005.

McClive, P., Pall, G., Newton, K., Lee, M., Mullins, J., and Forrester, L. (1998). Gene trap integrations expressed in the developing heart: Insertion site affects splicing of the PT1-ATG vector. Dev. Dyn. *212*, 267–276.

McGlashan, S. r., Cluett, E. c., Jensen, C. g., and Poole, C. a. (2008). Primary cilia in osteoarthritic chondrocytes: From chondrons to clusters. Dev. Dyn. *237*, 2013–2020.

von Melchner, H., and Ruley, H.E. (1989). Identification of cellular promoters by using a retrovirus promoter trap. J. Virol. *63*, 3227–3233.

Menju, T., Hashimoto, S., Hashimoto, A., Otsuka, Y., Handa, H., Ogawa, E., Toda, Y., Wada, H., Date, H., and Sabe, H. (2011). Engagement of Overexpressed Her2 with GEP100 Induces Autonomous Invasive Activities and Provides a Biomarker for Metastases of Lung Adenocarcinoma. PLoS One *6*.

Meyer, D.S., Brinkhaus, H., Müller, U., Müller, M., Cardiff, R.D., and Bentires-Alj, M. (2011). Luminal expression of PIK3CA mutant H1047R in the mammary gland induces heterogeneous tumors. Cancer Res. *71*, 4344–4351.

Minn, A.J., Gupta, G.P., Siegel, P.M., Bos, P.D., Shu, W., Giri, D.D., Viale, A., Olshen, A.B., Gerald, W.L., and Massagué, J. (2005). Genes that mediate breast cancer metastasis to lung. Nature *436*, 518–524.

Molyneux, G., Geyer, F.C., Magnay, F.-A., McCarthy, A., Kendrick, H., Natrajan, R., Mackay, A., Grigoriadis, A., Tutt, A., Ashworth, A., et al. (2010a). BRCA1 basal-like breast cancers originate from luminal epithelial progenitors and not from basal stem cells. Cell Stem Cell *7*, 403–417.

Molyneux, G., Geyer, F.C., Magnay, F.-A., McCarthy, A., Kendrick, H., Natrajan, R., Mackay, A., Grigoriadis, A., Tutt, A., Ashworth, A., et al. (2010b). BRCA1 basal-like breast cancers originate from luminal epithelial progenitors and not from basal stem

cells. Cell Stem Cell *7*, 403–417.

Morishige, M., Hashimoto, S., Ogawa, E., Toda, Y., Kotani, H., Hirose, M., Wei, S., Hashimoto, A., Yamada, A., Yano, H., et al. (2008). GEP100 links epidermal growth factor receptor signalling to Arf6 activation to induce breast cancer invasion. Nat. Cell Biol. *10*, 85–92.

Mosser, D.M., and Edwards, J.P. (2008). Exploring the full spectrum of macrophage activation. Nat Rev Immunol *8*, 958–969.

Mueller, S.C., Yeh, Y., and Chen, W.T. (1992). Tyrosine phosphorylation of membrane proteins mediates cellular invasion by transformed cells. J. Cell Biol. *119*, 1309–1325.

Muglia, L., Jacobson, L., Dikkes, P., and Majzoub, J.A. (1995). Corticotropin-releasing hormone deficiency reveals major fetal but not adult glucocorticoid need. Nature *373*, 427–432.

Müller, A., Homey, B., Soto, H., Ge, N., Catron, D., Buchanan, M.E., McClanahan, T., Murphy, E., Yuan, W., Wagner, S.N., et al. (2001). Involvement of chemokine receptors in breast cancer metastasis. Nature *410*, 50–56.

Müller, T., Stein, U., Poletti, A., Garzia, L., Rothley, M., Plaumann, D., Thiele, W., Bauer, M., Galasso, A., Schlag, P., et al. (2010). ASAP1 promotes tumor cell motility and invasiveness, stimulates metastasis formation in vivo, and correlates with poor survival in colorectal cancer patients. Oncogene *29*, 2393–2403.

Nabeshima, Y., Hanaoka, K., Hayasaka, M., Esumi, E., Li, S., Nonaka, I., and Nabeshima, Y. (1993). Myogenin gene disruption results in perinatal lethality because of severe muscle defect. Nature *364*, 532–535.

Nam, J.-M., Onodera, Y., Mazaki, Y., Miyoshi, H., Hashimoto, S., and Sabe, H. (2007). CIN85, a Cbl-interacting protein, is a component of AMAP1-mediated breast cancer invasion machinery. EMBO J. *26*, 647–656.

Nelson, C.M., and Bissell, M.J. (2006). Of Extracellular Matrix, Scaffolds, and Signaling: Tissue Architecture Regulates Development, Homeostasis, and Cancer. Annual Review of Cell and Developmental Biology *22*, 287–309.

Nestl, A., Von Stein, O.D., Zatloukal, K., Thies, W.G., Herrlich, P., Hofmann, M., and Sleeman, J.P. (2001). Gene expression patterns associated with the metastatic phenotype in rodent and human tumors. Cancer Res. *61*, 1569–1577.

Nguyen, D.X., Bos, P.D., and Massagué, J. (2009). Metastasis: from dissemination to organ-specific colonization. Nat. Rev. Cancer *9*, 274–284.

Nie, Z., Stanley, K.T., Stauffer, S., Jacques, K.M., Hirsch, D.S., Takei, J., and Randazzo, P.A. (2002). AGAP1, an Endosome-associated, Phosphoinositide-dependent ADP-ribosylation Factor GTPase-activating Protein That Affects Actin

Cytoskeleton. J. Biol. Chem. *277*, 48965–48975.

Nie, Z., Hirsch, D.S., Luo, R., Jian, X., Stauffer, S., Cremesti, A., Andrade, J., Lebowitz, J., Marino, M., Ahvazi, B., et al. (2006). A BAR Domain in the N Terminus of the Arf GAP ASAP1 Affects Membrane Structure and Trafficking of Epidermal Growth Factor Receptor. Current Biology *16*, 130–139.

Nobes, C.D., and Hall, A. (1995). Rho, rac, and cdc42 GTPases regulate the assembly of multimolecular focal complexes associated with actin stress fibers, lamellipodia, and filopodia. Cell *81*, 53–62.

Nusse, R., and Varmus, H.E. (1982). Many tumors induced by the mouse mammary tumor virus contain a provirus integrated in the same region of the host genome. Cell *31*, 99–109.

Obenauf, A.C., Zou, Y., Ji, A.L., Vanharanta, S., Shu, W., Shi, H., Kong, X., Bosenberg, M.C., Wiesner, T., Rosen, N., et al. (2015). Therapy-induced tumour secretomes promote resistance and tumour progression. Nature *520*, 368–372.

Oda, A., Wada, I., Miura, K., Okawa, K., Kadoya, T., Kato, T., Nishihara, H., Maeda, M., Tanaka, S., Nagashima, K., et al. (2003). CrkL directs ASAP1 to peripheral focal adhesions. J. Biol. Chem. *278*, 6456–6460.

Okabe, H., Furukawa, Y., Kato, T., Hasegawa, S., Yamaoka, Y., and Nakamura, Y. (2004). Isolation of development and differentiation enhancing factor-like 1 (DDEFL1) as a drug target for hepatocellular carcinomas. Int. J. Oncol. *24*, 43–48.

Oliver, G., and Alitalo, K. (2005). The lymphatic vasculature: recent progress and paradigms. Annu. Rev. Cell Dev. Biol. *21*, 457–483.

Olumi, A.F., Grossfeld, G.D., Hayward, S.W., Carroll, P.R., Tlsty, T.D., and Cunha, G.R. (1999). Carcinoma-associated fibroblasts direct tumor progression of initiated human prostatic epithelium. Cancer Res. *59*, 5002–5011.

Onodera, Y., Hashimoto, S., Hashimoto, A., Morishige, M., Mazaki, Y., Yamada, A., Ogawa, E., Adachi, M., Sakurai, T., Manabe, T., et al. (2005). Expression of AMAP1, an ArfGAP, provides novel targets to inhibit breast cancer invasive activities. EMBO J. *24*, 963–973.

Onodera, Y., Nam, J.-M., Hashimoto, A., Norman, J.C., Shirato, H., Hashimoto, S., and Sabe, H. (2012). Rab5c promotes AMAP1–PRKD2 complex formation to enhance β1 integrin recycling in EGF-induced cancer invasion. J Cell Biol *197*, 983–996.

Oshiro, T., Koyama, S., Sugiyama, S., Kondo, A., Onodera, Y., Asahara, T., Sabe, H., and Kikuchi, A. (2002). Interaction of POB1, a Downstream Molecule of Small G Protein Ral, with PAG2, a Paxillin-binding Protein, Is Involved in Cell Migration. J. Biol. Chem. *277*, 38618–38626.

Oskarsson, T., Acharyya, S., Zhang, X.H.-F., Vanharanta, S., Tavazoie, S.F., Morris, P.G., Downey, R.J., Manova-Todorova, K., Brogi, E., and Massagué, J. (2011). Breast cancer cells produce tenascin C as a metastatic niche component to colonize the lungs. Nat Med *17*, 867–874.

Ottewell, P.D., Coleman, R.E., and Holen, I. (2006). From genetic abnormality to metastases: murine models of breast cancer and their use in the development of anticancer therapies. Breast Cancer Res. Treat. *96*, 101–113.

Özdemir, B.C., Pentcheva-Hoang, T., Carstens, J.L., Zheng, X., Wu, C.-C., Simpson, T.R., Laklai, H., Sugimoto, H., Kahlert, C., Novitskiy, S.V., et al. (2014). Depletion of carcinoma-associated fibroblasts and fibrosis induces immunosuppression and accelerates pancreas cancer with reduced survival. Cancer Cell *25*, 719–734.

Paget, S. (1889). THE DISTRIBUTION OF SECONDARY GROWTHS IN CANCER OF THE BREAST. The Lancet *133*, 571–573.

Paik, S., Shak, S., Tang, G., Kim, C., Baker, J., Cronin, M., Baehner, F.L., Walker, M.G., Watson, D., Park, T., et al. (2004). A Multigene Assay to Predict Recurrence of Tamoxifen-Treated, Node-Negative Breast Cancer. New England Journal of Medicine *351*, 2817–2826.

Palacios, F., Schweitzer, J.K., Boshans, R.L., and D'Souza-Schorey, C. (2002). ARF6-GTP recruits Nm23-H1 to facilitate dynamin-mediated endocytosis during adherens junctions disassembly. Nat. Cell Biol. *4*, 929–936.

Palumbo, J.S., Talmage, K.E., Massari, J.V., La Jeunesse, C.M., Flick, M.J., Kombrinck, K.W., Hu, Z., Barney, K.A., and Degen, J.L. (2007). Tumor cell-associated tissue factor and circulating hemostatic factors cooperate to increase metastatic potential through natural killer cell-dependent and-independent mechanisms. Blood *110*, 133–141.

Parsons, J.T., Horwitz, A.R., and Schwartz, M.A. (2010). Cell adhesion: integrating cytoskeletal dynamics and cellular tension. Nat. Rev. Mol. Cell Biol. *11*, 633–643.

Péchoux, C., Gudjonsson, T., Ronnov-Jessen, L., Bissell, M.J., and Petersen, O.W. (1999). Human mammary luminal epithelial cells contain progenitors to myoepithelial cells. Dev. Biol. *206*, 88–99.

Peter, B.J., Kent, H.M., Mills, I.G., Vallis, Y., Butler, P.J.G., Evans, P.R., and McMahon, H.T. (2004). BAR Domains as Sensors of Membrane Curvature: The Amphiphysin BAR Structure. Science *303*, 495–499.

Petersen, O.W., and van Deurs, B. (1988). Growth factor control of myoepithelial-cell differentiation in cultures of human mammary gland. Differentiation *39*, 197–215.

Prat, A., Parker, J.S., Karginova, O., Fan, C., Livasy, C., Herschkowitz, J.I., He, X., and Perou, C.M. (2010). Phenotypic and molecular characterization of the claudin-low intrinsic subtype of breast cancer. Breast Cancer Research *12*, R68.

Provenzano, P.P., Eliceiri, K.W., Campbell, J.M., Inman, D.R., White, J.G., and Keely, P.J. (2006). Collagen reorganization at the tumor-stromal interface facilitates local invasion. BMC Medicine *4*, 38.

Provenzano, P.P., Inman, D.R., Eliceiri, K.W., Knittel, J.G., Yan, L., Rueden, C.T., White, J.G., and Keely, P.J. (2008). Collagen density promotes mammary tumor initiation and progression. BMC Med *6*, 11.

Psaila, B., and Lyden, D. (2009). The metastatic niche: adapting the foreign soil. Nat. Rev. Cancer *9*, 285–293.

Quail, D., and Joyce, J. (2013). Microenvironmental regulation of tumor progression and metastasis. Nat Med *19*, 1423–1437.

Randazzo, P.A., and Hirsch, D.S. (2004). Arf GAPs: multifunctional proteins that regulate membrane traffic and actin remodelling. Cell. Signal. *16*, 401–413.

Randazzo, P.A., Andrade, J., Miura, K., Brown, M.T., Long, Y.Q., Stauffer, S., Roller, P., and Cooper, J.A. (2000a). The Arf GTPase-activating protein ASAP1 regulates the actin cytoskeleton. Proc. Natl. Acad. Sci. U.S.A. *97*, 4011–4016.

Randazzo, P.A., Andrade, J., Miura, K., Brown, M.T., Long, Y.-Q., Stauffer, S., Roller, P., and Cooper, J.A. (2000b). The Arf GTPase-activating protein ASAP1 regulates the actin cytoskeleton. PNAS *97*, 4011–4016.

Randazzo, P.A., Inoue, H., and Bharti, S. (2007). Arf GAPs as regulators of the actin cytoskeleton. Biol. Cell *99*, 583–600.

Rhim, A.D., Oberstein, P.E., Thomas, D.H., Mirek, E.T., Palermo, C.F., Sastra, S.A., Dekleva, E.N., Saunders, T., Becerra, C.P., Tattersall, I.W., et al. (2014). Stromal elements act to restrain, rather than support, pancreatic ductal adenocarcinoma. Cancer Cell *25*, 735–747.

Ribeiro, F.R., Jerónimo, C., Henrique, R., Fonseca, D., Oliveira, J., Lothe, R.A., and Teixeira, M.R. (2006). 8q gain is an independent predictor of poor survival in diagnostic needle biopsies from prostate cancer suspects. Clin. Cancer Res. *12*, 3961–3970.

Rodrigues, F.F., Shao, W., and Harris, T.J.C. (2016a). The Arf GAP Asap promotes Arf1 function at the Golgi for cleavage furrow biosynthesis in Drosophila. Mol. Biol. Cell mbc.E16-05-0272.

Rodrigues, F.F., Shao, W., and Harris, T.J.C. (2016b). The Arf GAP Asap promotes Arf1 function at the Golgi for cleavage furrow biosynthesis in Drosophila. Mol. Biol. Cell mbc.E16-05-0272.

Rodrigues, F.F., Shao, W., and Harris, T.J.C. (2016c). The Arf GAP Asap promotes Arf1 function at the Golgi for cleavage furrow biosynthesis in Drosophila. Mol. Biol. Cell mbc.E16-05-0272.

Roh-Johnson, M., Bravo-Cordero, J.J., Patsialou, A., Sharma, V.P., Guo, P., Liu, H., Hodgson, L., and Condeelis, J. (2014). Macrophage contact induces RhoA GTPase signaling to trigger tumor cell intravasation. Oncogene *33*, 4203–4212.

Rønnov-Jessen, L., Petersen, O.W., Koteliansky, V.E., and Bissell, M.J. (1995). The origin of the myofibroblasts in breast cancer. Recapitulation of tumor environment in culture unravels diversity and implicates converted fibroblasts and recruited smooth muscle cells. J. Clin. Invest. *95*, 859–873.

Rønnov-Jessen, L., Petersen, O.W., and Bissell, M.J. (1996a). Cellular changes involved in conversion of normal to malignant breast: importance of the stromal reaction. Physiol. Rev. *76*, 69–125.

Rønnov-Jessen, L., Petersen, O.W., and Bissell, M.J. (1996b). Cellular changes involved in conversion of normal to malignant breast: importance of the stromal reaction. Physiol. Rev. *76*, 69–125.

Rudnicki, M.A., Schnegelsberg, P.N., Stead, R.H., Braun, T., Arnold, H.H., and Jaenisch, R. (1993). MyoD or Myf-5 is required for the formation of skeletal muscle. Cell *75*, 1351–1359.

Russo, I.H., and Russo, J. (1998). Role of hormones in mammary cancer initiation and progression. J Mammary Gland Biol Neoplasia *3*, 49–61.

Sabe, H. (2003). Requirement for Arf6 in cell adhesion, migration, and cancer cell invasion. J. Biochem. *134*, 485–489.

Sabe, H., Onodera, Y., Mazaki, Y., and Hashimoto, S. (2006). ArfGAP family proteins in cell adhesion, migration and tumor invasion. Current Opinion in Cell Biology *18*, 558–564.

Sabe, H., Hashimoto, S., Morishige, M., Ogawa, E., Hashimoto, A., Nam, J.-M., Miura, K., Yano, H., and Onodera, Y. (2009). The EGFR-GEP100-Arf6-AMAP1 signaling pathway specific to breast cancer invasion and metastasis. Traffic *10*, 982–993.

Sappino, A.P., Skalli, O., Jackson, B., Schürch, W., and Gabbiani, G. (1988). Smooth-muscle differentiation in stromal cells of malignant and non-malignant breast tissues. Int. J. Cancer *41*, 707–712.

Sato, H., Hatanaka, K.C., Hatanaka, Y., Hatakeyama, H., Hashimoto, A., Matsuno, Y., Fukuda, S., and Sabe, H. (2014). High level expression of AMAP1 protein correlates with poor prognosis and survival after surgery of head and neck squamous cell carcinoma patients. Cell Commun. Signal *12*, 17.

Sceneay, J., Chow, M.T., Chen, A., Halse, H.M., Wong, C.S.F., Andrews, D.M., Sloan, E.K., Parker, B.S., Bowtell, D.D., Smyth, M.J., et al. (2012). Primary tumor hypoxia recruits CD11b+/Ly6Cmed/Ly6G+ immune suppressor cells and compromises NK cell cytotoxicity in the premetastatic niche. Cancer Res. *72*, 3906–3911.

Schlüter, K., Gassmann, P., Enns, A., Korb, T., Hemping-Bovenkerk, A., Hölzen, J., and Haier, J. (2006). Organ-specific metastatic tumor cell adhesion and extravasation of colon carcinoma cells with different metastatic potential. Am. J. Pathol. *169*, 1064–1073.

Schmalzigaug, R., Phee, H., Davidson, C.E., Weiss, A., and Premont, R.T. (2007). Differential expression of the ARF GAP genes GIT1 and GIT2 in mouse tissues. J. Histochem. Cytochem. *55*, 1039–1048.

Segi, E., Sugimoto, Y., Yamasaki, A., Aze, Y., Oida, H., Nishimura, T., Murata, T., Matsuoka, T., Ushikubi, F., Hirose, M., et al. (1998). Patent ductus arteriosus and neonatal death in prostaglandin receptor EP4-deficient mice. Biochem. Biophys. Res. Commun. *246*, 7–12.

Senkus, E., Kyriakides, S., Ohno, S., Penault-Llorca, F., Poortmans, P., Rutgers, E., Zackrisson, S., and Cardoso, F. (2015). Primary breast cancer: ESMO Clinical Practice Guidelines for diagnosis, treatment and follow-up. Ann Oncol *26*, v8–v30.

Serrels, B., Serrels, A., Brunton, V.G., Holt, M., McLean, G.W., Gray, C.H., Jones, G.E., and Frame, M.C. (2007). Focal adhesion kinase controls actin assembly via a FERM-mediated interaction with the Arp2/3 complex. Nat. Cell Biol. *9*, 1046–1056.

Sharili, A.S., Kenny, F.N., Vartiainen, M.K., and Connelly, J.T. (2016). Nuclear actin modulates cell motility via transcriptional regulation of adhesive and cytoskeletal genes. Scientific Reports *6*, 33893.

Sheetz, M.P. (1999). Motor and cargo interactions. Eur. J. Biochem. *262*, 19–25.

Sheridan, J.M., Ritchie, M.E., Best, S.A., Jiang, K., Beck, T.J., Vaillant, F., Liu, K., Dickins, R.A., Smyth, G.K., Lindeman, G.J., et al. (2015a). A pooled shRNA screen for regulators of primary mammary stem and progenitor cells identifies roles for Asap1 and Prox1. BMC Cancer *15*, 221.

Sheridan, J.M., Ritchie, M.E., Best, S.A., Jiang, K., Beck, T.J., Vaillant, F., Liu, K., Dickins, R.A., Smyth, G.K., Lindeman, G.J., et al. (2015b). A pooled shRNA screen for regulators of primary mammary stem and progenitor cells identifies roles for Asap1 and Prox1. BMC Cancer *15*, 221.

Shiba, Y., and Randazzo, P.A. (2011). GEFH1 binds ASAP1 and regulates podosome formation. Biochem. Biophys. Res. Commun. *406*, 574–579.

Shree, T., Olson, O.C., Elie, B.T., Kester, J.C., Garfall, A.L., Simpson, K., Bell-McGuinn, K.M., Zabor, E.C., Brogi, E., and Joyce, J.A. (2011). Macrophages and cathepsin proteases blunt chemotherapeutic response in breast cancer. Genes Dev. *25*, 2465–2479.

Shu, W., Jiang, Y.Q., Lu, M.M., and Morrisey, E.E. (2002). Wnt7b regulates mesenchymal proliferation and vascular development in the lung. Development *129*, 4831–4842.

Sieweke, M.H., Thompson, N.L., Sporn, M.B., and Bissell, M.J. (1990). Mediation of wound-related Rous sarcoma virus tumorigenesis by TGF-beta. Science *248*, 1656–1660.

Simian, M., Hirai, Y., Navre, M., Werb, Z., Lochter, A., and Bissell, M.J. (2001). The interplay of matrix metalloproteinases, morphogens and growth factors is necessary for branching of mammary epithelial cells. Development *128*, 3117–3131.

Sleeman, J.P. (2000). The lymph node as a bridgehead in the metastatic dissemination of tumors. Recent Results Cancer Res. *157*, 55–81.

Sleeman, J.P. (2012a). The metastatic niche and stromal progression. Cancer Metastasis Rev *31*, 429–440.

Sleeman, J.P. (2012b). The metastatic niche and stromal progression. Cancer Metastasis Rev *31*, 429–440.

Sleeman, J.P., and Cremers, N. (2007). New concepts in breast cancer metastasis: tumor initiating cells and the microenvironment. Clin Exp Metastasis *24*, 707–715.

Sleeman, J.P., Nazarenko, I., and Thiele, W. (2011). Do all roads lead to Rome? Routes to metastasis development. Int. J. Cancer *128*, 2511–2526.

Sleeman, J.P., Christofori, G., Fodde, R., Collard, J.G., Berx, G., Decraene, C., and Rüegg, C. (2012a). Concepts of metastasis in flux: The stromal progression model. Seminars in Cancer Biology *22*, 174–186.

Sleeman, J.P., Christofori, G., Fodde, R., Collard, J.G., Berx, G., Decraene, C., and Rüegg, C. (2012b). Concepts of metastasis in flux: The stromal progression model. Seminars in Cancer Biology *22*, 174–186.

Someya, A., Sata, M., Takeda, K., Pacheco-Rodriguez, G., Ferrans, V.J., Moss, J., and Vaughan, M. (2001). ARF-GEP(100), a guanine nucleotide-exchange protein for ADP-ribosylation factor 6. Proc. Natl. Acad. Sci. U.S.A. *98*, 2413–2418.

Song, J., Khachikian, Z., Radhakrishna, H., and Donaldson, J.G. (1998). Localization of endogenous ARF6 to sites of cortical actin rearrangement and involvement of ARF6 in cell spreading. J. Cell. Sci. *111 (Pt 15)*, 2257–2267.

Sørlie, T., Perou, C.M., Tibshirani, R., Aas, T., Geisler, S., Johnsen, H., Hastie, T., Eisen, M.B., van de Rijn, M., Jeffrey, S.S., et al. (2001). Gene expression patterns of breast carcinomas distinguish tumor subclasses with clinical implications. Proc. Natl. Acad. Sci. U.S.A. *98*, 10869–10874.

Sørlie, T., Tibshirani, R., Parker, J., Hastie, T., Marron, J.S., Nobel, A., Deng, S., Johnsen, H., Pesich, R., Geisler, S., et al. (2003). Repeated observation of breast tumor subtypes in independent gene expression data sets. Proc Natl Acad Sci U S A *100*, 8418–8423.

Stacey, T.T.I., Nie, Z., Stewart, A., Najdovska, M., Hall, N.E., He, H., Randazzo, P.A., and Lock, P. (2004). ARAP3 is transiently tyrosine phosphorylated in cells attaching to fibronectin and inhibits cell spreading in a RhoGAP-dependent manner. Journal of Cell Science *117*, 6071–6084.

Stahl, A., Connor, K.M., Sapieha, P., Chen, J., Dennison, R.J., Krah, N.M., Seaward, M.R., Willett, K.L., Aderman, C.M., Guerin, K.I., et al. (2010). The Mouse Retina as an Angiogenesis Model. Invest Ophthalmol Vis Sci *51*, 2813–2826.

Stoker, M.G., Shearer, M., and O'Neill, C. (1966). Growth inhibition of polyoma-transformed cells by contact with static normal fibroblasts. J. Cell. Sci. *1*, 297–310.

Strutz, F., Zeisberg, M., Hemmerlein, B., Sattler, B., Hummel, K., Becker, V., and Müller, G.A. (2000). Basic fibroblast growth factor expression is increased in human renal fibrogenesis and may mediate autocrine fibroblast proliferation. Kidney Int. *57*, 1521–1538.

Tague, S.E., Muralidharan, V., and D'Souza-Schorey, C. (2004). ADP-ribosylation factor 6 regulates tumor cell invasion through the activation of the MEK/ERK signaling pathway. Proc. Natl. Acad. Sci. U.S.A. *101*, 9671–9676.

Talmadge, J.E., and Fidler, I.J. (2010). AACR centennial series: the biology of cancer metastasis: historical perspective. Cancer Res. *70*, 5649–5669.

Tarin, D., and Croft, C.B. (1969). Ultrastructural features of wound healing in mouse skin. J. Anat. *105*, 189–190.

Tian, S., Roepman, P., Van't Veer, L.J., Bernards, R., de Snoo, F., and Glas, A.M. (2010). Biological functions of the genes in the mammaprint breast cancer profile reflect the hallmarks of cancer. Biomark Insights *5*, 129–138.

Tomasek, J.J., Gabbiani, G., Hinz, B., Chaponnier, C., and Brown, R.A. (2002). Myofibroblasts and mechano-regulation of connective tissue remodelling. Nat. Rev. Mol. Cell Biol. *3*, 349–363.

Tsukamoto, A.S., Grosschedl, R., Guzman, R.C., Parslow, T., and Varmus, H.E. (1988). Expression of the int-1 gene in transgenic mice is associated with mammary gland hyperplasia and adenocarcinomas in male and female mice. Cell *55*, 619–625.

Turgeon, B., and Meloche, S. (2009). Interpreting neonatal lethal phenotypes in mouse mutants: insights into gene function and human diseases. Physiol. Rev. *89*, 1–26.

Varfolomeev, E.E., Schuchmann, M., Luria, V., Chiannilkulchai, N., Beckmann, J.S., Mett, I.L., Rebrikov, D., Brodianski, V.M., Kemper, O.C., Kollet, O., et al. (1998). Targeted Disruption of the Mouse Caspase 8 Gene Ablates Cell Death Induction by the TNF Receptors, Fas/Apo1, and DR3 and Is Lethal Prenatally. Immunity *9*, 267–276.

Vargo-Gogola, T., and Rosen, J.M. (2007). Modelling breast cancer: one size does not

fit all. Nat Rev Cancer *7*, 659–672.

van ’t Veer, L.J., Dai, H., van de Vijver, M.J., He, Y.D., Hart, A.A.M., Mao, M., Peterse, H.L., van der Kooy, K., Marton, M.J., Witteveen, A.T., et al. (2002). Gene expression profiling predicts clinical outcome of breast cancer. Nature *415*, 530–536.

Vetter, I.R., and Wittinghofer, A. (2001). The guanine nucleotide-binding switch in three dimensions. Science *294*, 1299–1304.

van de Vijver, M.J., He, Y.D., van’t Veer, L.J., Dai, H., Hart, A.A.M., Voskuil, D.W., Schreiber, G.J., Peterse, J.L., Roberts, C., Marton, M.J., et al. (2002a). A gene-expression signature as a predictor of survival in breast cancer. N. Engl. J. Med. *347*, 1999–2009.

van de Vijver, M.J., He, Y.D., van ’t Veer, L.J., Dai, H., Hart, A.A.M., Voskuil, D.W., Schreiber, G.J., Peterse, J.L., Roberts, C., Marton, M.J., et al. (2002b). A Gene-Expression Signature as a Predictor of Survival in Breast Cancer. New England Journal of Medicine *347*, 1999–2009.

Voduc, K.D., Cheang, M.C.U., Tyldesley, S., Gelmon, K., Nielsen, T.O., and Kennecke, H. (2010). Breast Cancer Subtypes and the Risk of Local and Regional Relapse. JCO *28*, 1684–1691.

Wagner, K.U., McAllister, K., Ward, T., Davis, B., Wiseman, R., and Hennighausen, L. (2001). Spatial and temporal expression of the Cre gene under the control of the MMTV-LTR in different lines of transgenic mice. Transgenic Res. *10*, 545–553.

Wagner, S., Flood, T.A., O’Reilly, P., Hume, K., and Sabourin, L.A. (2002). Association of the Ste20-like kinase (SLK) with the microtubule. Role in Rac1-mediated regulation of actin dynamics during cell adhesion and spreading. J. Biol. Chem. *277*, 37685–37692.

Wang, J., and Deretic, D. (2015). The Arf and Rab11 effector FIP3 acts synergistically with ASAP1 to direct Rabin8 in ciliary receptor targeting. J Cell Sci *128*, 1375–1385.

Wang, J., Morita, Y., Mazelova, J., and Deretic, D. (2012a). The Arf GAP ASAP1 provides a platform to regulate Arf4- and Rab11-Rab8-mediated ciliary receptor targeting. EMBO J. *31*, 4057–4071.

Wang, J., Morita, Y., Mazelova, J., and Deretic, D. (2012b). The Arf GAP ASAP1 provides a platform to regulate Arf4- and Rab11-Rab8-mediated ciliary receptor targeting. EMBO J. *31*, 4057–4071.

Wang, W., Goswami, S., Sahai, E., Wyckoff, J.B., Segall, J.E., and Condeelis, J.S. (2005). Tumor cells caught in the act of invading: their strategy for enhanced cell motility. Trends Cell Biol. *15*, 138–145.

Weaver, A.M. (2006). Invadopodia: Specialized Cell Structures for Cancer Invasion. Clin Exp Metastasis *23*, 97–105.

Webb, B.A., Eves, R., Crawley, S.W., Zhou, S., Côté, G.P., and Mak, A.S. (2005). PAK1 induces podosome formation in A7r5 vascular smooth muscle cells in a PAK-interacting exchange factor-dependent manner. Am. J. Physiol., Cell Physiol. *289*, C898-907.

Weigelt, B., Peterse, J.L., and van 't Veer, L.J. (2005). Breast cancer metastasis: markers and models. Nat. Rev. Cancer *5*, 591–602.

Wennerberg, K., Rossman, K.L., and Der, C.J. (2005). The Ras superfamily at a glance. J Cell Sci *118*, 843–846.

West, D.B., Engelhard, E.K., Adkisson, M., Nava, A.J., Kirov, J.V., Cipollone, A., Willis, B., Rapp, J., Jong, P.J. de, and Lloyd, K.C. (2016). Transcriptome Analysis of Targeted Mouse Mutations Reveals the Topography of Local Changes in Gene Expression. PLOS Genetics *12*, e1005691.

Wigge, P., and McMahon, H.T. (1998). The amphiphysin family of proteins and their role in endocytosis at the synapse. Trends Neurosci. *21*, 339–344.

William Petersen, O., Lind Nielsen, H., Gudjonsson, T., Villadsen, R., Rønnov-Jessen, L., and Bissell, M.J. (2001a). The plasticity of human breast carcinoma cells is more than epithelial to mesenchymal conversion. Breast Cancer Research *3*, 213.

William Petersen, O., Lind Nielsen, H., Gudjonsson, T., Villadsen, R., Rønnov-Jessen, L., and Bissell, M.J. (2001b). The plasticity of human breast carcinoma cells is more than epithelial to mesenchymal conversion. Breast Cancer Research *3*, 213.

Wyckoff, J., Wang, W., Lin, E.Y., Wang, Y., Pixley, F., Stanley, E.R., Graf, T., Pollard, J.W., Segall, J., and Condeelis, J. (2004). A paracrine loop between tumor cells and macrophages is required for tumor cell migration in mammary tumors. Cancer Res. *64*, 7022–7029.

Ye, L., Mishina, Y., Chen, D., Huang, H., Dallas, S.L., Dallas, M.R., Sivakumar, P., Kunieda, T., Tsutsui, T.W., Boskey, A., et al. (2005). Dmp1-deficient Mice Display Severe Defects in Cartilage Formation Responsible for a Chondrodysplasia-like Phenotype. J. Biol. Chem. *280*, 6197–6203.

Zhang, B., and Zelhof, A.C. (2002a). Amphiphysins: raising the BAR for synaptic vesicle recycling and membrane dynamics. Bin-Amphiphysin-Rvsp. Traffic *3*, 452–460.

Zhang, B., and Zelhof, A.C. (2002b). Amphiphysins: raising the BAR for synaptic vesicle recycling and membrane dynamics. Bin-Amphiphysin-Rvsp. Traffic *3*, 452–460.

Zhao, C., Takita, J., Tanaka, Y., Setou, M., Nakagawa, T., Takeda, S., Yang, H.W., Terada, S., Nakata, T., Takei, Y., et al. (2001). Charcot-Marie-Tooth disease type 2A caused by mutation in a microtubule motor KIF1Bbeta. Cell *105*, 587–597.

Zhou, S., Webb, B.A., Eves, R., and Mak, A.S. (2006). Effects of tyrosine phosphorylation of cortactin on podosome formation in A7r5 vascular smooth muscle

cells. American Journal of Physiology - Cell Physiology *290*, C463–C471.

Zhu, Y., Wu, Y., Kim, J.I., Wang, Z., Daaka, Y., and Nie, Z. (2009). Arf GTPase-activating protein AGAP2 regulates focal adhesion kinase activity and focal adhesion remodeling. J. Biol. Chem. *284*, 13489–13496.

Acknowledgements

But little Mouse, you are not alone,
In proving foresight may be vain:
The best laid schemes of mice and men
Go oft awry,
And leave us nothing but grief and pain,
For promised joy!

- Robert Burns, 1785.

I feel fortunate to have worked in the lab of Prof. Jonathan Sleeman, for when the best laid plans of mice and men did go awry, I had a positive and an encouraging mentor like him to guide me through. It is because you went beyond just being a supervisor, and became a guardian to me, that I am here today and I am grateful for all those times when you have looked out for me, shared your personal anecdotes and have advised me. I owe my PhD to you in more ways than one.

I gratefully acknowledge the funding received towards my PhD by Deutscher Akademischer Austausch Dienst (DAAD) PhD fellowship.

I express my gratitude to Anke, who has a patient ear and a heart of gold. Your emails, messages and phone calls have meant the world to me and I cannot thank you enough for always being there for me. I thank Justyna for her friendship both in the lab and outside of it. I have shared truly memorable moments with you and I found a friend in you.

I thank all the lab members, who have been very easy-going and helpful – Annette, Gitta, Vanessa, Sonja, Ruolin, Georg, Wilko, Melanie, Sandra, Anja, Susanne and specially Caro, who helped me find my way into the lab in the initial days. I will always remember our lab meetings, coffee and cake sessions and lab outings very fondly.

I thank all my friends – old and new. To Rosh, for being the sister I wasn't born with, but the one I was destined to have. Om, your friendship and your humor has kept me going. Samrat, you've known me the longest of them all and have let me know of your belief in me at all the times when I was unsure of myself, thank you. To my friends who started their PhD journey with me, I share a special bond with all of you. Vishnu, for the long ponderings over trying to make sense of life, I say Prost! Thank you for your unconditional help. Subhamoy, you have kept me constant company with your warm positivity through the harsh European winter. Mahak, you've introduced me to the world of superheroes and super scientists with equal ease. I thank you for your unwavering friendship despite the sinusoidal graph of my emotions.

At the end, I would like to thank my parents – Jaya and Pratul – to Ma, for being the deepest reservoir of strength for me and for her abundant love, and to Papa, for reminding me of the more important things in life. To my younger brother, Raghu, I thank you for finally growing up and finding your words to let me know you are there for me. I would also like to thank the rest of my family for their love and support, especially Mama for insisting that I am 'a tigress who thinks she is a cow', and Bunty bhaiya for giving me all the love, care and pampering a little sister could ask for.

I feel blessed to have the love from all of you.